UNIVERSITEIT VAN PRETORIA
UNIVERSITY OF PRETORIA
YUNIBESITHI YA PRETORIA

Structural integrity monitoring using vibration measurements

by

André Engelbrecht

Submitted in partial fulfilment of the requirements for the degree

Master of Engineering

in the Department of Mechanical and Aeronautical Engineering

of the Faculty of Engineering, the Built Environment and Information Technology

University of Pretoria

October 2000

© University of Pretoria

Abstract

The detection of damage in structures through the use of vibrational methods offers particular advantages, which makes it an attractive method to use in specific applications. In this work the advantages and some of the possible applications of vibrational damage detection methods will be discussed. A study of the field of damage detection using vibration techniques is undertaken. Available methods are categorised in general groups according to the underlying principles. The principle, on which each group functions, as well as the advantages and disadvantages of each, concerning the practical application thereof, is explained. The goal of this work, which entails developing a damage detection method using large amounts of raw data directly and combining some of the most favourable properties of the different groups to detect damage, are set. The new method is developed and compared both numerically as well as experimentally to two methods, chosen from the literature because of similar methodology and their reputation for effective damage detection. The methods will be tested numerically with respect to accuracy, sensitivity and multiple damage detection ability. Finally experimental data is gathered and used to verify the methods damage detection ability. The new method provides a different approach to damage detection, by combining an available vibration detection method with the maximum available amount of data in order to increase the damage detection ability.

Samevatting

Die opsporing van struktuurskade deur middel van vibrasietegnieke hou spesifieke voordele in wat die gebruik van die tegnieke aanloklik maak vir spesifieke aanwendings. In hierdie werk word die voordele en 'n paar moonlike aanwendings van 'n vibrasiegebaseerde skade opsporingstegniek bespreek. 'n Studie van die veld van skadeopsporing deur middel van vibrasietegnieke word onderneem. Die beskikbare metodes kan in groepe gekategoriseer word ten opsigte van die onderliggende beginsels van elke groep. Voordele en nadele van elke groep ten opsigte van die praktiese aanwending word verduidelik. Die mikpunt van die werk wat die ontwikkelling van 'n nuwe metode behels, wat die gebruik van die maksimum hoeveelheid rou data kombineer met sommige die mees voordelige eienskappe van al die groepe om skade op te spoor, word gestel. Die nuwe metode is ontwikkel en numeries sowel as eksperimenteel vergelyk met twee bestaande metodes met soortgelyke metodiek, wat bekend is vir hulle effektiewe opsporing van struktuurskade. Metodes word getoets vir hulle akuraatheid, sensitiviteit en hulle vermoë om meervuldige skade op te spoor. Die nuwe metode verskaf 'n ander benadering tot die opsporing van skade deur bestaande vibrasie skade opsporingstegnieke deur 'n bestaande metode te kombineer met die maksimum hoeveelheid beskikbare data om die opsporing van skade te verbeter.

Contents

Acknowledgement

The author would like to express his gratitude to the University of Pretoria and to the personnel who made the writing of this thesis possible. The following people are thanked in particular:

- Professor P.S. Heyns: Not only was he a tremendously patient and caring mentor, but also a role model and friend.
- Ms. M. Calder: Always helpful and cheerful, without her help, finishing this work from Witbank would have been much harder.
-Ms. A.Botha: My wife for support and inspiration, as well as helping with the editing of the work.
- Mr. T Marwala: A man from humble beginnings destined for great things, a colleague and a friend.
-LGI: For financial support during my studies.
-Gold Fields Dynamics Laboratory: For the use of their equipment.
-My Parents: For raising me and giving me the opportunity to pursue my interests.

Soli deo Gloria

Nomenclature

A_r	Modal constant
A_{rk}	Set of coefficients associated with mode r
$[A_{wi}]$	Combined graph matrix
$[A_u]$	Undamaged motion shape matrix
B(s)	Dynamic stiffness
[C]	Global damping matrix
C_{rj}	Combination of r^{th} modal stiffness
c_r	Viscous damping of r^{th} mode
[D]	Motion shape curvature difference matrix
D_j	Decision classes
E	Modulus of elasticity
[F]	Flexibility matrix
Fp	Phase window function
{f(t)}	Applied force vector
f(s)	Applied force Laplace transform
[ΔF]	Flexibility matrix perturbation
F_{rj}	Modal stiffness fraction
f_{rj}	Elements of flexibility matrix [F]
H_0	Null hypothesis test
H_1	Second hypothesis
$(\|\hat{H}\|)$	Maximum value of FRF
h	Average distance between measuring points
[I]	Unit matrix
I	Second moment of the area
i	Unit imaginary number
j	General index
[K]	Global stiffness matrix
k_r	r^{th} Modal stiffness

[M]	Global mass matrix
M(x)	Bending moment as function of position
m_r	Effective mass of r^{th} mode.
N	Number of degrees of freedom
p	Transfer function residue
R^n	Pattern space
r	General index
R_{ij}	Stiffness contribution
S	Cubic spline polynomial
S_{jj}	Auto spectrum
S_{jI}	Cross-spectral density
$T_{ij}(i\omega)$	Transmissibility between point j and reference i
$X(i\omega)$	Fourier transform of x (t)
k(x)	Bending stiffness
M (x)	Bending moment
$V''(x)$	Curvature of displacement mode shape as function of position
V''_{jr}	Curvature of mode shape
$[V''_u]$	Second derivative undamaged motion shape matrix
X	Random sample patterns
x	Displacement
$\dot{x}$	Velocity
$\ddot{x}$	Acceleration
Z	Damage location index

α_n	Fraction of stiffness loss
α_{ij}	Receptance transfer function
β_β	Indicator used for damage location
σ_β	Variance of a set of data
ω_i	i^{th} Modal vibration frequency (rad/s, Hz)
$\Delta\omega$	Frequency bandwith of a FRF
ζ_i	i^{th} Modal damping ratio
δ_j	Measure of flexibility change
μ	Mean value of a set of data
η_{ij}	Anti-resonance frequency of α_{ij}
η_r	Damping of mode r
λ	Complex eigenvalue
$[\Phi]$	Ortho-normalised mode shape matrix
$[\psi]$	Arbitrarily normalised mode shape matrix
$\{\ \}$	Vector
$[\ ]$	Matrix
$\{\ \}^T, [\ ]^T$	Transposed vector, matrix
$[\ ]^{-1}$	Matrix inverse

1. INTRODUCTION

1.1 Vibration and damage detection

Today's society relies on many structures, such as aircraft, wind turbines, bridges, offshore platforms, buildings and production plants, which are nearing the end of their design lifetimes. Damage of large structures caused by fatigue, corrosion and wear, pose a threat to the safety of people, as well as a financial risk. Companies that make use of large structural buildings in their production processes, are therefore forced to schedule shutdowns of equipment for inspection, to avoid progressive damage which could result in failure. Primarily visual inspections take place, which are costly and time consuming. Non-destructive methods are usually utilised for the detection of damage on critical structures.

Non-destructive methods that are available at present, such as X-ray, acoustic emission, magnetic resonance and ultrasonic testing, are time consuming and labour intensive, due to the fact that they are highly localised (Robinson, Peterson, James & Doebling, 1996). In addition, none of these approaches provide a quantitative assessment of the magnitude of the damage (Kaouk & Zimmerman, 1994). The field of non-destructive testing is still in development and a vast amount of research is still needed. The above mentioned drawbacks make inspection of large structures tedious. Technicians roam around the structures with their equipment. Isolation and fire resistant material must be removed and replaced after inspection at additional cost. In addition, production-time loss makes the entire process more costly. It is evident that there is a need for a simpler and more effective technique of inspection.

Rudimentary techniques of structural evaluation by vibration monitoring are thousands of years old. Examples of these techniques include the sounding of clay pots, which could reveal cracks and tapping on walls to find voids. A more recent example is the tapping of train wheels. Structural integrity monitoring by the use of vibration techniques, holds many advantages compared to non-destructive techniques in the industrial field. Vibration damage detection methods rely on the vibration response of the structure. No

vibration response can exist without some form of excitation. During normal production, the structure is excited, which means vibration methods can be implemented. This has the added advantage of minimising production time losses, through the minimisation of production downtime. In comparison to two non-destructive methods, vibration techniques are much quicker, because they are not limited to finding damage in small areas. Location and quantification of damage is possible using vibration techniques. Recent advances in integrated circuit technology and digital signal processing, allows real time analysis of vibration response, in frequency and time domains. If permanent transducers can be mounted on the structures, continuous monitoring will be possible, which could result in a much safer work environment. Maintenance on the structure could be scaled down, saving money and prolonging the life of the structure.

1.1.2 Vibration parameters

When considering vibration damage location methods, a good place to start is to look at which characteristics could be quantified. Two groups of characteristics exist which comprise of different parameters. Systems can be characterised in terms of their spatial characteristics, or in terms of their modal characteristics. The difference between the two should be understood. Spatial characteristics (of the first group) pertain to the physical parameters such as mass, stiffness and damping of the system. The second group (modal parameters) on the other hand, can be coupled to the vibration characteristics of a system, which can be measured by monitoring the system motion. Examples include natural frequency and mode shapes. The two groups are interdependent. A change in the spatial parameters will automatically cause a change in the modal parameters. This means that the vibrational response of the system will change if the stiffness, mass or damping (because of inflicted damage to the system) is varied.

All vibration damage location methods are based on the fact that when a structure is damaged, its spatial characteristics change, which in turn causes vibration characteristic changes (modal characteristics). The response of a system can be seen as a signature of the system. As soon as the signature changes, the damage location method assumes that

the change was caused by damage to the system. As long as the system was not modified in any way it is a valid assumption.

For damage detection purposes, changes caused by damage in the individual spatial parameters (first group), namely mass, damping and stiffness are only considered for some of the parameters. For instance, change in mass due to damage is usually not considered, because it is generally assumed that parts of the system would not break loose to cause the mass to change. While the mass of the structure might not change, the loading of the structure is seldom a static case. Research has shown that it is possible to distinguish between the change in response, because of mass fluctuation on a large structure (like changes in fluid level, or moving of equipment) and the change in response caused by damage (Shahrivar & Bouwkamp, 1986).

Changes in damping because of damage to the structure, is usually seen as an insensitive parameter for the detection of damage. For a steel structure the damping is very low to start off with, which makes any changes seem insignificant. Nevertheless, the influence a change in damping has on other parameters, should always be kept in mind. Stiffness is the parameter most widely used in the location and quantification of damage. The stiffness is dependent on the material's elastic properties and the area of a section. Damage reduces the area of the section and therefore alters the stiffness (Pandey, Biswas & Samman, 1991).

The effect of damage can also be detected in the modal parameters (second group). For any system containing mass and stiffness, the frequencies where the largest responses are observed for a constant excitation amplitude, are called natural frequencies. Natural frequency is a very popular damage detection parameter, because of the fact that it can be obtained from a vibration measurement anywhere on the system. If damage is inflicted on the system, its natural frequency shifts. A mode shape is an indication of the shape of vibrational deformation of the system, if it is excited at one of its natural frequencies. Theoretically large systems, like steel structures, have an infinite number of natural

frequencies and mode shapes, in practice, it is only possible to measure the first few (Farrar, Stubbs & Kim, 1995). Damage to a system causes both the natural frequency and the mode shapes to change. The change in natural frequency for minor damage is extremely small (Crawley & Adams, 1979). Other problems with the change in natural frequency, are that cracks at two different locations, associated with certain crack lengths, may cause the same amount of frequency change. Frequency changes are also sensitive to changes in environmental conditions like temperature (Pandey, Biswas & Samman, 1991). Despite its drawbacks, a frequency change provide a quick check for damage to a system and is useful in combination with other parameters. If in future more sensitive measuring can be achieved, and these systems are incorporated with effective noise handling methods, the natural frequency might be a viable parameter on its own. Since mode shapes are much more sensitive to system damage, it is more often used in damage location techniques (Shahrivar & Bouwkamp, 1986). To summarise, the two most sensitive and widely used parameters for the detection of damage, are stiffness (spatial parameter) and mode shapes (modal parameter). Structural damage weakens the structure resulting in a decrease in stiffness, which can be measured most effectively by looking at the mode shapes (momental vibrational bending shape of the structure).

1.1.2 Damage location

Vibration damage location and identification techniques can be subdivided in two main groups. Both of the groups are only able to identify and locate damage, which occur after the method was implemented. The methods need information from the undamaged system to compare with recent information to be able to detect any damage. Early implementation of a method on a system such as a structure is thus essential.

The first group of the two, makes use of a mathematical finite element model of the structure, which was updated (adjusted to give accurate answers) by the use of vibration measurements to form the baseline "undamaged" model. For the purpose of updating, different algorithms can be found in the literature. The vibration measurements are always measured at much fewer positions than can be modelled by the mathematical

model. To compare measured and modelled data, the same amount of information is needed. This means that either the model must be reduced, or interpolation through the measured points has to be introduced to make comparison possible. If the response given by the updated mathematical model, is later found to differ from the measured response, due to system damage, the extent and location of damage is found by observing which changes must be made to the mathematical model, to give similar responses as the ones measured. The need still exists to account for the uncertainty associated with modelling the properties and boundary conditions of real structures (Farrar, Stubbs & Kim, 1995).

The second group of damage location techniques makes use of vibration measurements only. Some techniques utilise the changes of vibration measurements over time periods to locate damage. From the vibration measurements, modal parameters are extracted for use in the damage location process. Mostly a process called experimental modal analysis is used. This involves finding the modal parameters through the use of curve fitting on vibration measurements (Frequency Response Function plots). By observing the changes in modal parameters as a function of time, it is possible to locate and quantify damage. A need remains to account for omnipresent errors in measuring modal parameters (Farrar, Stubbs & Kim, 1995).

For application to structures like spacecraft and other structures, that do not undergo structural modifications, the first group of methods (making use of finite element models) holds great promise. In industry though, there are some practical problems. Firstly, for most of the older structures, finite element models are not available. Setting up a finite element model for a large complex structure is time consuming and very expensive. Secondly, plant modifications pose a major problem. As soon as modifications have been done the spatial system changes, which means that the finite element model must be modified and updated to produce a new baseline model. As many of the modifications on a plant are not documented, this could be very inconvenient and costly. A method that utilises changes in vibrational data, does not require the time and finances going into setting up a finite element model. If it can be assumed that no damage was inflicted

while modifications on the plant were done, the next set of vibration readings can be used as a new baseline. Drawbacks in the use of these methods are the large number of vibration readings, from specific positions and of high quality, that are required. With advances in computer technology, storage space becomes less of a problem, but because modal parameters are obtained from curve fits (modal analysis techniques), the quality of the data remains the biggest problem.

Neural networks are becoming very popular in the field of damage location. (Kirkegaard & Rytter, 1994) Neural networks can basically be used to automate structural integrity monitoring by use of any of the above mentioned groups of methods. The neural network system is an artificial intelligence system, which is trained to recognise damage. A number of possible damage scenarios are fed into a finite element model of the structure. Vibration responses of these scenarios are stored in the neural network database, with the description of the damage induced. The neural network continually monitors the vibration response of the system and tries to fit any changes caused by damage to its library of information. If a match is found, the description of the damage is given to the user. Neural networks can only recognise damage for which it was trained to look for.

1.2 Literature survey

A system of classification for damage-identification methods, as presented by Rytter (1993), defines four levels of damage identification:

Level 1 : Determination that damage is present.

Level 2 : Determination of the geometric location of the damage.

Level 3 : Quantification of the severity of the damage.

Level 4 : Prediction of remaining service life of the structure.

The literature in this review can be classified as Level 1, Level 2 or Level 3 methods. Level 4 methods fall into the fatigue field, which is a field of study on its own. The

outcome of the literature survey suggested that the damage detection field is a relatively new field. The first work done on the study of damage detection in the vibration context, was a collection of suggestions on possible ways in which the problem could be approached, as well as a study on their feasibility. With these methods in place, follow-up work, building on the best of the early methods and combinations of them were done. For the purpose of this survey the methods will be divided into early methods (suggesting a solution to the problem of damage detection) and second-generation methods (developed from the early methods).

1.2.1 Early methods

Cawley and Adams (1979) demonstrated what could be achieved with quality instrumentation in a constant temperature enclosure. Their work describes the extension of the frequency method for locating damage on two-dimensional structures. Measuring the extent of structural damping was not undertaken. Tests were done to locate damage on aluminium and fibre-reinforced plastic plates. It was found that the rates of changes in two modes were only a function of the damage location. An eight-node, 40 degree-of freedom finite-element model, was used. Dynamic analysis, sensitivity analysis and stress calculations were performed at positions on a grid over the plates. The change in natural frequency because of damage was computed through the use of a sensitivity analysis at a series of grid points. These sensitivities were used to find an error function at each point. The point, at which the error was a minimum, gave the approximate position of the damage. Occasionally it was found that the results obtained by using the damage location scheme was incorrect, but that the error was rectified if the results were computed without using the readings from one mode. A method was developed to automate the procedure. Frequency changes were found to be very small, but all of the damage could be successfully located. Natural frequency, being dependent on mass and stiffness, will change because of a change in stiffness caused by damage. The change in natural frequency for minor damage is so small that the shift in natural frequency, caused by temperature changes, needs to be considered.

Afolabi (1987) developed a technique based on anti-resonance frequencies to determine the approximate location of defects in a structure. Afolabi reported that anti-resonance frequency exhibits significant variation, depending on the location of the measurement site. Data obtained for the undamaged state was compared with the damaged state. Numerical experiments with damage, due to loss of mass as well as local loss in stiffness, were simulated. As the point of measurement got closer to the location of the defect, fewer and fewer anti-resonance are shifted when compared to their undamaged values. The approximate location of the defect may thus be located rapidly without computing resonance mode shapes. Unfortunately the anti-resonance shift has the same problem as the frequency shifts of very small changes in the case of minor damage.

Chang and Ju (1988) established a theory based on the structural power to assess the damage status of a structure. In addition the established structural power could also be a material characteristic for non-linear structures, which is important for identification of non-linear structures as well as damage. During strong excitation, energy is dissipated through hysteresis loops. The area under a hysteresis loop represents the energy dissipation. It was demonstrated that the amount of energy dissipation could be used as an indicator for the level of damage. The structural power is frequency dependent. For wide band excitation constant structural power could be found statistically. As amplitude rises the value of the structural power also increases. The technique requires the measurement of structural velocity response. This method might hold promise for level 4 application (remaining service life) as soon as the damage has been detected. Fatigue analysis is based on the same fundamentals (Bannantine, Comer & Handrock, 1990). Because of the frequency and amplitude sensitivity, this method is not favoured for damage detection.

Tsai, Yang and Chen (1988) tested the cross-random decrement method for the detection and location of damage. The random decrement process is a signal processing technique which extracts the free decay response from the random responses, by removing the

contribution of the random input excitation. The cross random decrement technique uses two channels of measurement each time, obtaining the free decay responses and calculating the modal eigenvalues, relative amplitudes and phases between the two selected positions. By shifting positions of the selected measurement around the structure, complete modal vectors can be determined. The time signature resulting from the cross-random decrement process, provides information concerning the time lag between the responses of the two different locations. This information is used in the determination of the location of damage. Tests were done on a 1:13.8 scale model of an offshore platform. A pendulum was set up to provide random impact excitation. Two stages of damage were introduced namely a saw-cut (halfway through) and a complete cut-away at the same location. The correlation between the changes of the relative phases at various positions and the location of the damage has demonstrated the feasibility of the technique. However due to the complexity of the large structure, the relationship between phase changes and the damage location still requires more research.

Lew (1995) developed a coherence of the transfer function approach for locating the position of damage. The parameter change in transfer function was used to distinguish the structural damage from environmental changes. Only a few sensors were required in using the coherence approach for damage detection. The coherence between the parameter change of the tested system and the change due to damage was used to locate the position of damage. Better results were obtained when excitation was directed at an angle inclined to two planes. A numerical study was done on a nine-bay truss structure. For the system damage a beam was removed for each case. From the results obtained, it was observed that the system's natural frequencies changed little due to environmental changes, but changed dramatically due to the system damage. The results based on the analysis of noisy response showed that the coherence algorithm would identify the damaged element. This approach could also be applied to a multi-input and -output system. Considering the large amount of damage removal of a beam represented, findings about the sensitivity of large natural frequency changes compared with environmental changes could be expected.

Shahrivar and Bouwkamp (1986) built a 1:50 scale plastic model representing the structure of a typical offshore platform. Effects of severing of diagonal bracing members on selected vibrational frequencies and mode shape parameters at the deck, were investigated. The effect of changing deck mass on the selected parameters were also investigated. It was found that the mode shapes were much more sensitive to damage than its natural frequencies. Typical damage reduced the frequency by 1 to 4 percent but changed values of the normalised modes by 30 to 100 percent. It was also found that if the mass was increased so that the same change in mode shape as would be caused by damage was observed, the natural frequency would decrease by more than 45 percent. The effect of increases in mass was clearly distinct from those of damage.

Mode shape based methods started humbly by comparing actual mode shapes before and after damage, but grew quickly to comparing the curvature of the mode shape before and after damage. The fact that mode shapes were much more sensitive to damage moved the research direction in its favour. More and more new research is built on the mode shape parameter, or with mode shapes in combination with other parameters.

1.2.2 Second generation methods

The early methods were the first to be introduced by researchers as possible solutions to the problem of detecting damage with the use of vibrational techniques. Second generation methods involve the investigation and refinement of existing techniques and combinations of techniques.

Pandey, Biswas and Sammon (1991) investigated a new parameter called curvature mode shape, as a possible candidate for identifying and locating damage in a structure. Absolute changes in the curvature mode shape are localised in the region of damage and increased with an increase in the size of the damage. Curvature mode shapes can be obtained numerically from the displacement mode shapes. Numerical results for a cantilever beam and a simply supported beam model demonstrated the usefulness of the

method in locating a state of damage. To obtain curvature mode shape by experimental model analysis, a full set of measurements is required.

Salawu and Williams (1994) evaluated the performance of two damage location methods, both making use of mode shapes. The methods are the curvature mode shape method and the mode shape relative difference method. In the second method graphical comparison of the displacement mode shapes was used to indicate the position of damage. The procedures do not require extensive computations or any theoretical damage model. Performance of the curvature mode shape and mode shape relative difference methods on experimental data was poor. The most important factor in using these two methods, was determining which modes to use, since only some of the modes correctly identified and located the damage. Only the curvature mode shape method was able to give an indication of simulated multiple damage locations. The methods were unable to sufficiently differentiate the location of two damage cases with close degrees of damage severity. An explanation was suggested why only some of the mode curvature mode shapes gave the correct damage position. Damage at a certain position could be close to position of maximum displacement at mode 1 and 2 but near a node at mode 3. The method could be useful if there was a way of telling which of the mode shapes were relevant for the detection of damage. The method will definitely come in handy for the purposes of a second opinion on possible damage location.

The emphasis of the work of Pandey and Biswas (1995) was on the location of damage using the flexibility difference method. Cantilevered, simply supported and free-free beams were tested. For each case different results were obtained but damage location could still be found. For example, in the cantilever beam the position of damage was at the point from which the flexibility difference started to increase linearly. In the simply supported beam on the other hand, damage was located at the position of maximum flexibility difference. Damage in the beams was introduced by cutting through the beam using a saw. Experimental modal analysis techniques were used to estimate the natural frequencies and mode shapes for both the intact and damaged beams. The measured

1157857 50
b15237412

values were then used to estimate the flexibility matrix. Location of damage was found from flexibility differences. The advantage of using flexibility instead of stiffness is that the flexibility matrix of a structure can be accurately estimated using only a few of the lower frequency modes. Sometimes transverse direction measurements were more sensitive to damage. The method successfully located damage as well as multiple damage.

Farrar, Stubbs & Kim (1995) developed a non-destructive damage detection method that was used on a full-scale bridge, called the damage index method. Only a few mode shapes were needed in this analysis. Damage was detected without solving a system of equations and damage could be localised in structures containing many elements. An indicator is found at a specific location in terms of pre- and post-damage mode shapes. For every location there are as many indicators available as there are mode shapes. The value of the indicator is normalised and the damage pattern is then found via a statistical pattern recognition technique. Pre-damage and post-damage model data were extracted from a 1300 ft span bridge located in New Mexico. The span was modelled as a fifty-element beam on three linear axial springs. Results of the analysis indicated that the methodology accurately localised the damage.

Five different damage identification methods that have been reported in technical literature, were demonstrated and compared by Farrar and Jautegui (1996). They utilised experimental data from an undamaged and damaged bridge for this exercise. Four levels of damage were introduced to the middle span of the bridge. A course set and a refined set of accelerometers were used to obtain resonant frequencies, mode shapes and modal damping values. Modal data was determined from frequency response functions obtained during measured input, random, forced-vibration testing. All the methods used observed changes in the mode shape to locate the damage. The methods examined were the Damage index method, Mode shape curvature method, Change in flexibility method, Change in uniform flexibility curvature method and Change in stiffness method. In the study the Damage index method performed the best. The Mode shape curvature method

also performed well, although not as well as the Damage index method. The Change in flexibility method appeared to have problems identifying damage for situations when damage was not severe. The Change in uniform flexibility curvature method performed satisfactorily using the experimental modal data from the refined set of accelerometers. Surprisingly, the Change in stiffness method improved when applied to the modal data from the course set of accelerometers. Significant improvements were also achieved when only the first two modes were used instead of all six. An observation from the author was that the Damage index method was the only method tested that had a specific criterion for determining if damage has occurred at a particular location. The other methods were only sensitive to the largest change in a particular parameter, and it is ambiguous at times to determine if these changes indicate damage at more than one location.

A structural damage location procedure, which does not require the use of an original analytical model, was presented by Zimmerman and Kaouk (1994). The only information needed in this procedure is pre- and post-damage vibration measurements. First arbitrary mass and stiffness matrixes are chosen. Using the pre-damage vibration measurements in an iterative algorithm the matrixes are refined to produce a baseline (undamaged) model. It should be noted that this baseline model might not be physically meaningful. Once damaged, the post-damage parameters of the structure are used to further refine the refined analytical model. This results in perturbation of the refined analytical model. Analysis of the resulting perturbation could indicate the damage location and extent. An experimental study using damage cases associated with a NASA eight-bay hybrid-scale cantilevered truss test-bed was used. The results of the proposed procedure were compared to results generated using a finite element model. Fourteen damage cases, for which five modes of vibration were identified, were used. The location algorithm only failed in one case. If this procedure is used with a finite element model it provides much better results. This work was a good attempt at cutting back on the large amount of work that goes into setting up a finite element model of a large structure. The fact that the baseline model may not be physically meaningful is a drawback of this method.

Kirkegaard and Rytter (1994) investigated the use of artificial neural networks for damage assessment of civil engineering structures. Training of the network was performed with patterns of the relative changes of the natural frequencies that occured due to damage. Measured data from an undamaged structure must be distinguished from measured data from a damaged structure. This is called pattern recognition. Pattern recognition techniques are presented to determine the damage location but not the magnitude of damage. The structure considered was a 20 m high steel lattice mast subjected to wind excitation. First a neural network was trained with simulated estimates of the relative changes of the lowest five natural frequencies. The changes were estimated for a 20, 40, 60, 80 and 100 percent reduction of the selected areas of diagonals. Twenty-one training sets were implemented. By trial-and-error it was found that a 4 layer neural network with 5 input nodes, 5 nodes in each of the two hidden layers and 4 output nodes gave the network with smallest output error. The results showed that the neural network was capable of locating damage corresponding to the removal of a diagonal in the mast. It was possible to detect damage corresponding to a 50 percent reduction of the diagonal, but it was not possible to quantify the size of the damage.

1.3 Scope of this work

From the literature survey, advantages, shortcomings and problems were revealed for the different methods. One of the largest problems seems to be the loss and under-utilisation of information. Damage detection methods (Pandey & Biswas, 1995) and (Stubbs, Kim and Farrar, 1995) seem to be focused on acquiring the best result with the least amount of data. Raw data contains a large amount of information. This includes information about damping, frequency and mode shapes. Methods utilising mode shapes have to make use of modal analysis to find the mode shapes from frequency response functions. The curve fitting involved results in the loss of vital information from the system. The under-utilisation of information comes from the fact that theoretically a large number of structural motion shapes can be measured. These shapes at resonant frequency are known

as mode shapes. For an aluminium cantilever beam, (length 0.8 m) if tested from 1 to 600 Hz at 1 Hz intervals, mode shapes used for the detection of damage usually amount to less than one percent of the total number of possible motion shapes. A large percentage of these motion shapes (measured near to an anti-resonance frequency) are relatively small and difficult to use, but better utilisation of the information is still possible.

In this work a new method utilising large amounts of raw data and at the same time side-stepping the time consuming work of setting up a finite element model similar to the efforts of Zimmerman and Kaouk (1994), will be developed. By not using a finite element model, it will make the method easier to use on systems subjected to structural changes. The method is an extension of the Curvature mode shape method investigated by Pandy, Biswas and Sammon (1991), chosen because it is easy to apply to raw data. Curvature mode shape method, was also chosen above the mode shape relative difference method, because of the findings from the comparison by Salawu and Williams (1994). The main problem of the Curvature mode shape method, namely which mode shapes to choose (as stated by Salawu and Williams (1994)) will be addressed.

To overcome the problem of loss of information through the fitting of curves to raw data, an alternative to the classical modal analysis technique was developed. In essence the new method developed is a mode shape method modified to utilise large amounts of data and using an alternative modal analysis technique. To obtain the mode shapes and the additional motion shapes, some process of converting the raw data to motion shapes is needed. The alternative method concentrates on using the measured data values instead of the modified values after the curve was fitted to the data. The alternative technique is valid for lightly damped structures. To test the efficiency of the new method, a numerical evaluation of the new damage location method comparing it to two established methods that were reported to give good results, will be undertaken. The two methods used to evaluate the new method are both mode shape methods using modal analysis to obtain the mode shapes required. The formulation of the new method makes the incorporation of

noise into the numerical data extremely difficult. To implement noise in numerically generated data is possible but the numerical method utilised for testing generates frequency response functions. In practice frequency response functions are generated by the combination of two measured signals, an excitation and a response signal. Normally noise is included in the two signals, which are then mathematically manipulated to provide the frequency response function. Noise will not be incorporated into the numerical data used in the numerical evaluations of the damage detection methods. The ability of the methods to locate damage as well as the effect different support types have will be investigated. The ability of the methods to locate multiple damage will also be investigated. Finally the method will be tested using experimental data. Comparison of the new method to the two chosen methods, will be made on the basis of numerical and experimental test results.

2. EXISTING DAMAGE DETECTION METHODS AND RELEVANT TECHNIQUES

All methods using mode shapes as a basis for the detection of damage obtain the mode shapes from measured data. The technique used for obtaining the mode shapes is called modal analysis. A short explanation of the modal analyses technique as well as the technique used as a basis for developing an alternative method used in the new method (Operational deflection shapes method) will be presented. The most promising existing damage detection methods in the literature will be outlined. These methods will be used to evaluate the effectiveness of the new method, which will be developed in the following chapter. The two methods chosen are the Flexibility difference method (Panday & Biswas, 1995) and the Damage index method (Farrar & Stubbs, 1995). Also outlined, is the change in curvature mode shape method and the operational deflection shape technique, which form the basis of the new method.

2.1 Modal analysis

Many procedures are available for the task of extracting the mode shapes from the measured frequency response function. In this work only the simplest approach will be discussed. The method is sometimes referred to as the 'peak-picking' method. This is a method which works adequately for structures whose FRFs exhibit well-separated modes, which are not so lightly-damped that accurate measurements at resonance are difficult to obtain but which, on the other hand, are not so heavily damped that the response at a resonance is strongly influenced by more than one mode (Ewins, 1994). Basically all modal analysis techniques involves two different parts. The first part consists of curve-fitting a theoretical expression for an individual FRF to the actual measured data to find coefficients, which most closely match the measured data. In increased complexity, different procedures (not discussed in this work) involve the curve fitting, first as part of a single FRF curve, then as a complete curve encompassing several resonance and finally to a set of many FRF plots. The second part is a mathematical root-finding or eigen-solution exercise.

The method is applied as follows (Ewins, 1994):

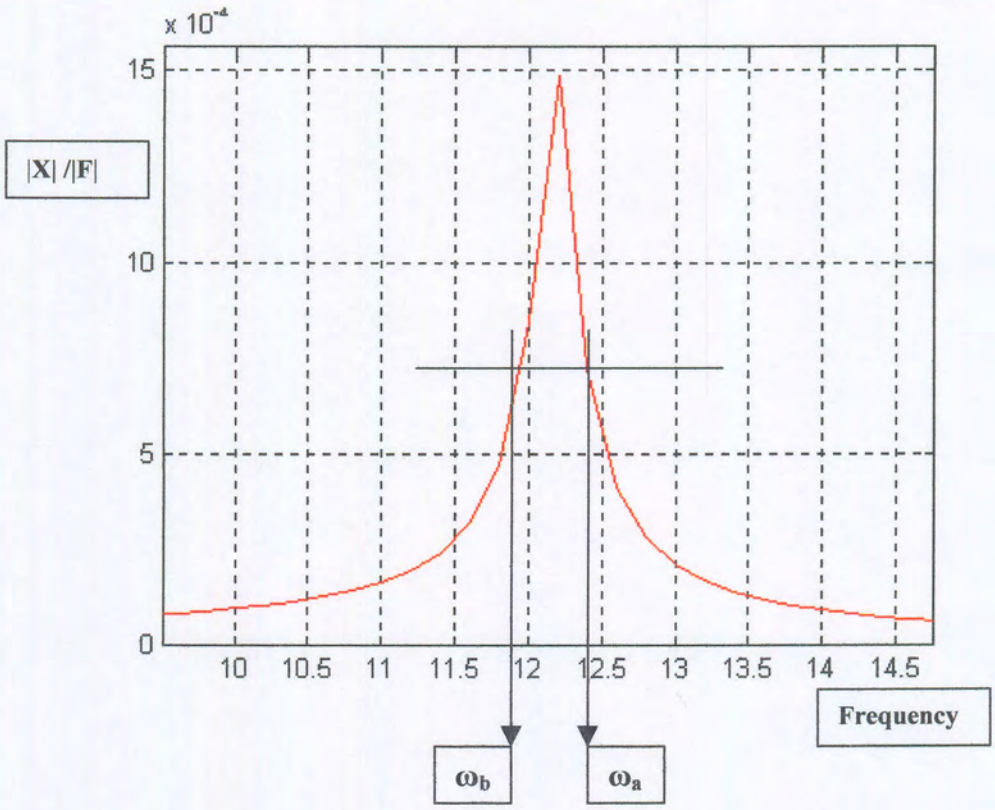

Figure 2.1 Parameter estimation through peak-picking.

1) First the individual resonance peaks are detected on the FRF plot and the frequency of maximum response taken as the natural frequency of the mode (ω_r).
2) Secondly the maximum value of the FRF is noted $\left(\left|\hat{H}\right|\right)$ and frequency bandwidth of the function for a response level of $\frac{1}{\sqrt{2}} \times \left(\left|\hat{H}\right|\right)$ is denoted as ($\Delta\omega$). The two points thus identified as ω_a and ω_b are the 'half-power points' (see Figure 2.1)

The damping of the mode in question can now be estimated from the following formula.

$$\eta_r = \frac{\left(\omega_a^2 - \omega_b^2\right)}{2 \times \omega_r^2} \approx \frac{\Delta\omega}{\omega_r} \tag{2.1.1}$$

The modal constant of the mode being analysed can now be calculated, by assuming that the total response in the resonant region is attributed to a single term in the general FRF series.

$$\frac{X}{F} = \frac{1}{\left(k - \omega^2 m\right) + i\omega c} \tag{2.1.2}$$

The modal constant (A_r) can be found from the equation

$$\left|\hat{\mathrm{H}}\right| = \frac{A_r}{\omega_r^2 \eta_r}$$

$$A_r = \left|\hat{\mathrm{H}}\right| \omega_r^2 \eta_r \tag{2.1.3}$$

2.2 Operational deflection shapes (Døssing & Staker, 1987)

Operational deflection shape (ODS) analysis involves measurement of the complex transmissibility between a fixed transducer and a second transducer roving to all points of interest on the structure. At each frequency of interest the relative magnitude and phase are extracted from the measurement. These extracted values, assembled in a vector, represent the operational deflection shape at the specific frequency of the measured point, relative to a reference point. The complex transmissibility function is defined in terms of the Fourier transform X(iω) of the measured x (t):

$$T_{ij}(i\omega) = \frac{X_i(i\omega)}{X_j(i\omega)} \tag{2.2.1}$$

where j is the reference DOF and i is an arbitrary DOF.

As no mathematical model exists for transmissibility, curve fitting of the data is not possible. Modal analysis software can however be used to extract the complex ratios at the desired frequencies using the 'peak picking' procedure (Ewins, 1994).

In practice $T_{ij}(i\omega)$ is approximated by one of several estimators

$$T_{ij} = \frac{S_{ji}}{S_{jj}} \tag{2.2.2}$$

$$T_{ij} = \frac{S_{ii}}{S_{ij}} \tag{2.2.3}$$

The choice of estimator for $T_{ij}(i\omega)$ depends on the noise situation, which can be judged by looking at the coherence. If the coherence of the measurements is unity at the frequency of interest, any of the estimators can be used and the same results will be obtained. If the coherency is less than unity at the frequency of interest, the approximations will be biased, and therefore more sophisticated estimators should be used. Possible reasons for coherence being less than unity is:

a) Noise in the input and/or output measurement.
b) Non-linearity of the system.

$$T_{ij} = \frac{X_i}{X_j} \qquad \omega = \omega_s \tag{2.2.4}$$

The extracted set of $T(i\,\omega)$ at $\omega=\omega_s$, constitute the ODS:

$$ODS = \{T_{ij}\}_s \tag{2.2.5}$$

The operational deflection is obtained by multiplying each ODS by the corresponding RMS value of the associated line reference auto-spectrum(S_{jj}).

$$\{x\} = \{T_{ij}\}\sqrt{S_{jj}(\omega_s)} \tag{2.2.6}$$

If the operational deflection is entered into a geometrical model, animation of the model can assist in visualising the dynamic behaviour of the system.

2.3 Changes in curvature mode shapes (Panday, Biswas & Sammon, 1991)

Existence of damage in a structure reduces the stiffness (as represented by *EI*) at the crack location. E is the modulus of elasticity, *I* is the second moment of area and *M(x)* is the bending moment as a function of position. Reduction in *EI* leads to an increase in the magnitude of the curvature $V''(x)$ at the section, as given by (Gere & Timoshenko, 1991)

$$V''(x) = \frac{M(x)}{EI} \tag{2.3.1}$$

Since the change in curvature is local and dependant on the reduction in (*EI*), the curvature change can be used to detect, locate and quantify damage. From the mode shapes the shape of the beam at the natural frequency can be found. Usually the mode shapes are ortho-normalised so that,

$$[\Phi]^T[M][\Phi] = [I] \tag{2.3.2}$$

If the curvature of the structure changed because of damage, it will be reflected in the curvature of the mode shapes. The absolute difference in the curvature mode shape between the damaged and undamaged structures is expected to show a maximum at the damaged region. The curvatures of a mode shape may be computed from the displacement mode shapes using a central difference approximation,

$$V''_{jr} = \frac{(\Phi_{(j+1)r} - 2\Phi_{jr} + \Phi_{(j-1)r})}{h^2} \quad \text{j} = 2, 3, 4 \ldots, \text{n} - 1 \tag{2.3.3}$$

where h is the distance between measuring points, V''_{jr} and Φ_{jr} are respectively elements of the curvature and displacement mode shape for the mode r at measurement point j. An element length is regarded as being the distance between two consecutive measuring points.

2.4 Flexibility difference method (Panday & Biswas, 1995)

Since flexibility is the inverse of stiffness, reduction in stiffness will result in an increase in flexibility of the structure. If the mode shapes are ortho-normalised to unit mass,

$$[\Phi]^T[M][\Phi]=[I] \tag{2.4.1}$$

the flexibility matrix, [F] can be obtained from the modal data as

$$[F]=[\Phi]\,[\overline{K}]^{-1}[\Phi]^T=\sum_{i=1}^{m}(1/\omega^2{}_r)\Phi_r\Phi_r^T \tag{2.4.2}$$

were m is the number of degrees of freedom, [M] is the mass matrix, Φ_r is r^{th} mode shape, ω_r is the r^{th} modal frequency and

$$[K]^{-1} = \text{diag}\,(1/\omega_r{}^2) \tag{2.4.3}$$

If two sets of measurements, one set for the undamaged structure and another for the damaged structure, are taken and modal parameters are estimated from the measurements, then by using equation (2.4.2), the flexibility for the two cases can be found. From the flexibility matrix, flexibility difference [ΔF] can be obtained as

$$[\Delta F] = [F_2] - [F_1] \tag{2.4.4}$$

where $[F_1]$ and $[F_2]$ are the flexibility matrices for the undamaged and damaged cases respectively. Since it is difficult to measure the rotational degree of freedom, only the translational degrees of freedom are used in the calculation of the flexibility matrix. For each translational degree of freedom, j, let δ_j be the maximum absolute value of the element in the corresponding column of $[\Delta F]$ *i.e.*

$$\delta_j = \max |\delta f_{rj}| \tag{2.4.5}$$

where δf_{rj} are elements of $[\Delta F]$. To locate damage, the quantity δ_j is used as the measure of change in flexibility for each measurement location.

2.5 Damage index method (Farrar & Stubbs, 1995)

The theory of damage location will be limited to beams. The approach presented can be routinely extended to plates or other arbitrary three-dimensional structures. Consider an arbitrary homogeneous 1-D beam with N members (in the finite element sense) and n nodes. Assume that the beam behaves linearly. On solving the eigenvalue problem, the r^{th} modal stiffness, K_r, of the beam is given by

$$K_r = \int_0^L k(x)[\Phi_r''(x)]^2 dx \tag{2.5.1}$$

where Φ_r'' is the second derivative of the mode shape of r^{th} modal vector, $k(x)$ is the bending stiffens of the beam (i.e. the product of Young's modulus and second moment of area). The contribution of the j^{th} member of the r^{th} modal stiffness, C_{rj}, is given by

$$C_{rj} = k_j \int_j [\Phi''_r(x)]^2 dx \tag{2.5.2}$$

where k_j is the stiffness of the j^{th} member. The fraction of the modal stiffness (element sensitivity) for the r^{th} mode that is concentrated in the j^{th} member is given by

$$F_{rj} = \frac{C_{rj}}{K_r} \tag{2.5.3}$$

Let the corresponding modal parameter in equations. (2.5.1) to (2.5.3) associated with damage structure be characterised by asterisks. Then for the damaged structure

$$F^*_{rj} = \frac{C^*_{rj}}{K^*_r} = F_{rj}(1 + \sum_{n=1}^{N} A_{rn}\alpha_n + H.O.T.) \tag{2.5.4}$$

where scalars C_{rj}^* and K_{rj}^* are given by:

$$C^*_{rj} = k^*_j \int_j [\Phi''^*_r(x)]^2 dx \tag{2.5.5}$$

$$K^*_r = \int_0^L k^* [\Phi''^*_r(x)]^2 dx \tag{2.5.6}$$

The constants A_{rk} represent a set of coefficients associated with the mode r and location k,

$$\alpha_n = \frac{(k^*_n - k_n)}{k_n} \tag{2.5. 7}$$

is the fraction of stiffness loss at location n in the structure and $H.O.T.$ stands for higher order terms. In Eqs. (2.5.1) to (2.5.7), note that for any mode r, the terms F_{rj} and F_{rj}^* have the following properties:

$$\sum_{j=1}^{N} F_{rj} = \sum_{j=1}^{N} F^*_{rj} = 1 \tag{2.5.8}$$

and $F_{rj} << 1$, $F_{rj}^* << 1$

Therefore, an expression which connects the behaviour of the damaged and undamaged structure may be developed from the approximation:

$$1 + F_{rj} \cong 1 + F_{rj}^{*} \tag{2.5.9}$$

Eq. (2.5.9) is used to derive a consistent indicator of damage localisation. The validity of using Eq. (2.5.9) to derive a consistent indicator of damage localisation will be examined in the next section. Substituting into Eq. (2.3.9) for H_{rj} and H_{rj}^{*} using Eqs. (2.5.3) and (2.3.4) yields

$$1 = \frac{(C_{rj}^{*} + K_{r}^{*})K_{r}}{(C_{rj} + K_{r})K_{r}^{*}} \tag{2.5.10}$$

Utilising expressions for C_{rj} and C_{rj}^{*} in Eqs. (2.5.5) and (2.5.6) and the Mean Value Theorem of Calculus, Eq. (2.5.10) is transformed to (2.5.11)

$$1 = \frac{k_j^{*}\left(\int_j [\Phi_r''^{*}(x)]^2 dx + \frac{1}{k_j^{*}} \int_0^L k^{*}[\Phi_r''^{*}(x)]^2 dx\right)\ k(x)\int_0^L [\Phi_r''(x)]^2 dx}{k_j\left(\int_j [\Phi_r''(x)]^2 dx + \frac{1}{k_j} \int_0^L k(x)[\Phi_r''(x)]^2 dx\right)\ k^{*}(x)\int_0^L [\Phi_r''^{*}(x)]^2 dx} \tag{2.5. 11}$$

By approximating $k(x) \cong k^{*}(x)$, the following equation is obtained

$$\beta_{\beta} = \frac{k_j}{k_j^{*}} = \frac{\left(\int_j [\Phi_r''^{*}(x)]^2 dx + \int_0^L [\Phi_r''^{*}(x)]^2 dx\right)\ \int_0^L [\Phi_r''(x)]^2 dx}{\left(\int_j [\Phi_r''(x)]^2 dx + \int_0^L [\Phi_r''(x)]^2 dx\right)\ \int_0^L [\Phi_r''^{*}(x)]^2 dx} \tag{2.5. 12}$$

$$\beta_\beta = \frac{NUM_\beta}{DEN_\beta}$$

There are two important features of the indicator β_β. Firstly, the expression attempts to express the changes in stiffness at a specific location in terms of pre-damage and post-damage mode shapes. Secondly, the terms on the right hand side of Eq. (2.5.11) can be measured. Thus for each damage location j, there are as many β_β available as there are mode shapes. The latter values of β_β define the feature space. To account for all available modes a single indicator for each location is formed as

$$\beta_j = \frac{\sum_r NUM_{jr}}{\sum_r DEN_{jr}} \qquad \textbf{(2.5. 13)}$$

Values of the indicator is normalised according to the rule

$$Z_j = \frac{(\beta_j - \mu_\beta)}{\sigma_\beta} \qquad \textbf{(2.5. 14)}$$

where σ_β is the variance and μ_β is the mean of the set of data. The next problem is to develop an algorithm that would classify Z_j's into damaged and undamaged location. The damage pattern will be classified by a statistical pattern recognition technique. Statistical pattern-recognition systems map randomly sampled patterns $X \in R^n$ to pattern k decision classes $D_j \subset R^n$. The decision classes (D_j) partition the pattern space R^n:

$$R^n = \bigcup_{j=1}^{k} D_j, \quad D_j \cap D_r = \phi \text{ if } r \neq j \qquad \textbf{(2.5. 15)}$$

Pattern recognition is supervised if the decision classes are known. The technique used here to classify a member is hypothesis testing. It is assumed that there are two

hypotheses concerning the value Z_j. The first is the null hypothesis, H_0, assumes that the value of Z_j consists of only noise so that $Z_j = N$. In the second hypothesis, H_1, the location is assumed to be damaged so that $Z_j = N + D$. Let D_0 denote the choice of H_0 hypothesis and D_1 denote the choice of the H_1 hypothesis.

Four outcomes based on a set of samples of Z_j are possible:

1. The presence of damage is correctly identified. The probability of this outcome is called the probability of detection (P_D) denoted by $P(D_1/H_1)$;
2. The damage is incorrectly declared as present when in fact there is no damage present. This is the probability of a false alarm (P_{fa}) denoted by $P(D_1/H_0)$;
3. It is incorrectly declared that there is no damage present. This is denoted by $P(D_0/H_1)$;
4. It is correctly declared that the location is undamaged. This case is denoted by $P(D_0/H_o)$.

Damage localisation is accomplished in five steps:

1. Compute fractional modal stiffness for each member.
2. Compute β_β.
3. Compute β_j.

Compute Z_j and classify location j.

3. NEW METHOD

In this chapter a new method called the *Combined curvature motion shape method*, will be developed. This method will be a combination of different methods and techniques, which are applied directly to the measured FRFs. The method starts off by converting each measured FRF (Bode diagram format) to single graphs, which represent the relative motion to the excitation at the measurement point for a wide range of frequencies. Combining these graphs gives an indication of the relative motion of the entire system over a wide range of frequencies. The *Difference in curvature mode shape method* (Panday, Biswas & Sammon, 1990) principle is applied to this vast amount of information to yield possible damage positions.

3.1 Introduction

To visualise the development of the method, a step by step explanation follows. Consider a typical FRF function. Each FRF is representative of a specific response, excitation ratio and measuring point. Other FRFs can be generated by either varying the point of measurement, and keeping the point of excitation static, or vice versa. If fixed excitation is used, the point of measurement is varied. As can be seen from Figure 3.1, the FRF in Bode diagram form, consist of two graphs. Figure 3.1(a) shows the ratio of response amplitude at the measurement point to excitation force, as a function of excitation frequency. Figure 3.1 (b) is the phase of the FRF, also as a function of frequency, which shows whether the motion at the point of measurement and the excitation force is in the same or the opposite direction as the excitation force.

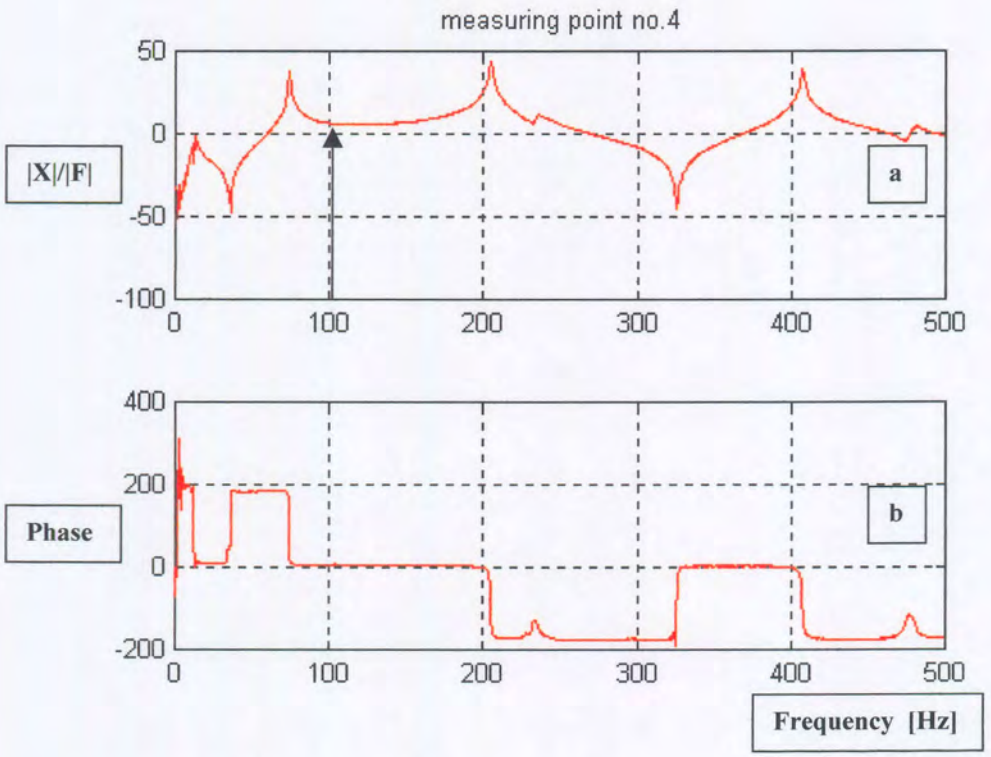

Figure 3.1a & b Typical frequency response function Bode Format

Because the moduli of all the FRFs (Figure 3.1 (a)) are scaled to a unit input force, it is easy to predict the motion of the measurement point caused by any harmonic excitation force with a specific frequency. For example, for an excitation frequency of 100 Hz (Figure 3.1), the response at the measuring point is approximately in phase with excitation force and the ratio of response amplitude to force is approximately $1x10^{-5}$ m/N.

The first step of the new proposed method is to combine the information on the bode graphs into a single graph, which better indicates what is physically happening at the measuring point relative to the excitation force. For lightly damped systems, the phase shifts, as read from the FRFs, are primarily either 0° or 180° (Figure 3.1b). The fact that the phase shift is so well defined, makes it easy to use the phase as a means to show if the motion should be in phase or out of phase to the excitation force, at the measurement

position. The new graph is constructed by taking the modulus of the FRF (Figure 3.1a) and multiplying it by a Phase window function. The phase window function is equal to one, if the absolute value of the phase is smaller than 90° at a specific input frequency, otherwise the function is equal to minus one. From the combined graph (Figure 3.2) the same relative motion predictions can be made as with the bode FRF graphs. A positive value is taken to be in phase while a negative value is out of phase. The characteristic phase change of the movement as the beam passes a natural frequency is easily observed in the combined graph.

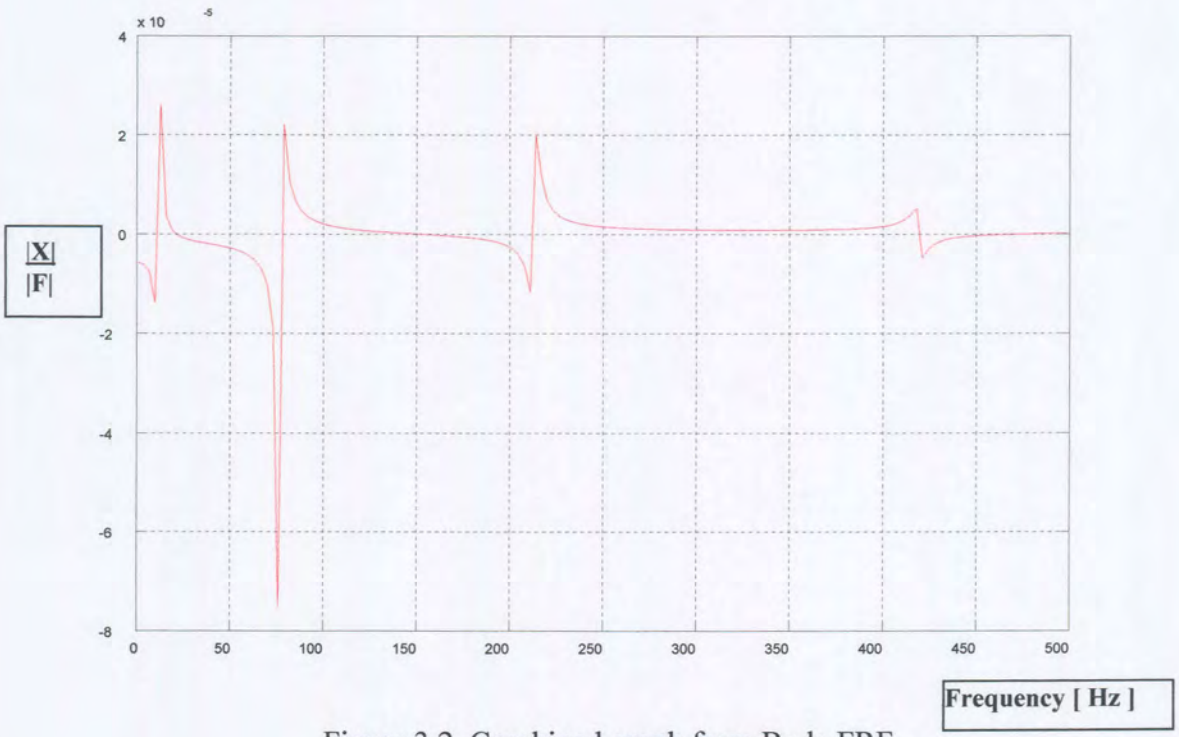

Figure 3.2 Combined graph from Bode FRF

The next step is to expand on what is explained above for a single measurement point, to generate an indication of the relative motion of the entire beam for any excitation frequency in the measured range. This is achieved by duplicating the process for a number of measured combined FRFs (Figure 3.2), spread over the length of the beam and incorporating the results in a 3D plot. In Figure 3.4 such a 3D plot has been generated for the cantilever beam of Figure 3.3. Note that the measurement nodes in Figure 3.3

correspond to the nodes in Figure 3.4. To obtain the estimation of the relative movement of a point between two measured FRFs, interpolation is used.

The process up to now bears a resemblance to the *Operational Deflection Shape technique* (see paragraph 2.1) with the exception that the plot is scaled relative to the excitation force, while the operational deflection is scaled relative to the motion of a chosen reference point. In both cases the aim is to find the actual motion of the structure for further analysis.

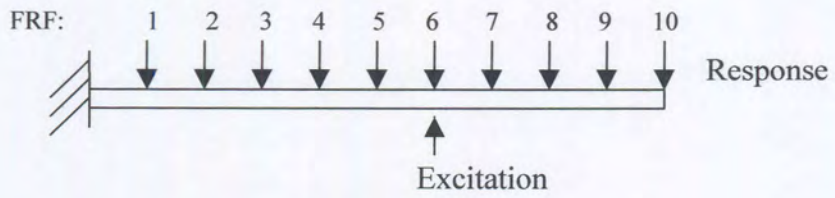

Figure 3.3 Cantilever beam

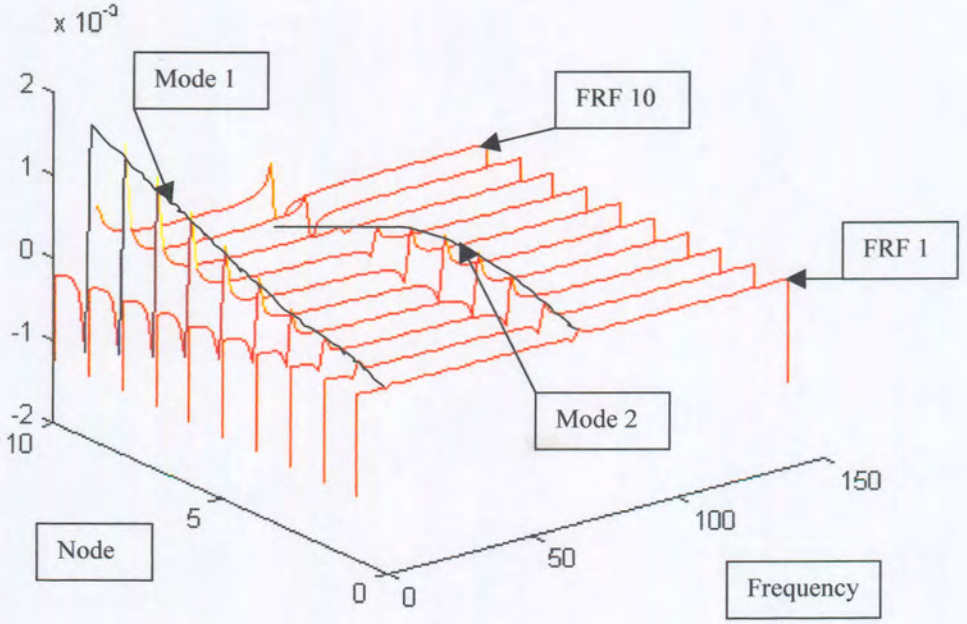

Figure 3.4 3D response plot of cantilever beam

The mode shapes correspond to the motion of the structure when it is excited at its natural frequencies. In the 3D plot (Figure 3.4) the mode shapes can be found by fitting a curve over the beam movement graph near the specific natural frequency. In essence the process followed thus far can be seen as an alternative to modal analysis. From it the mode shapes can be obtained, at the natural frequency, as well as other shapes, at other frequencies, which will be called "motion shapes" for this discussion. Now that the motion of the beam is known over a wide range of frequencies, the next step is to incorporate the theory behind the *Change in curvature mode shape method.* (Panday, Biswas & Sammon 1990 - See paragraph 3.1.1). Basically their theory relies on the excessive bending of a structure, at the point of damage relative to the bending of the undamaged structure. For the *Change in curvature mode shape method*, the method is applied to mode shapes that are extracted from the raw data via the modal analysis process (see paragraph 2.2). Rather than utilising only the mode shapes, as is the case for the *Change in curvature mode shape method*, the idea with the new method is to use all the motion shapes, to maximise data utilisation.

Once the motion shapes have been identified, the new method becomes an extension of the Change in curvature method. For continuity the explanation of the process will be completed. The next step is to evaluate the curvature of the undamaged and damaged beam by calculating their second derivatives of the motion shapes. The second derivative localises the position of change in bending on the structure. Theoretically the position of damage can be located by subtracting the two sets of derivatives (damaged and undamaged) from one another. In practice, as mentioned in the literature study, some of the mode shapes curvature differences points to the location of damage, while other mode shapes do not. It was mentioned (Panday, Biswas & Sammon 1991) that sometimes an incorrect damage position was detected, but it was rectified when one of the mode shapes was ignored. This phenomenon might be explained by a theory, which suggests that the location of the damage was close to the location of a node of a specific mode shape, making utilisation of that mode shape for the detection of damage ineffective. The

limited amount of data that is utilised in the application of the *Change in curvature mode shape method* causes the methods to be less effective. Each, of the many curvature motion shape differences show a possible damaged position. The final step of the new method is to sum all the absolute curvature differences values over all the motion shapes utilised, to give a better indication of the damage position.

3.2 Formulation

In this section the Combined curvature motion shape outlined in paragraph 3.1 will be mathematically formulated. The Frequency Response Function (FRF) which defines the relationship between the displacement at co-ordinate *i* and a unit excitation applied at co-ordinate *j*, may be written as a cross receptance, $\alpha_{r\,j}$. Due to reciprocity $\alpha_{rj}=\alpha_{jr.}$ (Ewins, 1994)

$$\alpha_{ij}(\omega) = \frac{X_i(\omega)}{F_j(\omega)} \qquad \textbf{(3.2.1)}$$

A combined graph is compiled by multiplying the modulus of the FRF by a "Phase window function" (Fp (ω)). The Phase window function is a function which is equal to one, if the absolute value of the FRF phase (Figure 3.1 b) is larger than 90° and equal to minus one otherwise. An arrow is used in the formulation (3.2.2) because the equation process is an element by element calculation obtained from the phase and absolute value Bode plot FRFs.

$$\left[A_{\omega\, i}\right] \Leftarrow Fp(\omega)_i \times \alpha_{i\,j}(\omega) \qquad \textbf{(3.2.2)}$$

To find the curvature motion shapes, a number of combined FRF values, compiled from pre- and post-damage data, are arranged in two separate matrices. In this formulation, matrices are used as a structure to store data. The matrix basically forms a numerical plan view of Figure 3.4. Each combined FRF (measured at a specific point) is placed in a separate column in matrix $[A_{\omega i}]$ (3.2.2), with the rows of the matrix corresponding to

similar excitation frequencies. If eleven FRFs are measured over the length of the system over a frequency range between zero and five hundred Hertz at 1 Hz intervals, a eleven by five hundred matrix will be generated. To construct a motion shape at a specific frequency, all the combined FRF values at that frequency should be used, thus making use of the matrix rows. If the system is clamped, a column of zeros is added to indicate zero motion at the clamped position for all frequencies. $[A_u]$ and $[A_d]$, constructed similarly (3.2.2), is the undamaged and damaged motion shapes. By looking at $[A_u]$ and $[A_d]$ separately, an image can be constructed resembling the motion of the damaged and undamaged structure at any frequency in the measured range. Both images are scaled relative to the excitation force and can thus be compared. When comparing motion shapes of the undamaged system to the damaged system an observation that can be made is that the comparative motion shape in the undamaged state shifts to a slightly lower frequency in the damaged state (Figure.3.5).

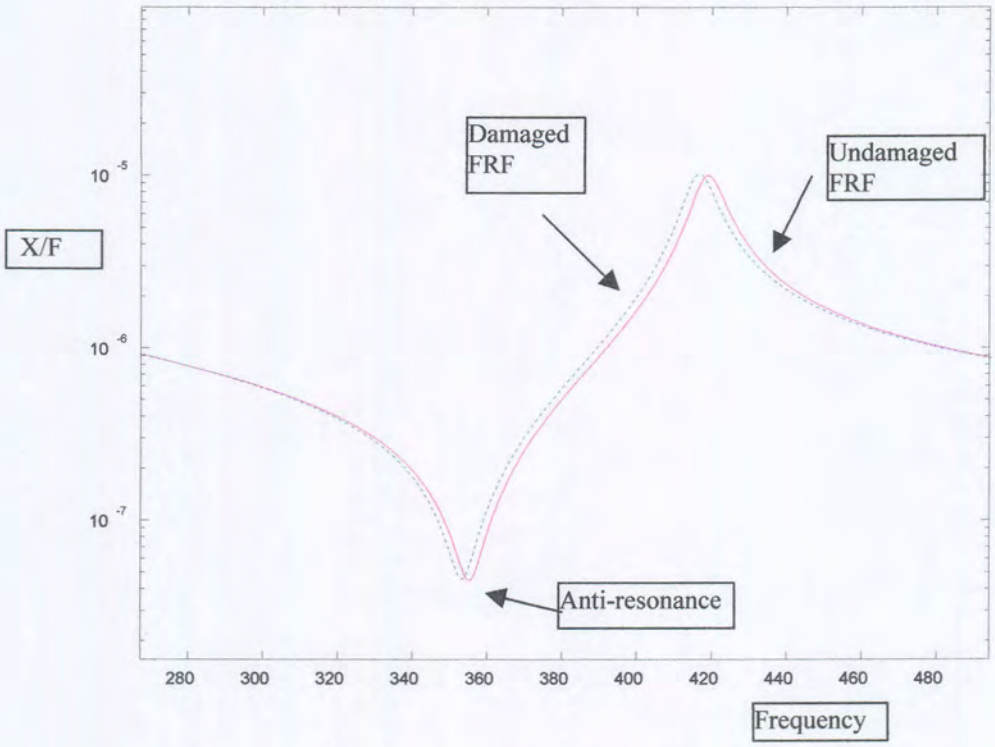

Figure 3.5. Frequency shift caused by damage

The shift in frequency is a direct result of the lowering of stiffness caused by damage. Fortunately the frequency shift for minor damage is very small, and should not have a large influence on the damage location method.

The curvature of the damaged and undamaged motion shapes are computed from the motion shapes using the second derivative of a cubic spline curve fit (Mathews, 1987) on the rows of the matrices $[A_u]$ and $[A_d]$. The cubic spline numerical curve fitting method was chosen because of its accuracy. High accuracy curve fit is essential for the next step, which requires the calculation of the second derivatives, of the motion shapes, at the measurement points. The cubic spline is a piece-wise third order polynomial curve fitted to a set of data points. The polynomials are calculated in such a way that the fitted curves form a continuous differentiable function over the data interval. (Burden & Faires, 1997)

S is a cubic polynomial, defined on the subinterval $[x_n \ x_{n+1}]$ for j = 0, 1, …, n-1.

$S(x_j) = f(x_j)$ for each j = 0, 1, ……n; **(3.2.3)**

$S_{j+1}(x_{j+1}) = S_j(x_{j+1})$ for each j = 0, 1, ……n - 2; **(3.2.4)**

$S'_{j+1}(x_{j+1}) = S'_j(x_{j+1})$ for each j = 0, 1, ……n - 2; **(2.2.5)**

$S''_{j+1}(x_{j+1}) = S''_j(x_{j+1})$ for each j = 0, 1, ……n - 2; **(3.2.6)**

One of the following sets of boundary conditions is satisfied: **(3.2.7)**

(i) $S''(x_o) = S''(x_n) = 0$ (*free or natural boundary*)

(ii) $S'(x_o) = f'(x_o)$ and $S'(x_n) = f'(x_n)$ (*clamped boundary*)

A cubic spline data fit is performed on each row of matrix $[A_u]$ and $[A_d]$ respectively giving the motion of the beam for each frequency for the damaged and undamaged system. The second derivative at the data point is obtained from the cubic polynomial and positioned in a matrix $[V''_u]$ and $[V''_d]$, in similar order as matrix $[A_u]$ and $[A_d]$. The Curvature motion shape difference is found by simply subtracting the elements of the two matrices from each other.

$$[D] = |V''_u| - |V''_d| \qquad \textbf{(3.2.8)}$$

Matrix [D] contains the motion shape curvature difference. Damage is indicated near the position where the structure bends the most compared to the undamaged state. Each row of matrix [D] gives a suggested damage position near the measurement point corresponding to the largest value in the row. As the columns of the [D] matrix coincide with the measurement positions, the largest value in each matrix row could suggest a possible damage position. To obtain a single index for the indication of the position of damage, the sum of the absolute curvature differences values for each position over all of the excitation frequencies are calculated. In matrix form it means summing the absolute values of the elements in each of the columns. The largest of these values indicate the position of damage.

4. Numerical investigation

4.1 Finite element models

Testing using numerically generated data was undertaken to evaluate and compare damage detection abilities thought to be of importance for effective damage detection methods. It is important to know how a damage detection method would perform under ideal data conditions, in order to know what to expect in its application. A successful method should be able to detect minor damage at any position in a damaged system, irrespective of the boundary conditions of the system. The multiple damage detection ability of the methods will be tested numerically. The ability to detect multiple damage will count in favour of a damage detection method.

A finite element model package was used to generate data for the numerical investigation. The scientific software *Structural Dynamic Toolbox* based on MATLAB (Balmès, 1995), was used to construct a finite element model for the beam. Aluminium beam of length 960 mm, width 31 mm and depth 9.5 mm was modelled. An aluminium beam with the same dimensions was used for experimental verification of the work (Chapter 5). Euler-Bernouli beam elements were used and damage was introduced in the form of a reduction in modulus of elasticity. The reduction in modulus of elasticity is a widely used method of modelling stiffness loss, caused by damage. To make the model of localised damage more realistic, the beam length was divided into fifty elements, where every fifth node coincided with one of the ten measuring points over the length of the beam. The modulus of elasticity of one of the five elements was reduced to generate data for a damaged case. Several damaged cases were modelled by varying the position of a single element on the beam of which the modulus of elasticity was reduced.

Three different programs were written using the same numerical data to evaluate the three different damage detection methods that were introduced in chapters 2 and 3. The methods tested are the Flexibility difference, Damage index and the new Combined curvature motion shape method. All the programs were constructed from the basis of

only having damaged and undamaged vibration data available. For *the Flexibility difference* and *Damage index methods*, mode shapes were generated. The *Combined curvature motion shape method* utilise numerically generated FRF data. The same mathematical model (modelling the specific damage test scenario) was used to generate test data for all the damage detection methods tested, and will be replaced by measured data in the following chapter. The programs that were compiled are presented in Appendix A. In constructing the computer programs for the different damage detection methods, similar numerical methods were used where possible as a basis for fair comparison.

4.2 Numerical methods

In this section the numerical methods that will be used in the modelling of the different damage detection methods are explained. Numerical methods are used in computer programs when mathematical manipulation of a discrete set of values is necessary. The *Flexibility difference method*, based essentially on simple mathematical manipulation did not require the use of unusual numerical methods for its working. The method's accuracy can not be improved by the introduction of a numerical method.

For the application of the *Combined curvature motion shape method*, the second derivative of the motion shapes have to be calculated. A central difference method can be utilised to calculate the second derivative, but the results at the beginning and end of the structure can never be as accurate as the results in the centre of the structure. Lack of accuracy for the end points is caused by the principle on which the method works. The central difference method utilises values on both sides of the position where the second derivative is being calculated to estimate the answer more accurately. Naturally the above mentioned refinement is not effective at the ends of the curve where values only exist on one side. A poor numerical method that is used extensively in the calculation of the position of damage can have a major influence on the accuracy of the damage detection method. The fact that a poor numerical method can cause a stable damage detection

method to fail can not be over emphasised. Multiple differentiation or integration processes occurring in the majority of the damage detection methods tend to magnify the slight inaccuracies, each time the process is repeated. A more stable numerical method that can be used, to calculate the second derivative, is to fit a curve to the discrete data and then calculating the second derivative algebraically. The entire damage detection method functions on the basis of manipulation of discrete values. The software used to program the damage detection methods, MATLAB, allows both algebraic and discrete mathematical manipulation. After the second derivative functions have been algebraically calculated, it is necessary to calculate discrete values from the functions, for further calculations. Obviously the method used for curve fitting should be accurate if the above mentioned route is to be followed.

The Cubic spline interpolation method was chosen to obtain the curve fit from the discrete data points. This method is well known for its application as an interpolation. method. The oscillating nature of high degree polynomials and the property that a fluctuation over a small portion of the interval can induce large fluctuations over the entire range, does not pose a problem to the Cubic spline interpolation method. The method's approach is to divide the interval of the discrete curve into a collection of subintervals. A (generally) different approximating polynomial is fitted on each subinterval. Approximation by functions of this type is called piecewise polynomial approximations. The simplest piecewise polynomial approximation is a piecewise linear interpolation, which consists of joining a set of data points by a series of straight lines. To obtain a function that is continuous and second order differentiable on an interval, it is necessary to make use of minimum cubic polynomials. The need remains to specify the boundary conditions (3.2.7), because not enough information exists to generate the angle of the curve at the boundaries automatically. Two types of boundary conditions can be specified namely natural boundary conditions and free boundary conditions. The natural boundary conditions gives the shape that a long flexible rod would assume if it were forced to go through each of the data points. For the free boundary condition it is necessary to either have the value of the derivative at each curve end or an accurate

approximation of it. For the damage detection method's formulation, the natural boundary conditions were used. It was chosen because of its practicality for the large numbers of times the method is used in the program.

To calculate the damage position the *Damage index method* makes use of integration over a single element, as well as over the elements along the entire length of the structure (2.5). For this purpose the Trapezoidal rule (Mathews, 1987) of numerical integration was used because of the ease of the application thereof to both single elements as well as all the elements over the length of the beam. The accuracy of the integration process was improved by using cubic spline interpolation to increase the discrete data points from eleven points to five hundred and one points. Other than integration, the Damage index method also makes use of double differentiation. The cubic spline based method developed for the differentiation process in the Combined curvature motion shape method was also used to obtain double differentiation in this method.

4.3 Validity of modelled damage

Six nodes (five elements) were chosen between each two measuring points, to better model the saw cut damage on a 0.08m element. In this section the amount of change in the damage location position between two measuring points, for each of the five elements (i.e. five tests in one), will be investigated. Each of the three damage detection methods were tested to determine what influence moving the damaged element between measuring points 4 and 5, would have on the resulting damage location position. The five results for each damage detection method are presented in 3D plots, containing five graphs (one for each damaged element). The first graph on the 3D plots (in front), represents damage closest to measuring point 4, while the last graph on the plot represents damage closest to point 5. To better represent the results, a second plot is presented with a different viewing angle on the 3D plot.

The results of the *Flexibility difference method* (Figures 4.1 and 4.2) indicate a gradual movement of the location of damage, as can be expected for the different modelled damage positions. It is important to focus on the change in gradient in the line, if there is a gradient change to be able to pinpoint the indicated position of damage. Damage position indication at measurement point no.4 and 5 is clear and effective. The slight curve of the lines in between the two measurement points makes exact damage position location difficult. Bending in the graph is probably due to the damage detection method that uses the values obtained at the measurement points to do all the damage indication calculations. Consequently the methods ability to indicate damage is better at the measurement points.

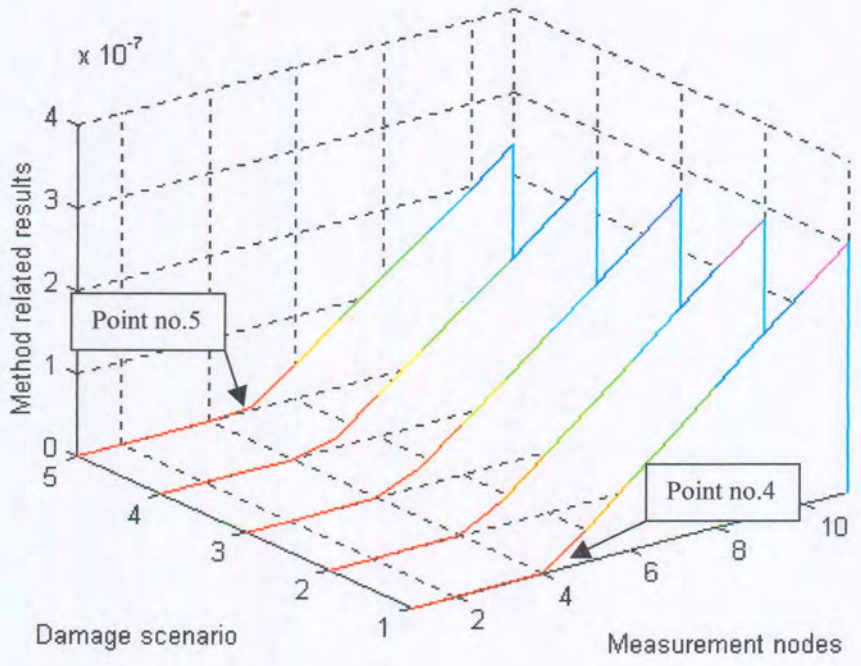

Figure 4.1 Damage detection between point 4 and 5 using the Flexibility difference method.

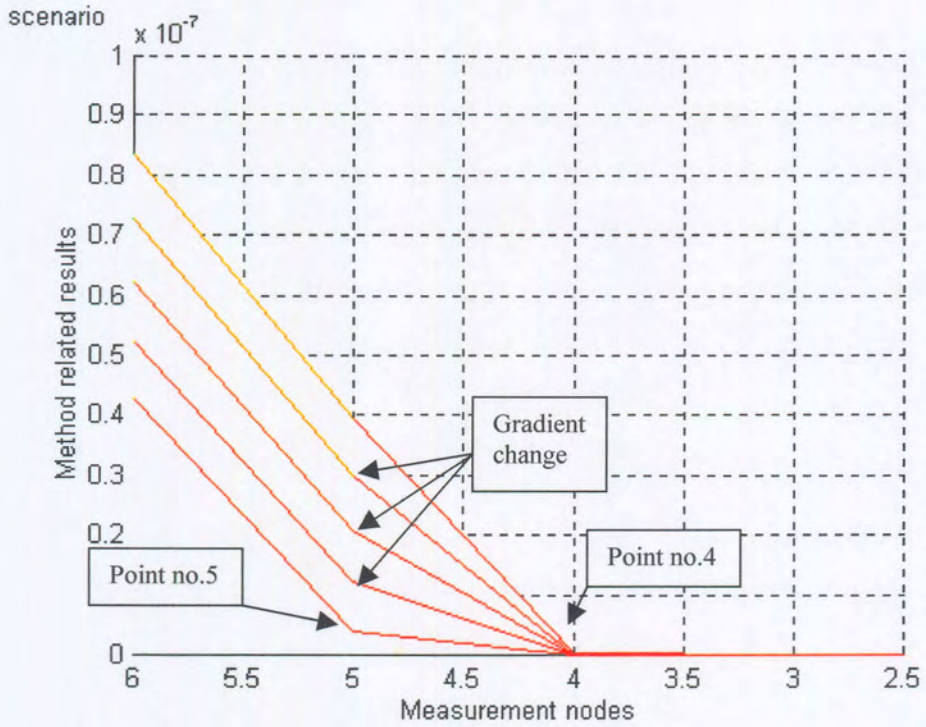

Figure 4.2 2D zoom in plot of Figure 4.1

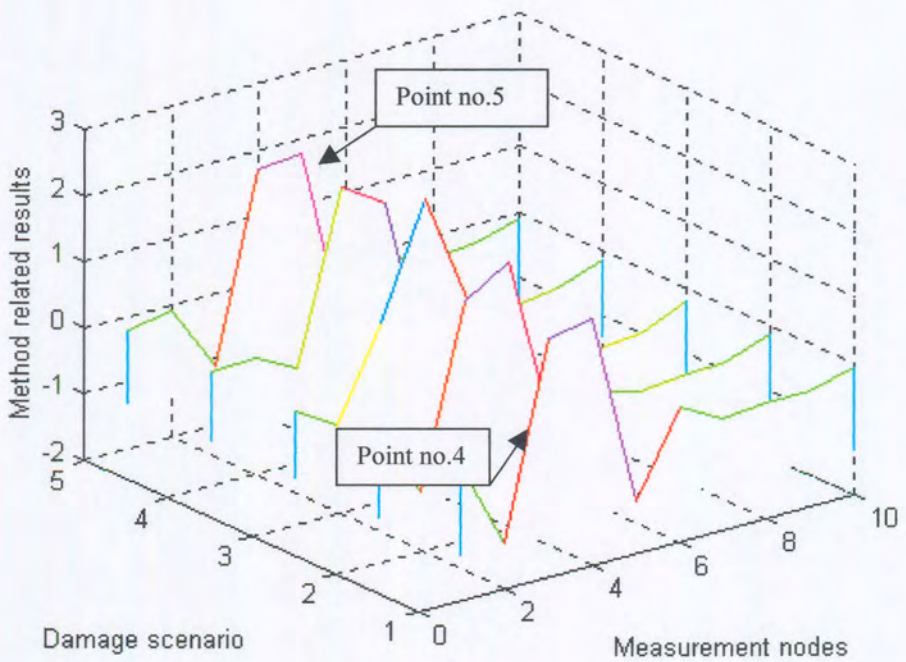

Figure 4.3 Damage detection between point 4 and 5 using the Damage index method.

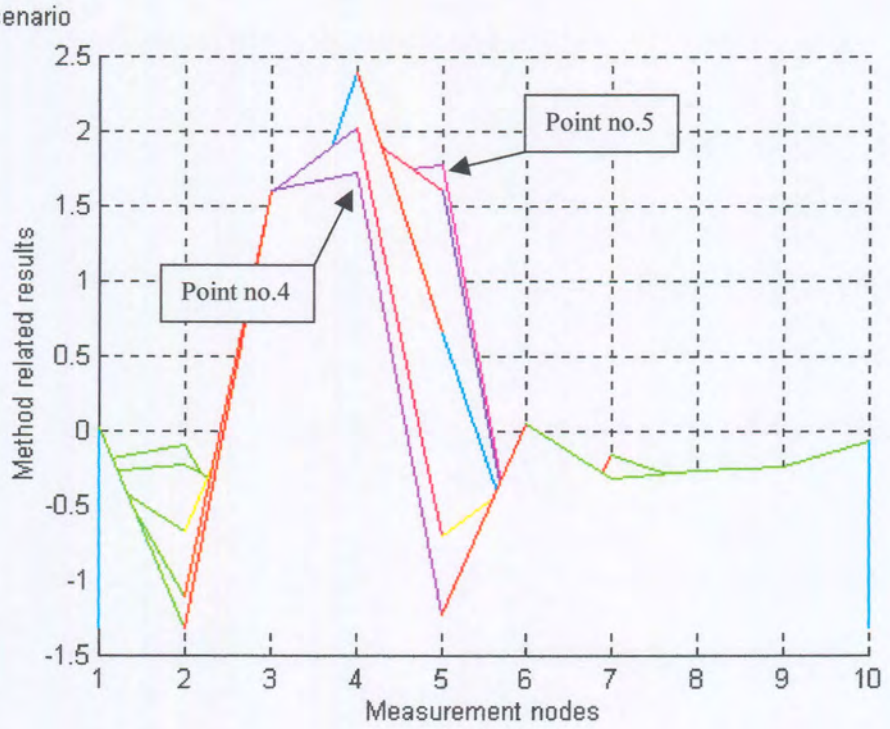

Figure 4.4 2D plot of Figure 4.3.

The results of the *Damage index method* (Figure 4.4) gives a clear indication of the position of damage. Figure 4.3 indicates a gradual movement of the second highest point in each graph from left to right. The second highest point indicates gradual shifting in the position of damage. Different from the *Flexibility difference method*, it seems that the best damage position indication is between two measurement points.(Figure 4.4)

The damage position results for the *Combined motion shape method* is presented in Figure 4.5. Figure 4.6 indicates that damaged position remains between the fourth and fifth measurement points. Unfortunately the damage is indicated in the opposite direction than expected, if the highest peak is taken into consideration.

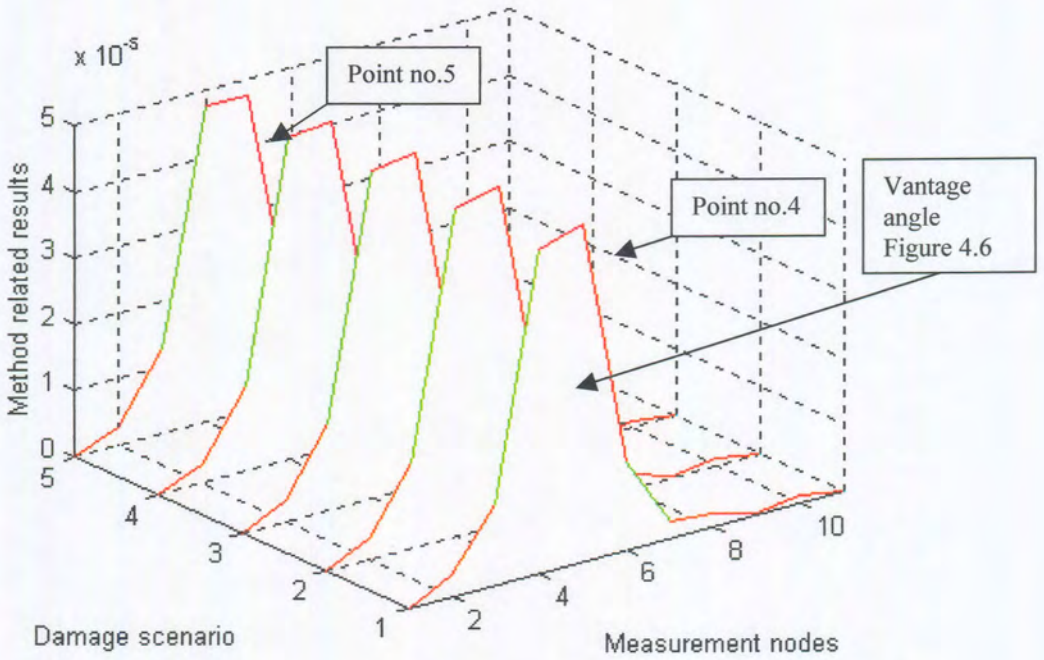

Figure 4.5 Damage detection between point 4 and 5 using the combined mode shape method

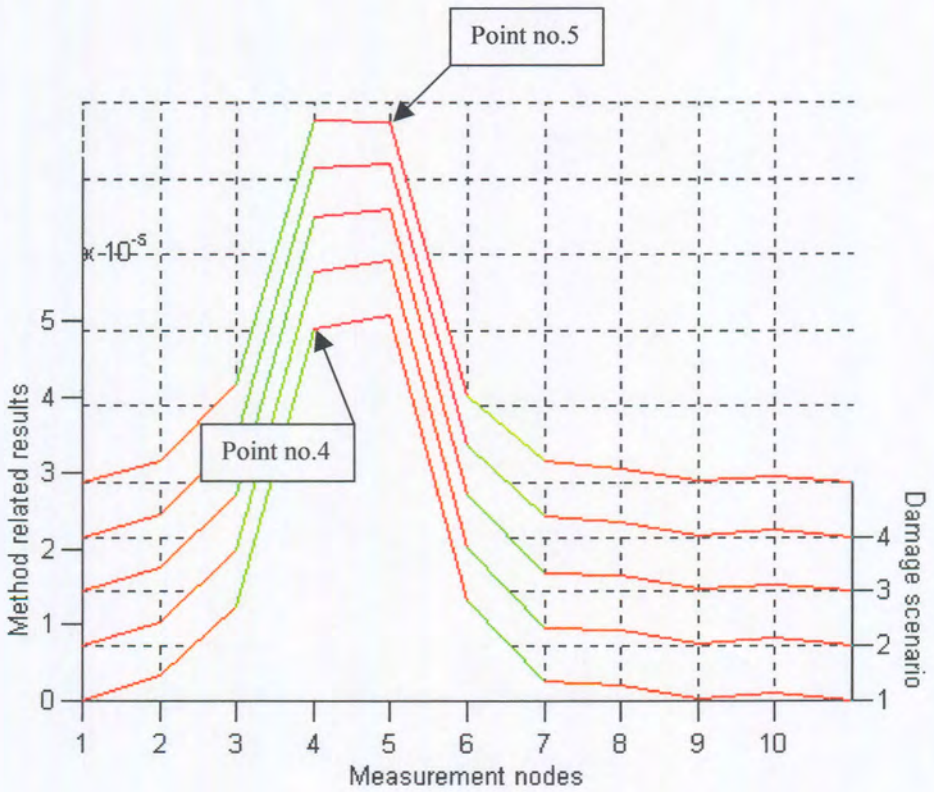

Figure 4.6 Different point of view as shown on Figure 4.5.

For all three methods tested, the position of damage remained between the two measurement points. In the following work, damage will be modelled in the centre element, because the centre position of modelled damage gives a stable damage indication result for all the methods tested.

4.4 Comparing accuracy and sensitivity of the different methods

In this section the ability of the three damage detection methods to detect damage anywhere in the damaged system will be tested and compared. The influence of boundary conditions on the detection ability of these methods will also be investigated.

4.4.1 Damage location

Since the main purpose of a damage detection method is to provide early warning regarding the presence of damage in a system the most important test will be to evaluate the ability of the various damage detection methods to locate damage spread over the length of a beam. In an effort to model damage more accurately the beam was divided into fifty elements. Eleven measuring points with five elements between each measuring point was modelled. For test data generation, the modulus of elasticity of ten different elements was reduced one by one to give ten different, but similar regarding the degree of damage scenarios. Each of the ten chosen elements were situated halfway between two different measuring points. This was done to test each method's ability to detect damage at any position throughout the system. A cantilever beam will be considered. For the first scenario, one percent damage was introduced in the centre element between the first two measuring points, leaving the rest of the structure undamaged. For the next scenario, one percent damage was introduced in the centre element between the second and third measuring points. This procedure was repeated stepwise progressing through the beam. As stated above, the position of damage for each damage scenario will be detected by the application of a specific damage detection method. The output given by a damage detection method investigating a single damage scenario, is ten numbers (Damage detection parameters). The ten damage detection parameters, for each specific damage scenario, represents the length of the beam and depending on the method applied, should

be evaluated in a specific way to pinpoint the position of damage. For two of the methods under consideration, the position of damage is given by the beam position related to the largest of the ten detection parameters. For the other method used the slope of the curve formed by the detection parameters is used to evaluate the position of damage. If the detected position of damage is similar or close to the modelled damage position, the method would prove effective. The results of the above mentioned tests will be presented as follow. A full test series of ten damage scenarios (equal in severity), will be presented in the form of three 3D plots, (Figure 4.7, Figure 4.9 and Figure 4.11) each representing the results of a different damage detection method. Ten curves, each consisting of ten damage detection parameters, will be presented on the 3D plot. The position where the damage will be modelled is different for each curve on the 3D plot. For the first scenario the damage model location will be between the fixed point and the first measuring position. In the second scenario (curve second from the front) the damage will be modelled between the first and the second measuring point. The other damaged cases will follow progressively through the system. By presenting the results on a 3D plot, it will possible to compare the damage detection ability of all the methods throughout the length of the beam, though it might still look confusing. It should be kept in mind that in practice the damage detection method will only produce one curve consisting of ten damage parameters. An adjusted view of the 3D plot will be presented for each method's results to simplify the evaluation. If the trend seen in Figure 4.8 is followed, which suggest that the bend in the graph indicate the position of damage, all of the damage scenarios is indicated to move one position forward. From scenario number seven and on recognising the exact damage location is more difficult because of the change in angle of the damage location graph.

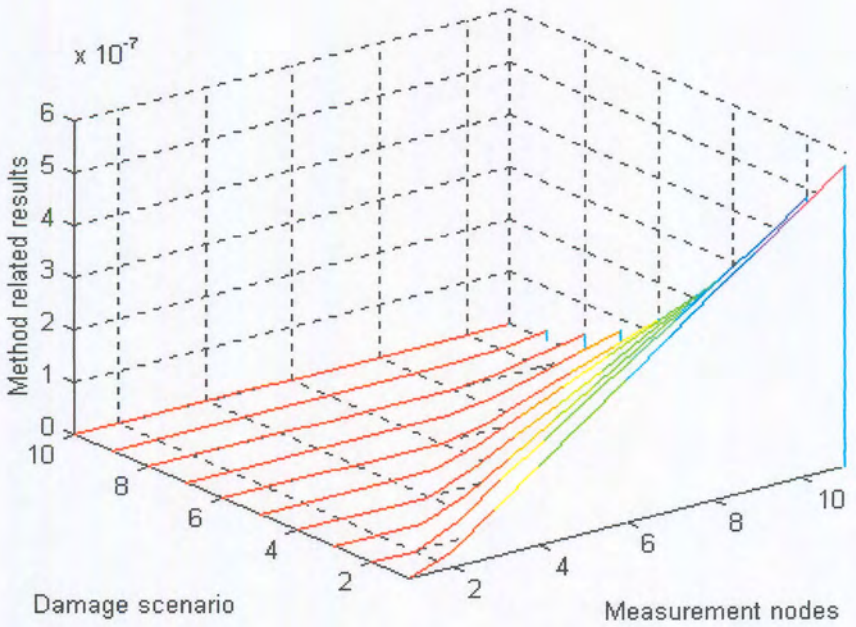

Figure 4.7 Damage location using the Flexibility difference method

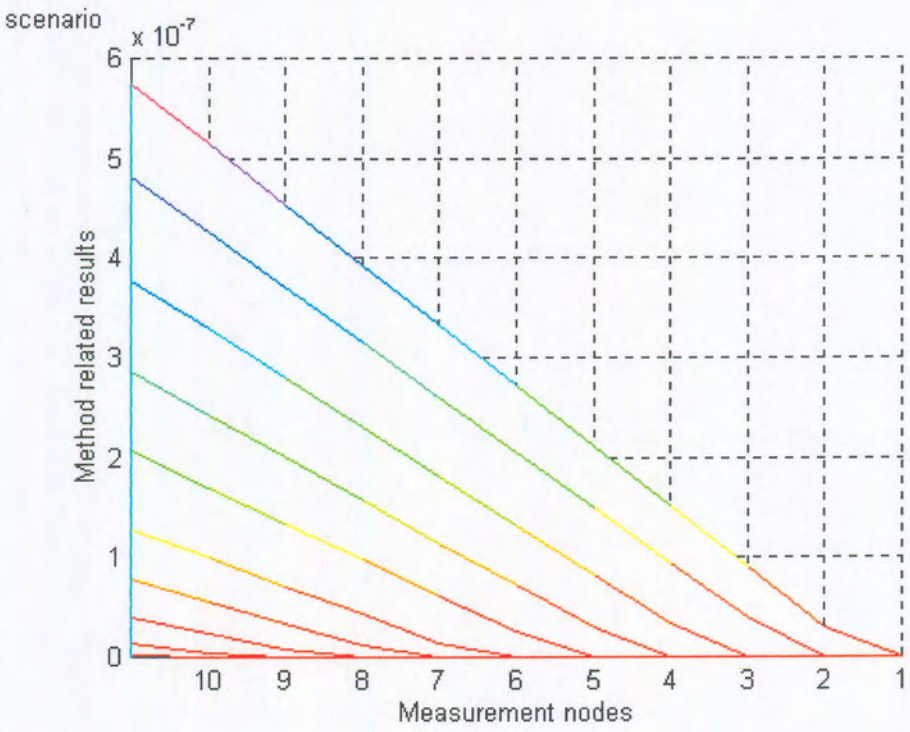

Figure 4.8 2D plot of Figure 4.7.

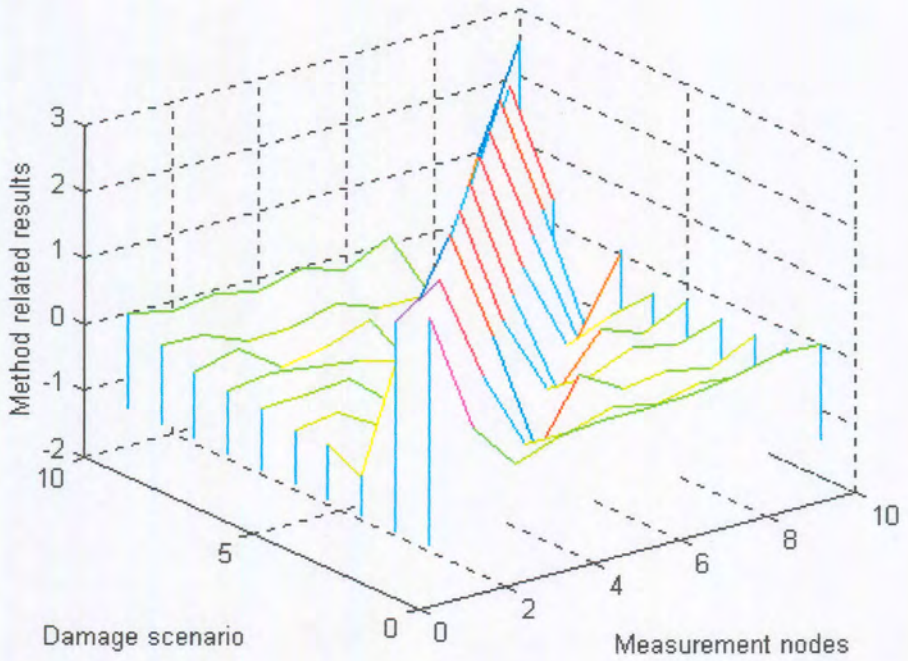

Figure 4.9 Damage location using Damage index method

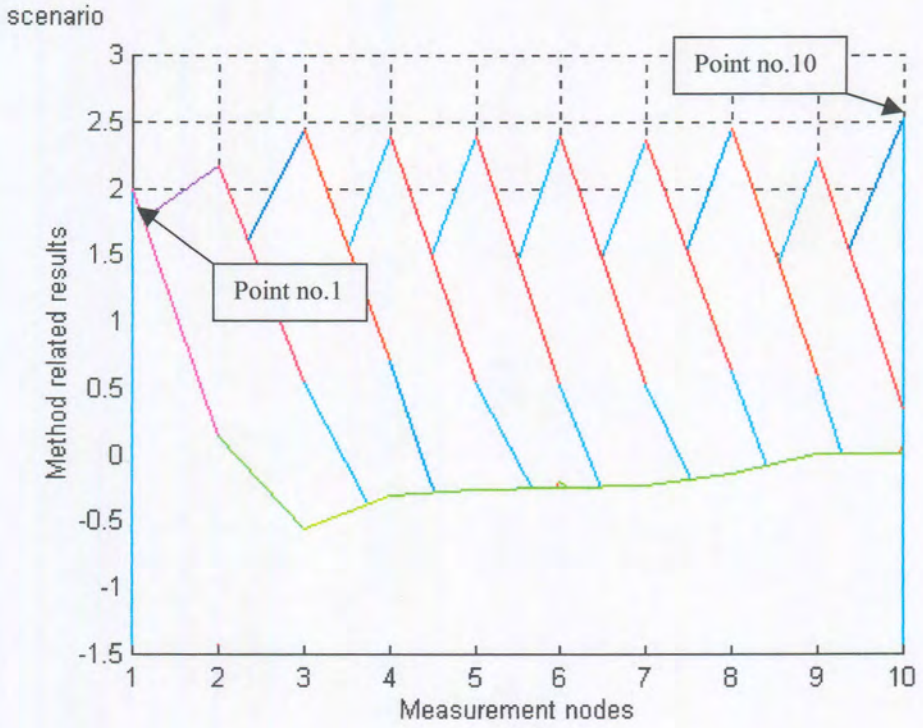

Figure 4.10 2D plot of Figure 4.9.

The *Damage index method* results illustrated in Figure 4.9 and 4.10 show excellent damage position detection ability. The location of damage is clear, exact and distinct. Tests where undertaken were the amount of points used for the integration process were gradually increased from the original eleven measured points to five hundred and one points. The second peak, peaking at point no.2 steadily sharpened as the integration points increased. The rest of the graph though remained unchanged.

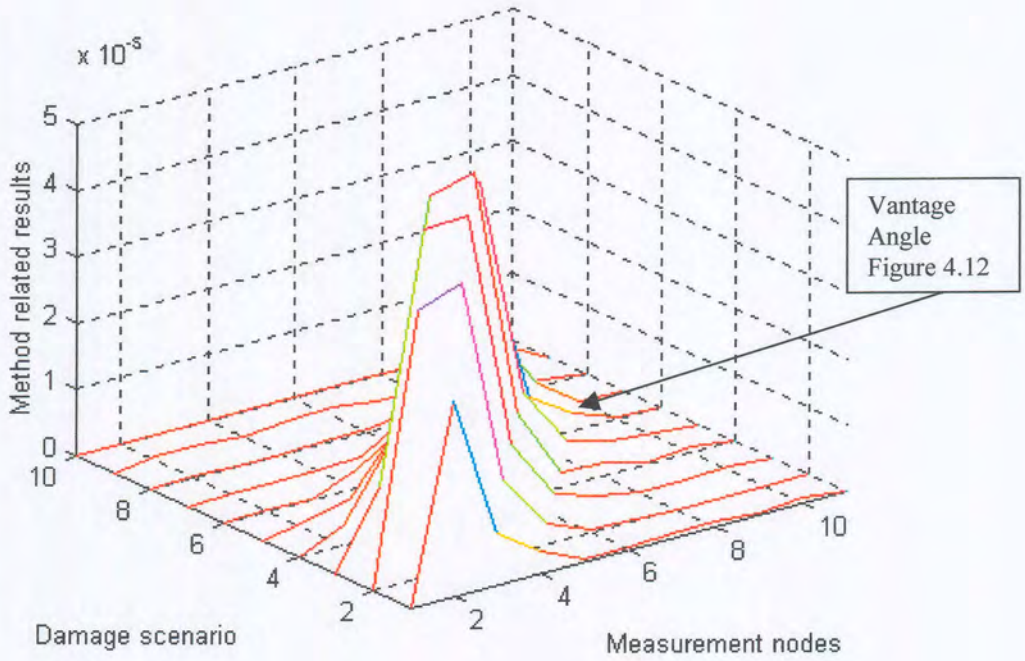

Figure 4.11 Damage location using Combined curvature motion shape method

From Figures 4.11 and 4.12 which illustrating the *Combined curvature motion shape's* ability to detect damage, it is evident that the method suffers from similar problems as the *Flexibility difference method.* The position of damage is shifted one position to the right compared to the modelled damage position. Similar to the *Flexibility difference method*, damage detection from scenario number 8 onwards becomes more difficult. Damage indication from scenario number 8 does indicate accurate damage position though.

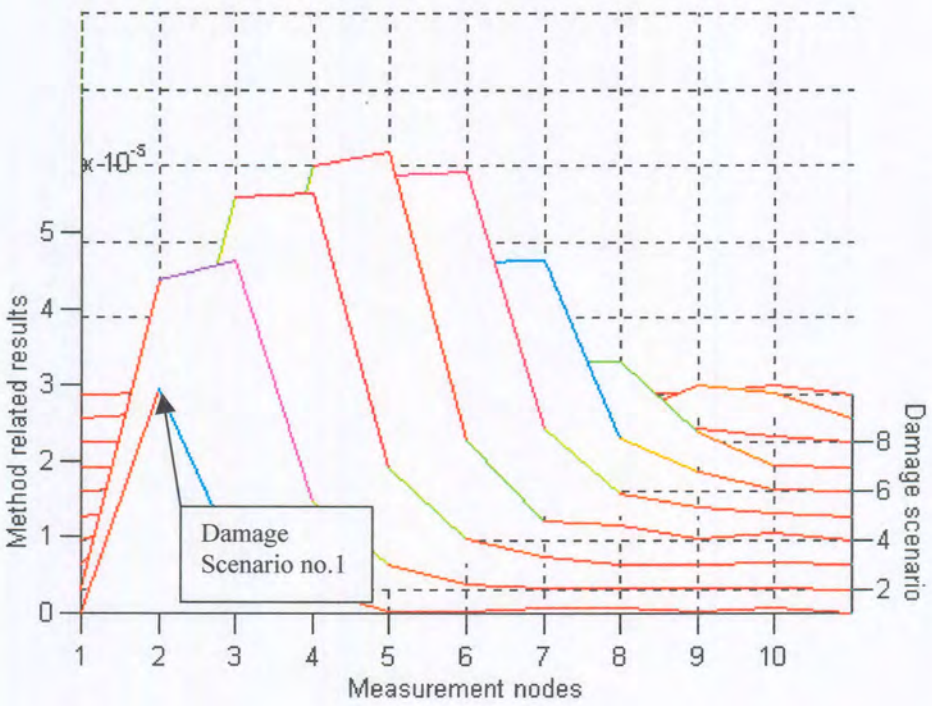

Figure 4.12.Different point of view on Figure 4.11.

It is evident from the results of the tests done, that the *Damage index method* is the most effective method where the indication of damage anywhere on a cantilever beam is concerned. The other two damage detection methods share similar disadvantages, like a slightly inaccurate damage position indication in some cases, which is not experienced by the *Damage index method*.

4.4.2 Different support configurations

It should be noted from the literature survey that when the boundary conditions were changed using the *Flexibility differance method*, a lack of consistency was observed in the way damage position was detected (Panday & Biswas, 1995). When the *Flexibility differance method* was used to detect damage on a cantilever beam, the position of damage was given by the position where the damage detection curve began to slope (Figure 4.7). When the method was used to detect damage on a simply supported beam,

the position of damage was given by the position of the largest damage detection parameter. Until now all the tests performed were done on a cantilever supported beam model. For the following tests the influence of a different structural support method will be evaluated. These tests were undertaken to determine if the other methods used (both mode shape based) would reveal the same characteristics. It should be kept in mind that the application of a damage detection method results in only one damage detection curve. If the method being used has a tendency to be dependant on the support configuration, the user should be aware of it to be able to correctly identify the position of damage. The influence of progressive damage on a beam pinned at both ends and analysed by each of the three damage detection methods will be investigated. Three 3D graphs showing each of the methods ability to detect ten percent damage throughout the structure, will be presented. The results of the pinned beam progressive damage detection will also be presented in from an alternative point of view for better clarity.

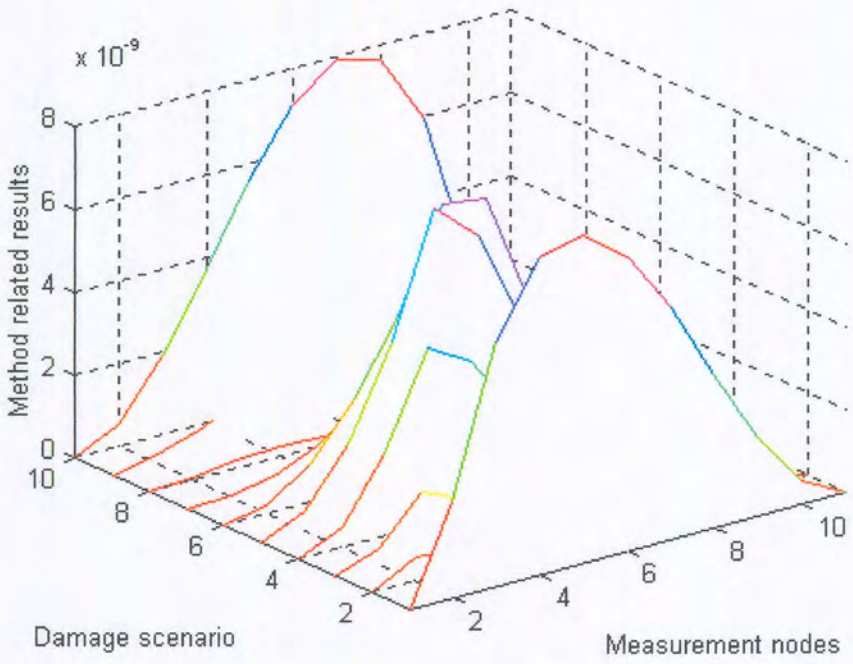

Figure 4.13 Damage detected on pinned beam using the Flexibility method.

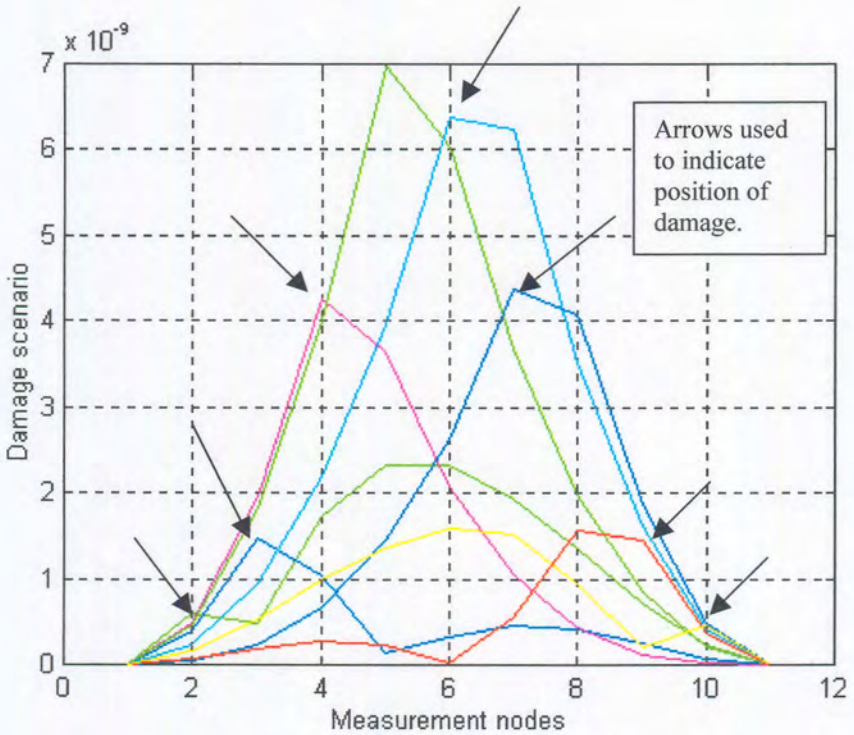

Figure 4.14 . 2D plot of Figure 4.13.

In the 2D plot the first and last scenario, that is obviously inaccurate, has been omitted from Figure 4.14. The remaining scenarios were plotted to illustrate the damage detection ability of the *Flexibility difference method* on a pinned beam between the pinned sides. When comparing Figure 4.13 with Figure 4.7, where a cantilever beam was modelled, it is evident that the results for the *Flexibility difference method* should be interpreted differently. Compared to the results obtained from the cantilever support model where the position of damage was detected at the position where the graph undergone a gradient change bend, the position of damage is obtained in most cases by finding the position of the largest detection parameter near the centre of the beam. Damage near the centre of the beam is easily detected, but detection becomes more difficult closer to the edges of the beam. Despite the problems mentioned, the method is accurate in the areas where damage is located.

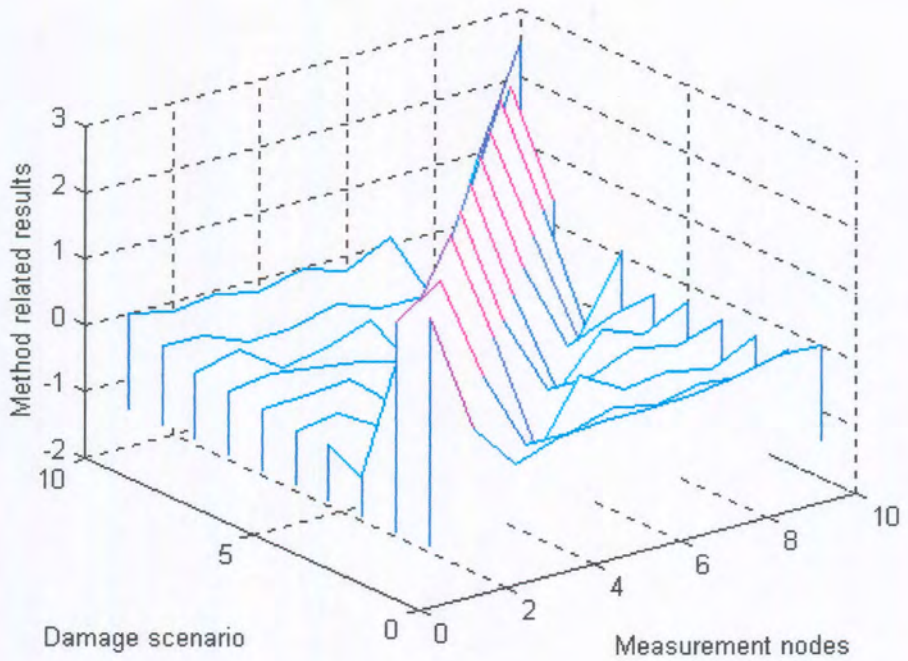

Figure 4.15 Damage detected on pinned beam using the Damage index method

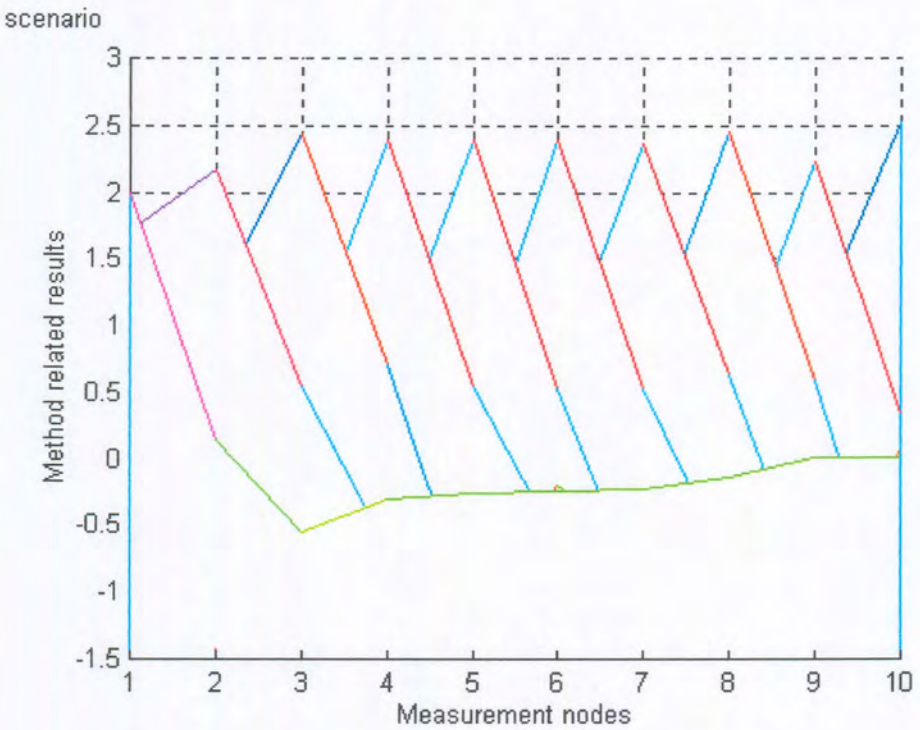

Figure 4.16 2D plot of Figure 4.15.

When comparing Figure 4.15 with Figure 4.9 it is evident that a change of the support configuration had no influence on the *Damage index method's* results. The figures are almost identical. The position of damage in Figure 4.15 can be identified just as easily as in Figure 4.9. The damage detection ability of the method remains impressive.

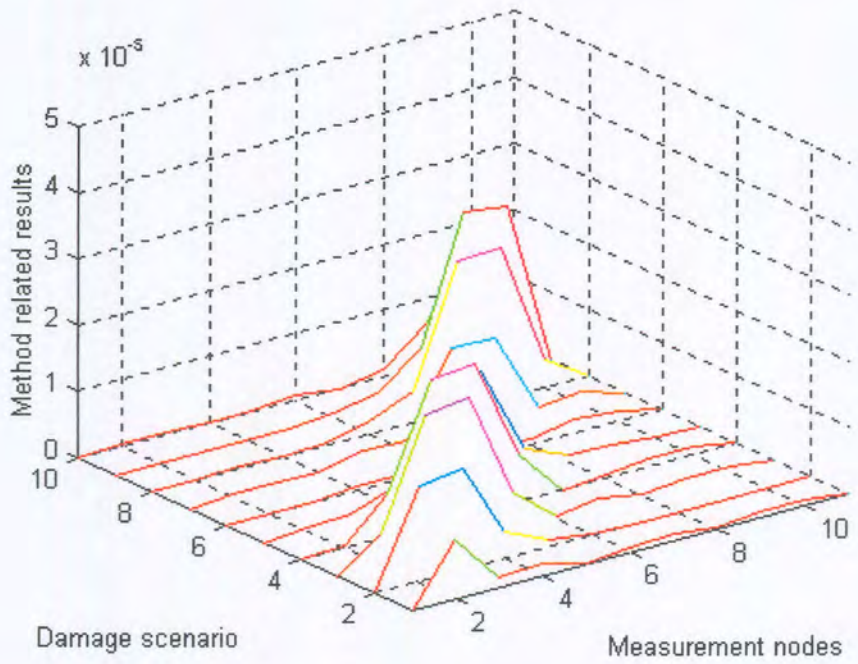

Figure 4.17 Damage detected on pinned beam using the Combined motion shape method

Comparing Figure 4.17 with Figure 4.11 it seems that a change in the support configuration has increased the damage detection ability of the *Combined motion shape method.* The position of damage is still located by identifying the position of the largest peak. The way in which damage is indicated has not changed. Damage detection up to the centre of the beam is out by one position (Figure 4.18) if the slopes of the peaks are taken as an indication of where damage is located. From the centre of the beam onwards, the position of damage is indicated correctly. Comparing Figure 4.18 to its counterpart where the cantilever damage was modelled, (Figure 4.12) the damage indication peaks seem to follow a parabolic pattern away from the pinned support configuration. In Figure 4.18 two parabolic figures can be seen clearly.

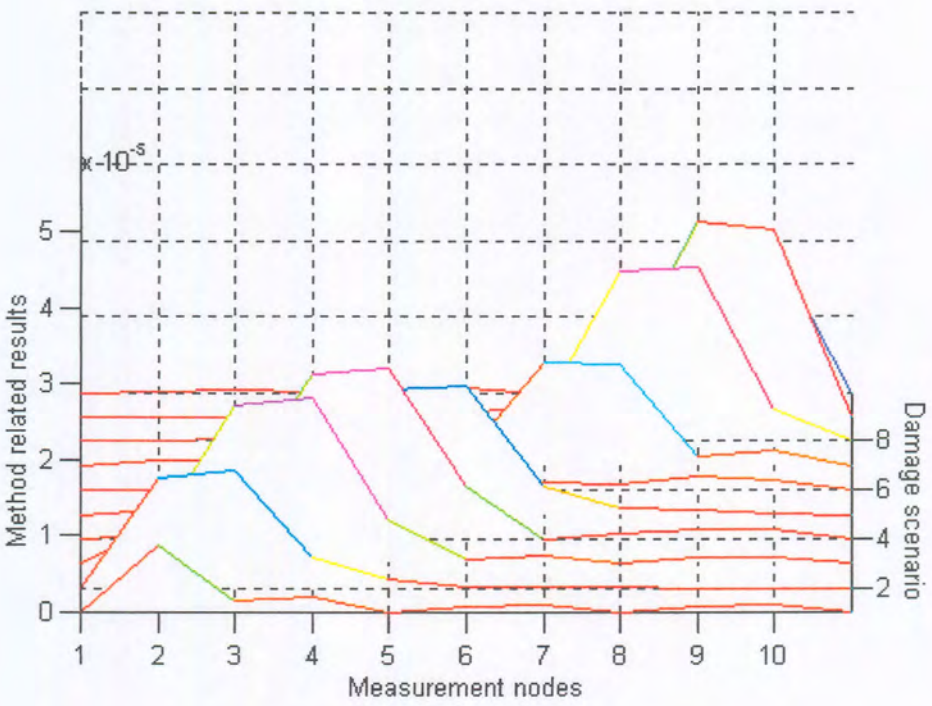

Figure 4.18 Different point of view on Figure 4.17.

4.5 Multiple damage location

It is a well-known fact from the literature (Jauregui & Farrar, 1996) that methods based on mode shapes have difficulty in detecting multiple damage. To test if the newly developed method will also experience difficulty, the ability of all the methods to detect multiple damage will be tested. Tests will be conducted using cantilever beams. Damage will be simulated at two locations. One damage location will be kept constant in element number six while the other location will be varied through the length of the beam. Two damaged cases will be modelled except at the point were the veritable damage and the static damage is equal at point number six.

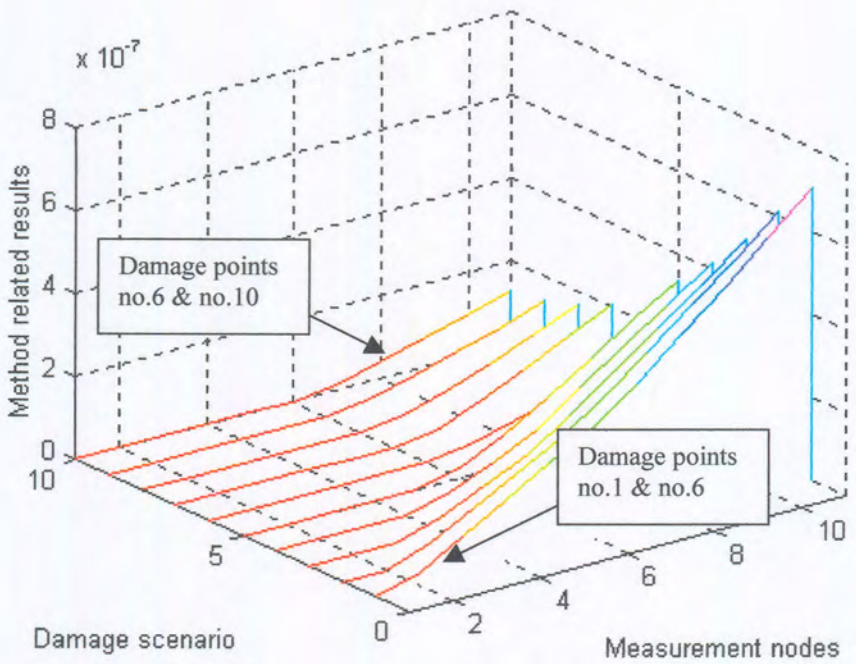

Figure 4.19 Multiple damage using the Flexibility method

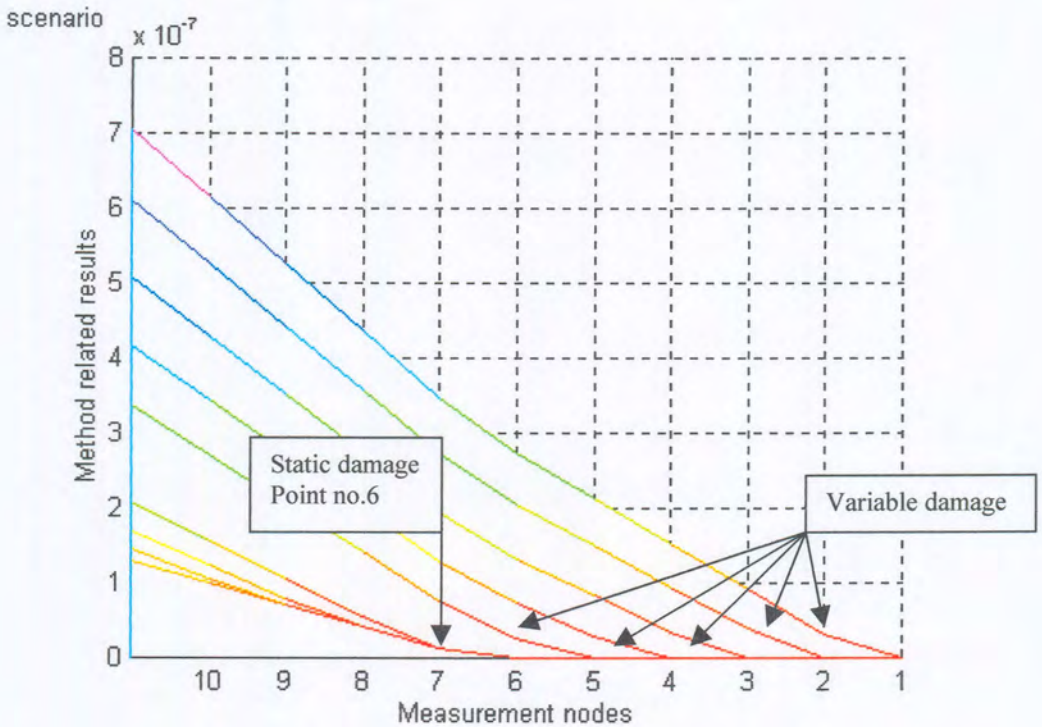

Figure 4.20 2D plot of Figure 4.19

The *Flexibility difference method* (Figure 4.19 and Figure 4.20) indicates the stationary point of damage at measuring point number six, but only after the variable damage position has passed the stationary position of damage. After the variable damage position has passed the static damage position, the variable damage can not be detected. It is clear that the *Flexibility difference method* is only capable of indicating a single position of damage. The position that is indicated, is for the damage position closest to the cantilever support.

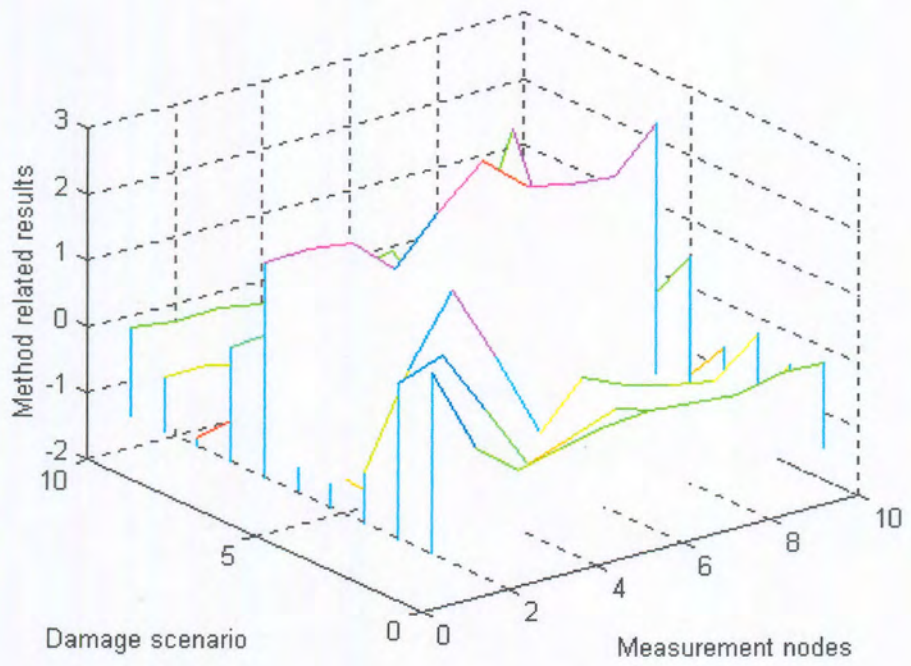

Figure 4.21. Multiple damage using the Damage index method.

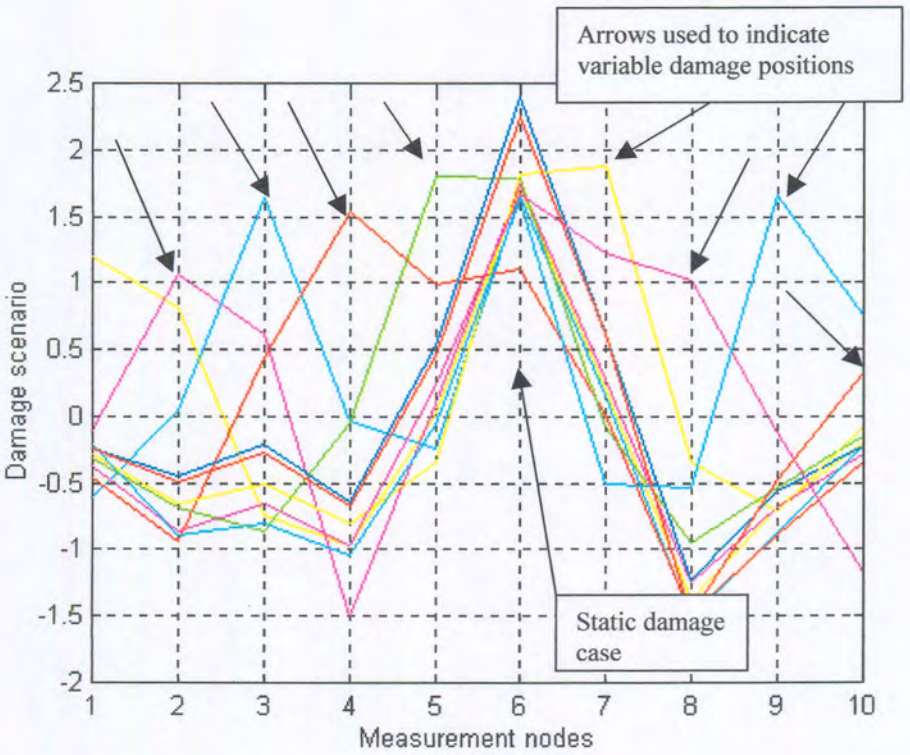

Figure 4.22 2D plot of Figure 4.21.

Figure 4.22 clearly illustrates that the *Damage index method* is capable of identifying two damaged cases. It was necessary to plot all the damage detection graphs on one graph (Figure 4.22) since Figure 4.21 does not illustrate the ability of the Damage detection method to indicate two simultaneous damaged cases. Note that the damaged position at point number one could not be found. The absence of the damage indication could probably be contributed to the cantilever at point number one. All the damage indication graphs identified the static damage point at point number six.

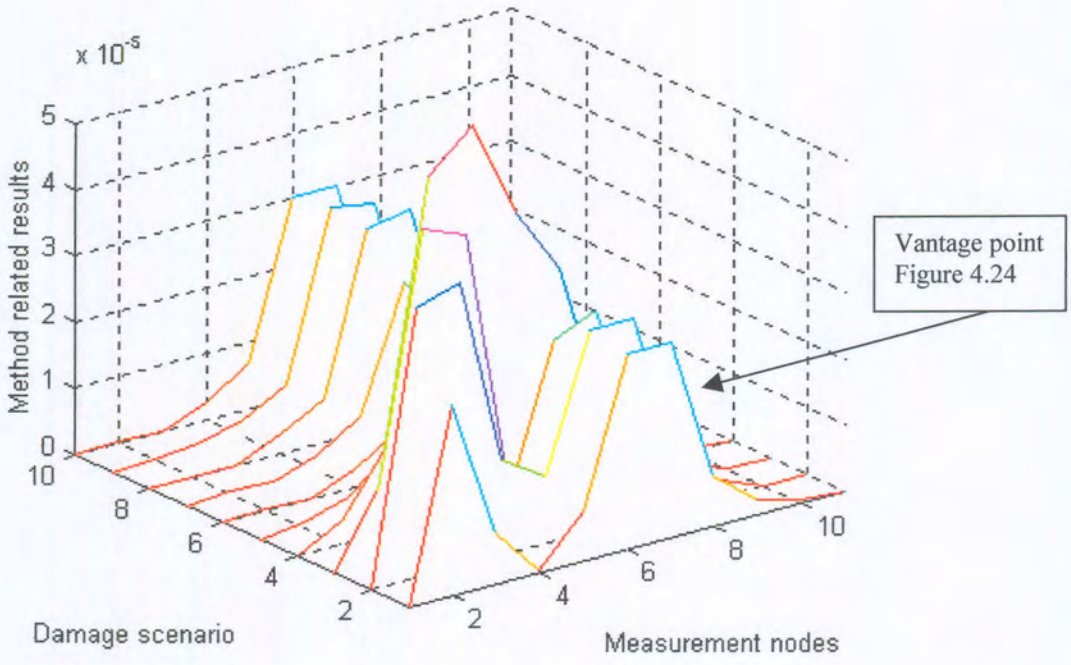

Figure 4.23 Multiple damage using Combined curvature mode shape method.

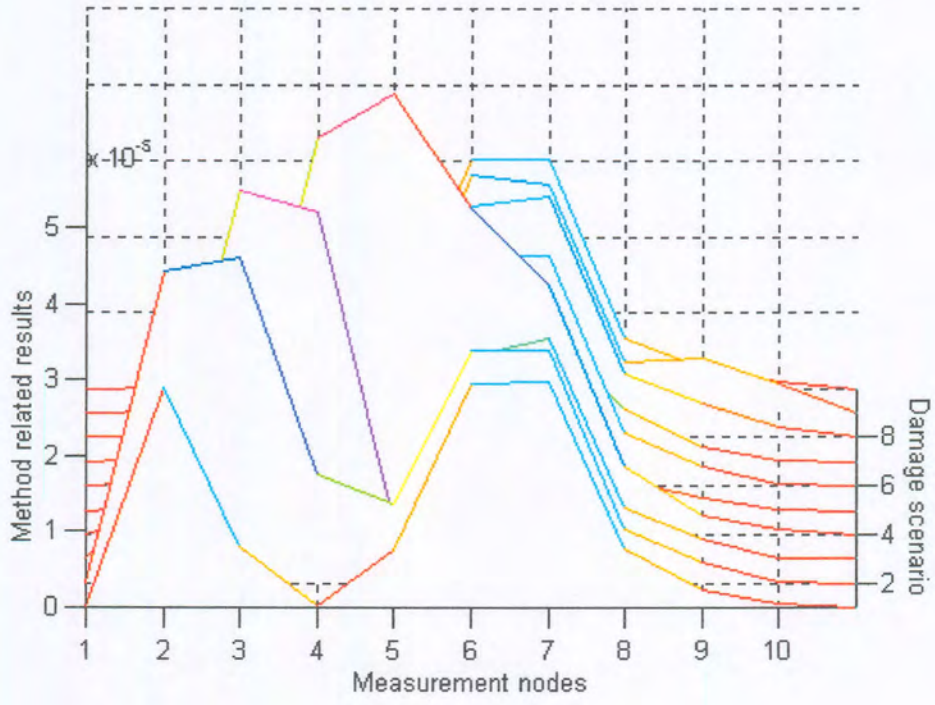

Figure 4.24 Different point of view on Figure 4.23.

It is evident from Figures 4.23 and 4.24. that the *Combined curvature motion shape method* is capable of successfully identifying two damage cases. All the damage indication graphs identify the static damage point at point number six. If the angles at the peaks are taken as an indication of the position of damage, the method sometimes indicates damage one position to the left of where it was modelled.

An earlier comment made on the inability of methods to locate multiple damage (Jauregui & Farrar, 1996) is only accurate in the case of the *Flexibility difference method.* The other two methods tested experienced minimal difficulty in detecting multiple damage. Whether damage could be identified easily if two damaged cases exist near one another will depend on how close the two cases are to each other. It should be noted that whenever a damage identification method is being implemented it would be advisable not to rule out the possibility of multiple damage at an indicated position.

4.6 Evaluation of different methods

A method performing well with numerical data will not necessarily ensure that the method will be able to give good results when measured data is used. Numerical testing does however give a good indication of what could be expected of a method under specific conditions.

A system of grading the damage detection methods on the numeric tests performed, has been devised. Four stars will be awarded to a damage detection method if all the damage cases were correctly detected or for excellent stability in the case of support configuration influence. Three stars will be awarded if all of the damaged locations are in close proximity of the modelled position. In the case of support configuration influence, tree stars will be awarded if influence is noticeable, but the technique of damage detection remains unchanged and accurate. Two stars will be awarded if less than fifty percent of the damage cases can be detected in close proximity of the modelled position. In the case

of support configuration influence, two stars will be awarded if the technique of damage detection changes but remains accurate. One star will be awarded for poor performance.

Table 4.1 Evaluation of different methods.

Numerical test	Damage index method	Flexibility difference method	Combined curvature motion shape method
Variable damage location	****	***	***
Consistency despite support configuration	****	**	***
Multiple damage detection	****	*	***

5 Experimental investigation

In this chapter experimental verification of the three damage detection methods will be undertaken. To obtain quality experimental data proved to be an extremely difficult task. On three different occasions the experimental setup had to be changed completely. Interference in the data, caused by the vibration response of the test beam clamping system, lead to an evolution in the experimental testing process, giving progressively improved measured data. In a process where any variation in data between the damaged and undamaged beam is exclusively contributed to the occurrence of damage and used to locate damage, good quality data is of the utmost importance. The final data used for experimental verification, although of greatly improved quality, is still far from perfect. To compensate for the lack of quality in measured data in practice, modal analysis is used to fit a curve to the data. Unlike the *Damage index* and the *Flexibility difference methods*, the new method does not make use of modal analysis. Because of the difficulty of obtaining good quality data, a more robust method of damage detection will be of great value.

5.1 Experimental set-up

Experimental data was obtained from a cantilever beam in the damaged and undamaged state. Damage was introduced in the form of a saw cut over the width of the beams between measuring point number four and five. The depth of the cut reached ±30 % into the beam. Aluminium beams of length 960 mm, width 31 mm and depth 9.5 mm were used. The beam was divided into twelve, 80 mm elements of which two were clamped in a clamp designed and built to provide a solid cantilever beam. Excitation was provided at the seventh measuring position by a Vibropet electromagnetic exciter, driven by a Rotel audio amplifier. Excitation signal generation as well as data gathering was done using a DSP Technology Siglab analyser, a piezoelectric PCB load cell and a 10 mV/g accelerometer. PCB 480B units were used to power the transducers and for noise reduction (Figure 5.1). Data was gathered on a laptop computer and converted for further

analysis in Matlab. Modal analysis was performed using the Scientific Software *Structural Dynamic Toolbox*. Plots of the frequency response data gathered is given in Appendix C. More pictures of the equipment used to obtain experimental data can be found in Appendix B.

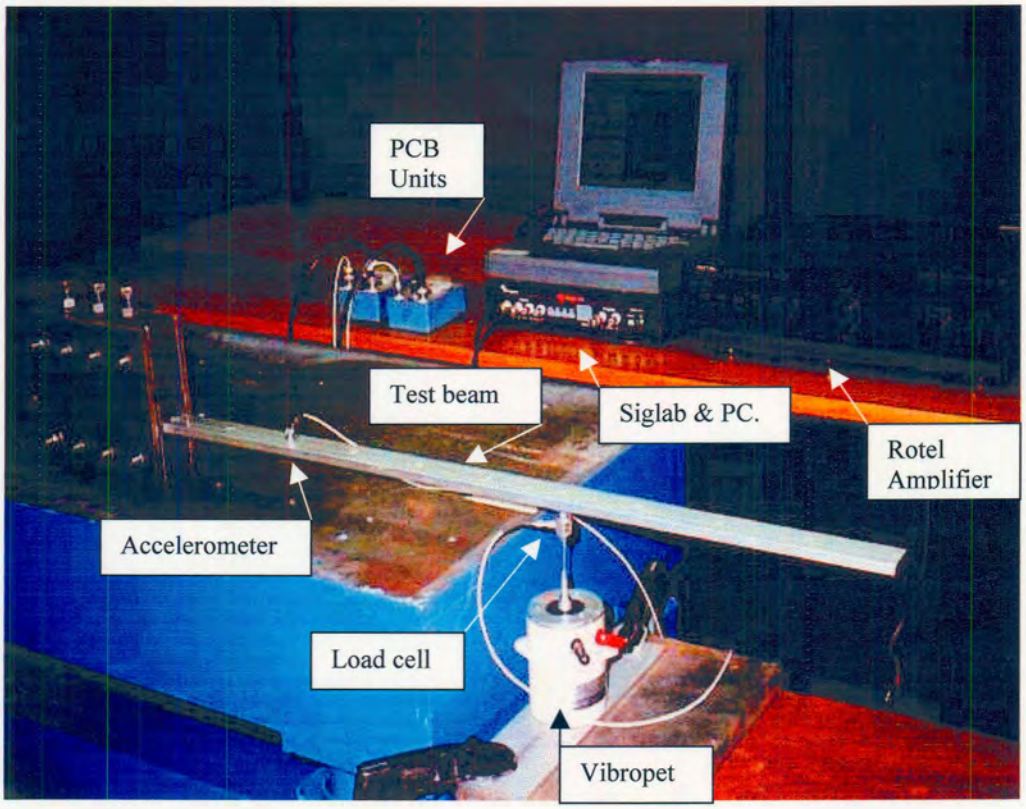

Figure 5.1 Experimental setup.

5.2 Experimental data quality

Figure 5.2 is a typical example of the experimental data gathered. Low frequency noise is present in the data. The noise is consistent in all the FRFs throughout the damaged and undamaged states. The cause of the fluctuation in the data can be contributed mainly to two factors. The first is the vibration interference of the base plate on which the clamping system was mounted and the other is the inability of the Rotel audio amplifier used to effectively amplify low frequencies used for excitation.

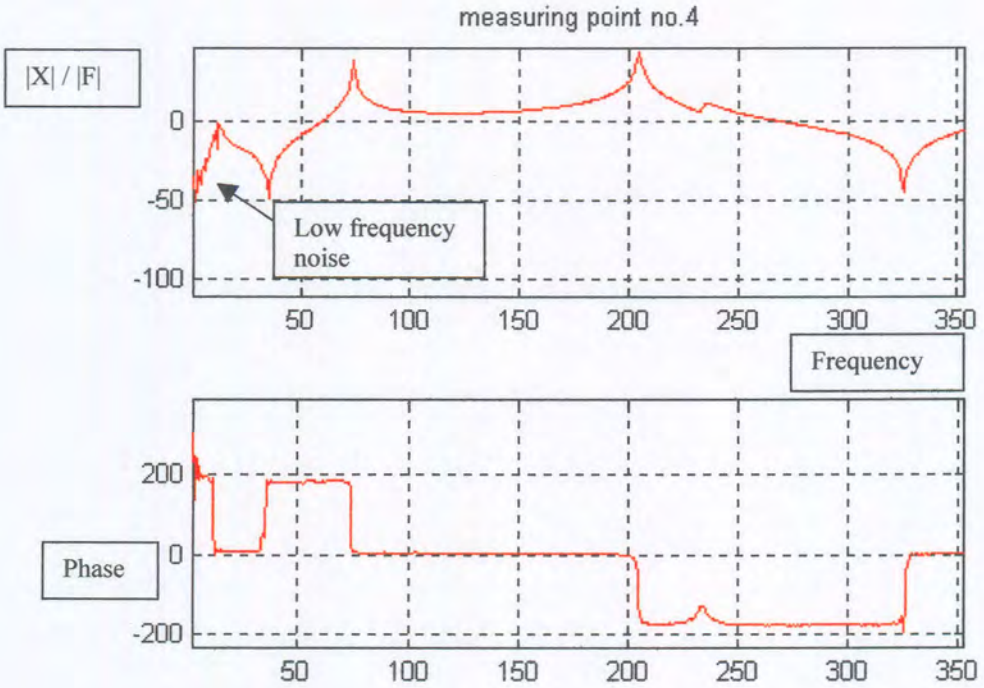

Figure 5.2 Example of experimental data.

Low frequency noise will be omitted before analysis is done. Ignoring low frequency noise, is common practice in the field of vibration. Modal analysis is complicated by excessive low frequency noise. When the modal analysis was done, data close up to the first peak was ignored. It is important to include the first peak of the FRFs to be able to calculate the first mode shape successfully. The accelerometer was attached to the beam using beeswax. Other methods of attaching the accelerometer to the test system is by cemented stud, magnet or the hand held method (Ewins, 1984). Not wishing to damage the structure or add too much weight to it, a lightweight accelerometer was fixed to the beam using bees wax. The load cell on the other hand was fastened to the beam by using a copper stud. The stud served a dual purpose. Firstly it connected the load cell to the beam and secondly excitation was transferred to the beam via the stud. Excitation was done by means of a drive-rod assembly (stinger) (Figure 5.1). The stinger is a thin flexible connection with sufficient stiffness to transfer axial forces to the beam, but is capable of bending to keep moment transfer to a minimum. Despite all the precautions and experimental setup changes, the modal analysis process proved to be extremely

difficult. The fact that near perfect experimental conditions compared with general conditions in practice, still caused difficult modal analysis, should indicate the sensitivity of the modal analysis process. An example of a curve fit used can be seen in Appendix C. Invariably the *Damage index* and *Flexibility difference methods* will be influenced by the results of the modal analysis.

5.3 Comparing damage detection ability of the different methods

In this section the methods that were evaluated numerically in the previous chapter are tested using the experimental data gathered. The same experimental data was used for all the damage detection methods under consideration. Modal analysis was done on the experimental data in order to provide the *Flexibility difference* and the *Damage index method* with mode shapes. Copies of the programs used are presented in Appendix A. The raw data was fed straight into the *Combined curvature motion shape method* to obtain damage indication results.

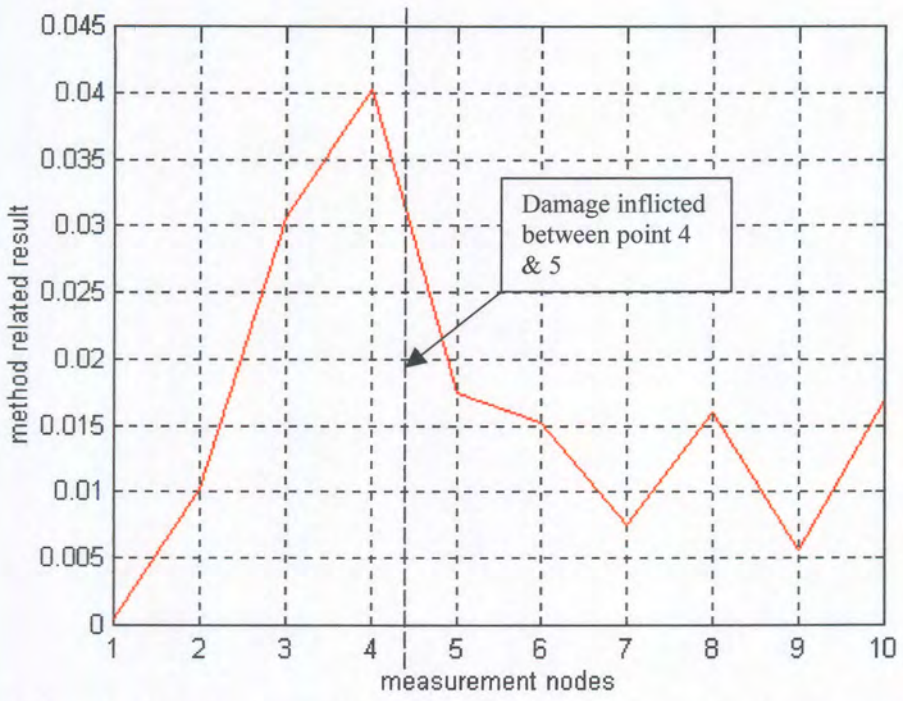

Figure 5.3 Damage detection using the Flexibility difference method on experimental data.

The damage detection result of the *Flexibility difference method* on the experimental data is somewhat unexpected. Looking at the numerical test results it would be expected to see a change in curvature at the point were damage was inflicted. The *Flexibility difference method* applied to a damaged cantilever beam (Figure 4.1) indicates the position of damage at the position where the curve changes. The experimental results indicate the correct position of damage, but not as expected. The results of Figure 5.3 follows the model Figure 4.13, where a pinned damaged beam was numerically modeled. In the case of the pinned beam the damage location was indicated by the maximum value on the curve. The result indicates the methods sensitivity towards modal analysis in practice.

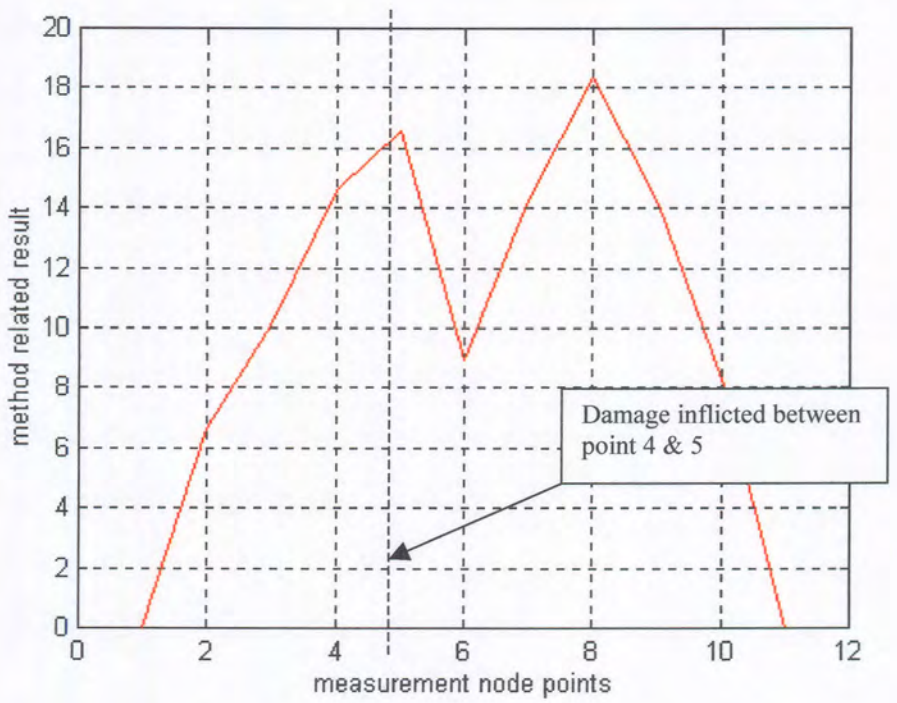

Figure 5.4 Damage detection using the Combined curvature mode shape method on the experimental data.

The result obtained for the *Combined curvature motion shape method* indicate two positions of damage. The first peak indicates the damage at the position where damage was inflicted on the experimental test beam. The second peak is close to the excitation

position at measuring point number seven. It is believed that the stinger which was screwed into the aluminum beam to provide excitation at point number seven, effectively created a point mass at that point. The stinger was manufactured by soldering two screws on both sides of a flexible rod, to provide a solid link between the beam and the load cell. A point mass was created because providing the right height for the vibrator to ensure that it does not hang or lift the beam is extremely difficult. Figure 5.5 shows the numerical evaluation results of the *Combined curvature motion shape method* where a point mass at measurement point number seven was modeled. A point mass was modeled by increasing the mass of the element at point number seven. From figure 5.5 it is evident that a point mass, as was caused by the vibrator-stinger assembly would have caused the second peak.

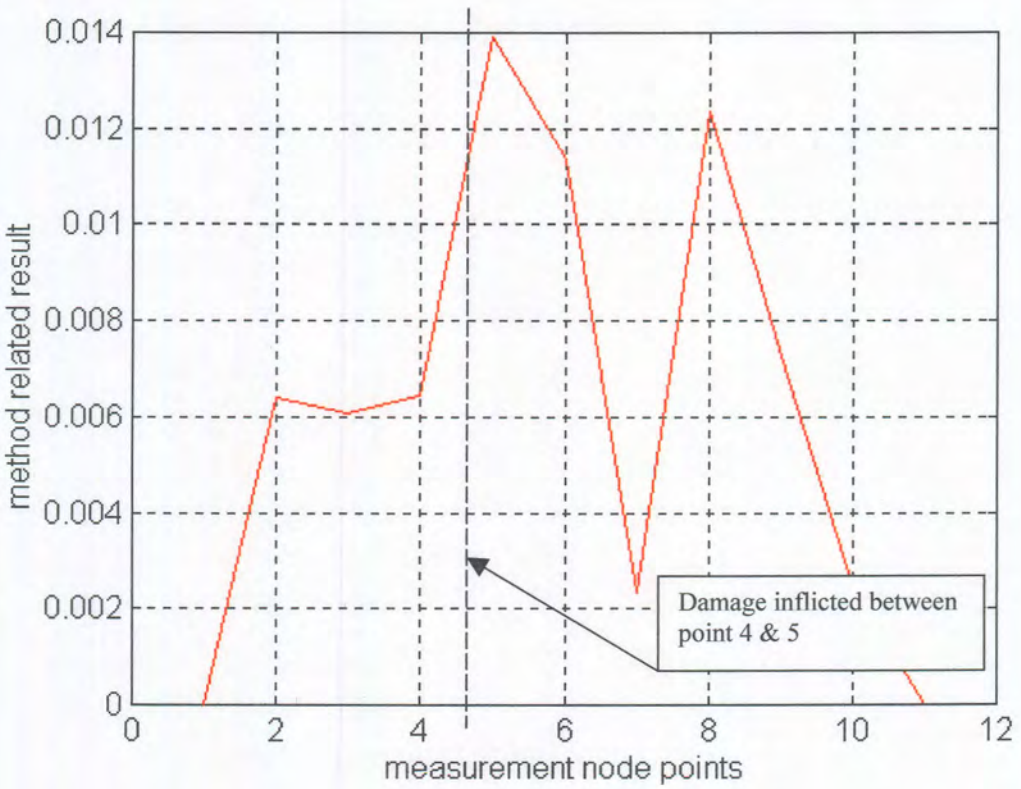

Figure 5.5 Damage detection using the Combined curvature mode shape method on the numerical point mass modulation.

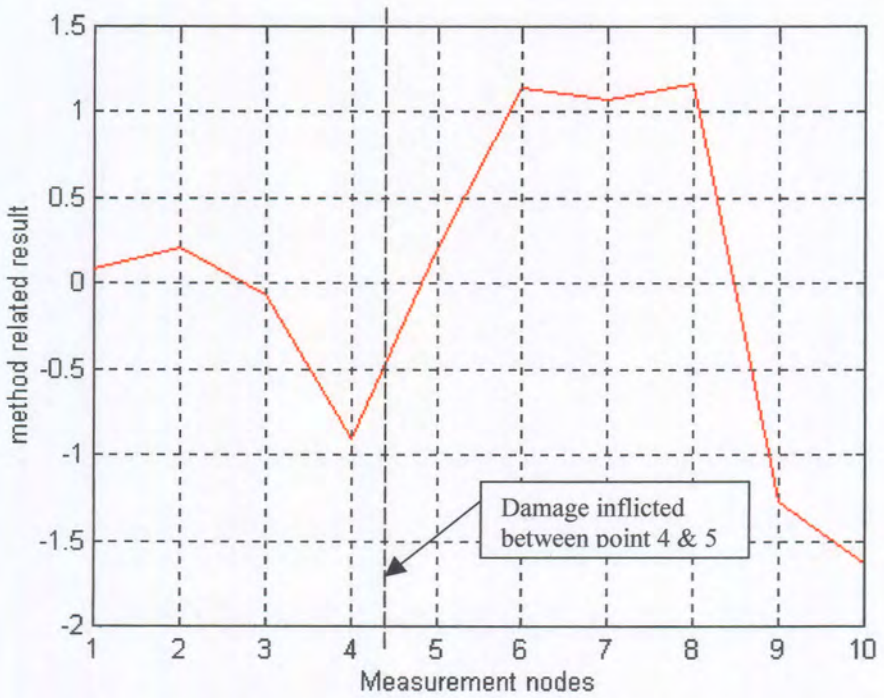

Figure 5.6 Damage detection using the Damage index method on experimental data.

The Damage index method performed better than the other two methods in the numerical evaluation of the methods. Unfortunately the experimental testing of the method does not indicate the position of inflicted damage. Again this can be attributed to difficulties experienced during the modal analysis process.

5.4. Evaluation of damage detection methods

The results of the damage detection methods tested experimentally, do not generally compare well with the numerical results in the previous chapter. Difficulties experienced during the modal analysis process are believed to have an influence on the mode shapes obtained. The mode shapes before and after damage are used as input data to two of the damage detection methods. The *Flexibility difference method,* indicates the position of damage correctly, but does not correspond to the numerical test results under similar

conditions. The *Damage index method* was unable to indicate the position of damage correctly. The *Combined curvature motion shape method* use damage and undamaged data directly and therefore provides the correct answer

6. Conclusion

The aim of this work was to develop a damage detection method, capable of using a large amount of raw experimental data to indicate the position of damage in a damaged structure. A literature study made it possible to identify current methods that are available to detect damage. The study included categorizing the available damage detection methods. From the classification of the methodology behind the available damage location methods, a refined objective was formed. It was decided to steer clear of utilizing finite element models as a means of detecting damage, because of its complexity and cost. A finite element model was only used to generate data for numerical testing purposes. The methodology that was decided on, was the comparison of damaged and undamaged data. The literature survey indicted that using mode shapes is the most practical and the most sensitive parameter to use for this damage detection methodology. The best available methods in the chosen area of damage detection were chosen to compare the performance of the new method.

In chapter 2 the two methods chosen for comparison purposes (*Flexibility difference and Damage index method*) were introduced. A brief introduction to modal analysis, essential for the working of the two comparing methods, was included in this chapter. In chapter 3, the *Combined curvature motion shape method* was introduced. The *Curvature difference method* from which the new method was developed was also introduced. A fair amount of emphasis was placed on the importance of using accurate numerical methods in programming the damage detection methods in general. For the purpose of fair comparison amongst the methods, similar numerical methods were used as far as possible in all the programs.

The numerical testing of the methods was undertaken in chapter 4. Test objectives following from the literature and the finite element model used to generate the data, were set. The objectives included testing for versatility in damage detection, testing to see if the methods would be able to identify multiple damage and to evaluate the degree in which the methods results could be influenced by changes in the support configurations. Firstly the viability of breaking up the model into more elements to enable a better

representation of localized damage was tested. The results indicated that the position of damage remained between the relevant measuring points, for all the damage indication methods. The results proved that the finite element model would represent localized damage more successfully. In the test category focusing on testing the versatility of damage detection methods to indicate damage using numerical data, the *Damage index method* proved superior to the other two methods. The *Flexibility difference* and the *Combined curvature motion shape methods* were able to detect all the damage introduced, but a slight shift in the indicated damage position was sometimes observed. The influence of change in the support configuration on the methods ability to detect damage, showed the least influence on the *Damage index method*. *The Flexibility difference method* proved to be very sensitive to support configuration changes. The *Flexibility difference method* experienced difficulty in detecting damage near pinned supports. Surprisingly the *Combined curvature motion shape method* showed a slight improvement in damage indication ability when tested on a pinned numerical model. The multiple damage indication test showed the *Flexibility difference method* to be unable to detect multiple damage. Both the *Damage index* and the *Combined curvature motion shape methods* were able to successfully indicate the position of two simultaneous damaged modeled cases. Emphasis was placed on the importance of checking for multiple damage in the vicinity of indicated damage, because none of the methods would be able to distinguish between closely spaced damaged cases.

In chapter 5 the different damage detection methods were tested using experimental data. Obtaining good quality data in practice is difficult in general. The quality of the experimental data and the reasons for data containing low frequency noise was discussed. Figures showing the experimental data obtained can be seen in Appendix C. Difficulties experienced during the modal analysis process to obtain damaged and undamaged mode shapes, caused the results of the *Flexibility difference* and the *Damage index method* to be influenced. The *Combined curvature motion shape method* which does not make use of the modal analysis process, indicated the position of damage correctly. A second damage position indicated by the results is believed to be caused by the stinger-vibrator configuration, creating a point load on the beam.

In conclusion, the damage detection results of the *Combined curvature motion shape method*, showed that it is possible to indicate the position of damage by using raw data. Numerical tests show that the new method performed better than the *Flexibility difference method* and fairly well compared to the *Damage index method*. The objectives set at the beginning of the study have been met. It might be of future benefit to the damage detection field, if large amounts of data can be incorporated into other existing damage detection methods to achieve better damage indication results.

References

Adams,R.D & Crawley,P, 1979. The location of defects in structures from measurements of natural frequencies, *Journal of Strain Analysis* , Vol. 14, No 2, pp 49-57.

Afolabi,D, 1987. An anti-resonance technique for detecting structural damage, *Proceedings of the 5th International Modal Analysis Conference, London, England,* Vol. 1, pp 491-495

Balmès,E, 1995. Structural Dynamics Toolbox for use with MATLAB. User's Guide. Scientific Software.

Bannantine,J, Comer,J.J & Handrock,J.L, 1990. Fundamentals of metal fatigue analysis, *Prentice-Hall, New Jersey*, pp 40-70.

Burden,R.L & Faires,J,F, 1997. Numerical Analysis, Fifth edition, *PWS publishing company, Boston.*

Chang,C.F & Ju,D, 1987. On the correlation between energy and deformation, *Advanced Topics in Vibration, ASME,* DE-Vol. 8, pp 67-75.

Chang,C.F & Ju,D, 1988. Damage assessment for non linear structures, *6th International Modal Analysis Conference*, Kissimee, Florida, *pp* 63-66.

Chen,J & Garba,J.A, 1988. On-orbit damage assessment for large space structures, *AAIA Journal*, Vol.26, No.9, pp1119-1126.

Døssing,O. & Staker,C. H, 1987. Operation deflection shapes: Background, measurement and application. *Proceedings of the 5th International Modal Analysis Conference.* London, England vol.2, pp1372 -1378

Ewins,D.J, 1996. Modal testing: Theory and practice, Tauton: Research Studies Press.

Farrar,C.R & Jaurequi,D.V, 1996. Comparison of damage identification algorithms on experimental modal data from a bridge, *Proceedings of the 14th International Modal Analysis Conference, Deardorn, Michigan,* Vol. 2.

Farrar,C.R, Stubbs,N & Kim,T, 1995. Field verification of a non-destructive damage location and severity estimation algorithm, *Proceedings of the 13th International Modal Analysis Conference, Nashville, TN,* pp 210-218.

Gere,J.F & Timoshenko,S.P, 1991. Mechanics of materials, *Chapman & Hall, UK.* pp 461-465.

Kirkegaard,P.H & Rytter,A, 1994. Use of networks for damage assessment in a steel mast, *Proceedings of the 12th International Modal Analysis Conference, Honolulu, Hawaii,* Vol. 2, pp 1128-1134.

Kopff,P. 1987. Experimental modal analysis for structural damage assessment: The case of natural convection cooling towers. *Proceedings of the 5th International Modal Analysis Conference, London, England,* Vol.12, pp122-126.

Lew,J, 1995. Using transfer function parameter changes for damage detection of structures, *AIAA Journal,* Vol.33, No.11, pp 2189-2193.

Law,S.S, Waldon,P & Taylor,C, 1992. Damage detection of a reinforced concrete bridge deck using the frequency response function, *Proceedings of the 10th International modal Analysis Conference, San Diego,* pp 772-778.

Mathews,J.H, 1987. Numerical methods for computer science, engineering, and mathematics, *Prentice-Hall International*, London, pp 312.

Panday,A.K & Biswas,M, 1995. Experimental verification of flexibility difference method for locating damage in structures, *Journal of Sound and Vibration* Vol.182,No.2, pp 311-328.

Panday,A.K, Biswas,M & Samman,M.M, 1991. Damage detection from changes in curvature mode shapes. *Journal of Sound and Vibration* Vol.145, No.2, pp221-332.

Robinson,N.A, Peterson,L.D, James,G.H & Doebling,S.W, 1996. Damage detection in aircraft structures using dynamically measured static flexibility matrices, *Proceedings of the 14th International Modal Analysis Conference, Dearborn, Michigan* Vol.2, pp857-865.

Rytter,A, 1993. Vibration based inspection of civil engineering structures, Ph.D Dissertation, Department of Building Technology and Structural Engineering, Aalborg University, Denmark.

Salawu,O.S & Williams,C, 1994. Damage location using vibration mode shapes, *Proceedings of the 12th International Modal Analysis Conference,* Vol.1, pp 933-939.

Shahrivar,F & Bouwkamp,J.G, 1986. Damage detection in offshore platforms using vibration information, *Journal of energy resources technology*, Vol. 108, No. 2, pp 97-106.

Springer,W.T, Lawrence,K.L & Lawley,T.J. 1988. Damage assessment based on the structural Frequency Response Function, *Experimental Mechanics March 1988.* pp 34-37.

Tsai,T & Yang,J.C.S, 1988. Detection of damage in structures by the Cross random decrement method, *Proceedings of the 3rd International Modal Analysis Conference, Orlando, Florida*, Vol.2, pp 691-700.

Walton,B.W, Ibanez,P & Yessaie,G, 1988. Remote structural damage detection via substructuring,*Proceedings of the 6th International Modal Analysis Conference Kissimmee, Florida*, pp 272-277.

Worden,K & Tomlinson,G.R, 1994. Damage location and quantification using neural networks, *Engineering Integrity Assessment* , Edwards,J.H, Kerr,J & Stanley,P, pp 11-31.

Worden,K, Ball,A.D & Tomlinson,G.R, 1993. Fault location in a framework structure using neural networks, *Smart Mater. Struct.,1993*, pp 189-200.

Zhang,Y.H, Friswell,M.I & Mottershead,J.E, 1994. A Comparison of methods to locate damage in structures, *ISMA 19 Tools for Noise and Vibration Analysis*, pp 683-696.

Zimmerman,D.C & Kaouk,M, 1992. Eigenstructure Assignment Approach for Structural Damage Detection, *AAIA Journal*, Vol.30, No.7, pp 1848-1855.

Zimmerman,D.C & Kaouk,M, 1994. Structural damage detection using measured modal data and no original analytical modal, *Proceedings of the 12th International Modal Analysis Conference*, Vol.1, pp 731-73

UNIVERSITEIT VAN PRETORIA
UNIVERSITY OF PRETORIA
YUNIBESITHI YA PRETORIA

Appendix A Matlab Software Programs

Numerical testing

Flexibility difference method

```
% nuflex.M
% Panday & Biswas 1995
% A Engelbrecht
% Damage anywhere in the system
clear all;
% Length        L [m]
   L=0.8;
% Width         b [m]
   b=0.0318;
% Thickness     h [m]
   h=0.00952;
   mes=0:0.08:0.8;   % Measurement points
                     % Consider beam with 50 elements
d=L/50;
Iz=(1/12)*b*h^3;
Iy=(1/12)*h*b^3;
Jx=(1/12)*b*h*(b^2 + h^2);
A =b*h;
IIw=1:0.25:500;
IIw=IIw';
% Coordinates of nodes
%     node#    unused        x     y     z
node=[ 1     0  0  0       0     0     0
       2     0  0  0         d     0     0
       3     0  0  0       2*d     0     0
       4     0  0  0       3*d     0     0
       5     0  0  0       4*d     0     0
       6     0  0  0       5*d     0     0
       7     0  0  0       6*d     0     0
       8     0  0  0       7*d     0     0
       9     0  0  0       8*d     0     0
      10     0  0  0       9*d     0     0
      11     0  0  0      10*d     0     0
      12     0  0  0      11*d     0     0
      13     0  0  0      12*d     0     0
      14     0  0  0      13*d     0     0
      15     0  0  0      14*d     0     0
      16     0  0  0      15*d     0     0
      17     0  0  0      16*d     0     0
      18     0  0  0      17*d     0     0
      19     0  0  0      18*d     0     0
      20     0  0  0      19*d     0     0
      21     0  0  0      20*d     0     0
      22     0  0  0      21*d     0     0
      23     0  0  0      22*d     0     0
      24     0  0  0      23*d     0     0
      25     0  0  0      24*d     0     0
      26     0  0  0      25*d     0     0
      27     0  0  0      26*d     0     0
      28     0  0  0      27*d     0     0
      29     0  0  0      28*d     0     0
      30     0  0  0      29*d     0     0
      31     0  0  0      30*d     0     0
      32     0  0  0      31*d     0     0
      33     0  0  0      32*d     0     0
      34     0  0  0      33*d     0     0
      35     0  0  0      34*d     0     0
      36     0  0  0      35*d     0     0
      37     0  0  0      36*d     0     0
      38     0  0  0      37*d     0     0
      39     0  0  0      38*d     0     0
```

```
      40     0   0   0     39*d     0     0
      41     0   0   0     40*d     0     0
      42     0   0   0     41*d     0     0
      43     0   0   0     42*d     0     0
      44     0   0   0     43*d     0     0
      45     0   0   0     44*d     0     0
      46     0   0   0     45*d     0     0
      47     0   0   0     46*d     0     0
      48     0   0   0     47*d     0     0
      49     0   0   0     48*d     0     0
      50     0   0   0     49*d     0     0
      51     0   0   0     50*d     0     0
      52     0   0   0        0     1     0];
% Use beam elements
elt1={ Inf abs('beam1')
% n#1   n#2 pl# il#  nr  0
   1    2    1    1    52  0
   2    3    1    1    52  0
   3    4    1    1    52  0
   4    5    1    1    52  0
   5    6    1    1    52  0
   6    7    1    1    52  0
   7    8    1    1    52  0
   8    9    1    1    52  0
   9   10    1    1    52  0
  10   11    1    1    52  0
  11    12    1    1    52  0
  12    13    1    1    52  0
  13    14    1    1    52  0
  14    15    1    1    52  0
  15    16    1    1    52  0
  16    17    1    1    52  0
  17    18    1    1    52  0
  18    19    1    1    52  0
  19    20    1    1    52  0
  20    21    1    1    52  0
  21    22    1    1    52  0
  22    23    1    1    52  0
  23    24    1    1    52  0
  24    25    1    1    52  0
  25    26    1    1    52  0
  26    27    1    1    52  0
  27    28    1    1    52  0
  28    29    1    1    52  0
  29    30    1    1    52  0
  30    31    1    1    52  0
  31    32    1    1    52  0
  32    33    1    1    52  0
  33    34    1    1    52  0
  34    35    1    1    52  0
  35    36    1    1    52  0
  36    37    1    1    52  0
  37    38    1    1    52  0
  38    39    1    1    52  0
  39    40    1    1    52  0
  40    41    1    1    52  0
  41    42    1    1    52  0
  42    43    1    1    52  0
  43    44    1    1    52  0
  44    45    1    1    52  0
  45    46    1    1    52  0
  46    47    1    1    52  0
  47    48    1    1    52  0
  48    49    1    1    52  0
  49    50    1    1    52  0
  50    51    1    1    52  0];

                % Material properties for Aluminium
   %     MatId MatType  E [N/m^2]     nu     rho [kg/m^3]
 pl={      1       1       7.1e10     0.35       2762
           2       1       7.029e10     0.35       2762]; % % damage
```

```
                % Section properties
  %    SecId SecType  Jx [kgm^2]  Iz [kgm^2]  Iy [kgm^2]   A [m^2]
il=[   1      1      Jx          Iy          Iz          A];
                % Assemble mass and stiffness matrix
[m1,k1,mdof1]=fe_mk(node,elt1,pl,il);
                % Active degrees of freedom
 % Consider 2 degrees of freedom .03 can be added
[adof1,ind1]=fe_c(mdof1,[.02 .06]);
                % Node 1 is fixed in translation and rotation
[adof1,ind1]=fe_c(adof1,[1],[],2);
                % Compute mass normalised normal modes
opt=[1 7 0 0 1e-05];
[mode1,freq1]=fe_eig(m1,k1,opt,mdof1,adof1);
%-----------------------------------------------------------------------
for np=1:10
np
pln=[1 1 1 1 1 1 1 1 1 1];
pln(np)=2;
                % Use beam elements
elt2=[ Inf abs('beam1')
% n#1   n#2 pl# il#  nr  0
   1    2    1    1    52  0
   2    3    1    1    52  0
   3    4    pln(1)    1    52  0
   4    5    1    1    52  0
   5    6    1    1    52  0
   6    7    1    1    52  0
   7    8    pln(2)    1    52  0
   8    9    1    1    52  0
   9   10    1    1    52  0
  10   11    1    1    52  0
  11    12    1    1    52  0
  12    13    pln(3)    1    52  0
  13    14    1    1    52  0
  14    15    1    1    52  0
  15    16    1    1    52  0
  16    17    1    1    52  0
  17    18    pln(4)    1    52  0
  18    19    1    1    52  0
  19    20    1    1    52  0
  20    21    1    1    52  0
  21    22    1    1    52  0
  22    23    pln(5)    1    52  0
  23    24    1    1    52  0
  24    25    1    1    52  0
  25    26    1    1    52  0
  26    27    1    1    52  0
  27    28    1    1    52  0
  28    29    pln(6)    1    52  0
  29    30    1    1    52  0
  30    31    1    1    52  0
  31    32    1    1    52  0
  32    33    1    1    52  0
  33    34    pln(7)    1    52  0
  34    35    1    1    52  0
  35    36    1    1    52  0
  36    37    1    1    52  0
  37    38    1    1    52  0
  38    39    pln(8)    1    52  0
  39    40    1    1    52  0
  40    41    1    1    52  0
  41    42    1    1    52  0
  42    43    1    1    52  0
  43    44    pln(9)    1    52  0
  44    45    1    1    52  0
  45    46    1    1    52  0
  46    47    1    1    52  0
  47    48    1    1    52  0
  48    49    pln(10)    1    52  0
  49    50    1    1    52  0
  50    51    1     1    52  0];
```

```
                % Assemble mass and stiffness matrix
[m2,k2,mdof2]=fe_mk(node,elt2,pl,il);
                % Active degrees of freedom
                % Consider 2 degrees of freedom .03 can be added
[adof2,ind2]=fe_c(mdof2,[.02 .06]);
                % Node 1 is fixed in translation and rotation
[adof2,ind2]=fe_c(adof2,[1],[],2);
                % Compute mass normalised normal modes
opt=[1 7 0 0 1e-05];            % 7 modes to de found
[mode2,freq2]=fe_eig(m2,k2,opt,mdof2,adof2);
%-------------------------------------------------------------
ra=5*(0:10);
rv=(ra)*6+2; % Translational DOF's
for i=1:11
 mode11(i)=mode1(rv(i),1);
 mode12(i)=mode1(rv(i),2);
 mode13(i)=mode1(rv(i),3);
 mode14(i)=mode1(rv(i),4);
 mode15(i)=mode1(rv(i),5);
end;
for i=1:11
 mode21(i)=mode2(rv(i),1);
 mode22(i)=mode2(rv(i),2);
 mode23(i)=mode2(rv(i),3);
 mode24(i)=mode2(rv(i),4);
 mode25(i)=mode2(rv(i),5);
end;
%-------------------------------------------------------------
 ma1=(1/freq1(1)^2)*(mode11'*mode11);
 ma2=(1/freq1(2)^2)*(mode12'*mode12);
 ma3=(1/freq1(3)^2)*(mode13'*mode13);
 ma4=(1/freq1(4)^2)*(mode14'*mode14);
 ma5=(1/freq1(5)^2)*(mode15'*mode15);
 F1=ma1+ma2+ma3+ma4+ma5;
 mb1=(1/freq2(1)^2)*(mode21'*mode21);
 mb2=(1/freq2(2)^2)*(mode22'*mode22);
 mb3=(1/freq2(3)^2)*(mode23'*mode23);
 mb4=(1/freq2(4)^2)*(mode24'*mode24);
 mb5=(1/freq2(5)^2)*(mode25'*mode25);
 F2=mb1+mb2+mb3+mb4+mb5;
DF=F2-F1;
d1=max(abs(DF(:,1)));
d2=max(abs(DF(:,2)));
d3=max(abs(DF(:,3)));
d4=max(abs(DF(:,4)));
d5=max(abs(DF(:,5)));
d6=max(abs(DF(:,6)));
d7=max(abs(DF(:,7)));
d8=max(abs(DF(:,8)));
d9=max(abs(DF(:,9)));
d10=max(abs(DF(:,10)));
d11=max(abs(DF(:,11)));
dd=[d1 d2 d3 d4 d5 d6 d7 d8 d9 d10 d11];
%-------------------------------------------------------------
Np(np)=np;
for n=1:length(dd)
  DD(n,np)=dd(n);
end;
end;
no=1:11;
        figure(1);
WATERFALL(no,Np,DD');
axis([1 11 1 10 0 6e-7]);
xlabel('Measurement nodes');
ylabel('Damage scenario');
zlabel('Method related results');
grid;
        figure(2);
WATERFALL(no,Np,DD');
axis([1 11 1 10 0 6e-7]);
VIEW(180,0);
```

```
xlabel('Measurement nodes');
ylabel('Damage scenario');
zlabel('Method related results');
grid;
```

Damage index Method

```
% nuindex.M
% Stubbs & Farrar 1995
% A Engelbrecht
% Fault finding
clear all;
% Length        L [m]
L=0.8;
% Width         b [m]
b=0.0318;
% Thickness     h [m]
h=0.00952;
                        % Consider beam with 50 elements
d=L/50;
Iz=(1/12)*b*h^3;
Iy=(1/12)*h*b^3;
Jx=(1/12)*b*h*(b^2 + h^2);
A =b*h;
IIw=1:0.25:500;
IIw=IIw';
                % Coordinates of nodes
%     node#    unused          x     y     z
node=[  1     0   0   0       0     0     0
        2     0   0   0         d     0     0
        3     0   0   0      2*d      0     0
        4     0   0   0      3*d      0     0
        5     0   0   0      4*d      0     0
        6     0   0   0      5*d      0     0
        7     0   0   0      6*d      0     0
        8     0   0   0      7*d      0     0
        9     0   0   0      8*d      0     0
       10     0   0   0      9*d      0     0
       11     0   0   0     10*d      0     0
       12     0   0   0     11*d      0     0
       13     0   0   0     12*d      0     0
       14     0   0   0     13*d      0     0
       15     0   0   0     14*d      0     0
       16     0   0   0     15*d      0     0
       17     0   0   0     16*d      0     0
       18     0   0   0     17*d      0     0
       19     0   0   0     18*d      0     0
       20     0   0   0     19*d      0     0
       21     0   0   0     20*d      0     0
       22     0   0   0     21*d      0     0
       23     0   0   0     22*d      0     0
       24     0   0   0     23*d      0     0
       25     0   0   0     24*d      0     0
       26     0   0   0     25*d      0     0
       27     0   0   0     26*d      0     0
       28     0   0   0     27*d      0     0
       29     0   0   0     28*d      0     0
       30     0   0   0     29*d      0     0
       31     0   0   0     30*d      0     0
       32     0   0   0     31*d      0     0
       33     0   0   0     32*d      0     0
       34     0   0   0     33*d      0     0
       35     0   0   0     34*d      0     0
       36     0   0   0     35*d      0     0
       37     0   0   0     36*d      0     0
       38     0   0   0     37*d      0     0
       39     0   0   0     38*d      0     0
       40     0   0   0     39*d      0     0
       41     0   0   0     40*d      0     0
```

```
      42     0   0   0     41*d     0     0
      43     0   0   0     42*d     0     0
      44     0   0   0     43*d     0     0
      45     0   0   0     44*d     0     0
      46     0   0   0     45*d     0     0
      47     0   0   0     46*d     0     0
      48     0   0   0     47*d     0     0
      49     0   0   0     48*d     0     0
      50     0   0   0     49*d     0     0
      51     0   0   0     50*d     0     0
      52     0   0   0        0     1     0];
                % Use beam elements
eltl=[ Inf abs('beam1')
% n#1   n#2 pl# il#  nr  0
   1    2    1    1    52  0
   2    3    1    1    52  0
   3    4    1    1    52  0
   4    5    1    1    52  0
   5    6    1    1    52  0
   6    7    1    1    52  0
   7    8    1    1    52  0
   8    9    1    1    52  0
   9   10    1    1    52  0
  10   11    1    1    52  0
  11    12    1    1    52  0
  12    13    1    1    52  0
  13    14    1    1    52  0
  14    15    1    1    52  0
  15    16    1    1    52  0
  16    17    1    1    52  0
  17    18    1    1    52  0
  18    19    1    1    52  0
  19    20    1    1    52  0
  20    21    1    1    52  0
  21    22    1    1    52  0
  22    23    1    1    52  0
  23    24    1    1    52  0
  24    25    1    1    52  0
  25    26    1    1    52  0
  26    27    1    1    52  0
  27    28    1    1    52  0
  28    29    1    1    52  0
  29    30    1    1    52  0
  30    31    1    1    52  0
  31    32    1    1    52  0
  32    33    1    1    52  0
  33    34    1    1    52  0
  34    35    1    1    52  0
  35    36    1    1    52  0
  36    37    1    1    52  0
  37    38    1    1    52  0
  38    39    1    1    52  0
  39    40    1    1    52  0
  40    41    1    1    52  0
  41    42    1    1    52  0
  42    43    1    1    52  0
  43    44    1    1    52  0
  44    45    1    1    52  0
  45    46    1    1    52  0
  46    47    1    1    52  0
  47    48    1    1    52  0
  48    49    1    1    52  0
  49    50    1    1    52  0
  50    51    1    1    52  0];
                % Material properties for Aluminium
  %     MatId MatType  E [N/m^2]     nu     rho [kg/m^3]
pl=[     1       1       7.1e10      0.35       2762
         2       1       6.035e10      0.35       2762]; %    % damage
                % Section properties
  %     SecId SecType  Jx [kgm^2]  Iz [kgm^2]  Iy [kgm^2]    A [m^2]
il=[   1       1      Jx           Iy           Iz           A];
```

```
                % Assemble mass and stiffness matrix
[m1,k1,mdof1]=fe_mk(node,elt1,pl,il);
                % Active degrees of freedom
                % Consider 2 degrees of freedom .03 can be added
[adof1,ind1]=fe_c(mdof1,[.02 .06]);
                % Node 1 is fixed in translation and rotation
[adof1,ind1]=fe_c(adof1,[1],[],2);  % [1,51]
  % Compute mass normalised normal modes
opt=[1 7 0 0 1e-05];
[model,freq1]=fe_eig(m1,k1,opt,mdof1,adof1);
%-----------------------------------------------------------------------
for np=1:10
np
pln=[1 1 1 1 1 1 1 1 1 1];
pln(np)=2;
% Use beam elements
elt2=[ Inf abs('beam1')
% n#1   n#2 pl# il#  nr  0
    1    2    1    1   52  0
    2    3    1    1   52  0
    3    4   pln(1)    1   52  0
    4    5    1    1   52  0
    5    6    1    1   52  0
    6    7    1    1   52  0
    7    8    1    1   52  0
    8    9   pln(2)    1   52  0
    9   10    1    1   52  0
   10   11    1    1   52  0
   11   12    1    1   52  0
   12   13    1    1   52  0
   13   14   pln(3)    1   52  0
   14   15    1    1   52  0
   15   16    1    1   52  0
   16   17    1    1   52  0
   17   18    1    1   52  0
   18   19   pln(4)    1   52  0
   19   20    1    1   52  0
   20   21    1    1   52  0
   21   22    1    1   52  0
   22   23    1    1   52  0
   23   24   pln(5)    1   52  0
   24   25    1    1   52  0
   25   26    1    1   52  0
   26   27    1    1   52  0
   27   28    1    1   52  0
   28   29   pln(6)    1   52  0
   29   30    1    1   52  0
   30   31    1    1   52  0
   31   32    1    1   52  0
   32   33    1    1   52  0
   33   34   pln(7)    1   52  0
   34   35    1    1   52  0
   35   36    1    1   52  0
   36   37    1    1   52  0
   37   38    1    1   52  0
   38   39   pln(8)    1   52  0
   39   40    1    1   52  0
   40   41    1    1   52  0
   41   42    1    1   52  0
   42   43    1    1   52  0
   43   44   pln(9)    1   52  0
   44   45    1    1   52  0
   45   46    1    1   52  0
   46   47    1    1   52  0
   47   48    1    1   52  0
   48   49   pln(10)    1   52  0
   49   50    1    1   52  0
   50   51    1    1   52  0];
                % Assemble mass and stiffness matrix
[m2,k2,mdof2]=fe_mk(node,elt2,pl,il);
                % Active degrees of freedom
```

```
                % Consider 2 degrees of freedom .03 can be added
[adof2,ind2]=fe_c(mdof2,[.02 .06]);
                % Node 1 is fixed in translation and rotation
[adof2,ind2]=fe_c(adof2,[1],[],2);  % [1,51]
                % Compute mass normalised normal modes
opt=[1 7 0 0 1e-05];
[mode2,freq2]=fe_eig(m2,k2,opt,mdof2,adof2);
%-------------------------------------------------------------
                % Translational DOF's
rc=0:10;
ra=5*rc;
rr=(ra)*6+2; % translasie modus 02 uit 06
rb=rc*d*5;    % x-koord
for j=1:5     % Mode shapes
 for i=1:11
  model1(i,j)=model(rr(i),j); % Undamaged
  mode22(i,j)=mode2(rr(i),j); % Damaged
 end;
end;
%-------------------------------------------------------------------
L=0.8;
d=L/10;                                 % elements
rc=0:10;
nn=rc*d;                                % element spacing
                                        % Undamaged
p10=pcs(nn,model1(:,1));        % second derivative
p20=pcs(nn,model1(:,2));
p30=pcs(nn,model1(:,3));
p40=pcs(nn,model1(:,4));
p50=pcs(nn,model1(:,5));
for n=1:11                              % matrix containing second
 PP(n,1)=p10(n).*p10(n);        % derivatives sqr.
 PP(n,2)=p20(n).*p20(n);
 PP(n,3)=p30(n).*p30(n);
 PP(n,4)=p40(n).*p40(n);
 PP(n,5)=p50(n).*p50(n);
end;
q10=pcs(nn,mode22(:,1));        % Damaged
q20=pcs(nn,mode22(:,2));
q30=pcs(nn,mode22(:,3));
q40=pcs(nn,mode22(:,4));
q50=pcs(nn,mode22(:,5));
for n=1:11
 QQ(n,1)=q10(n).*q10(n);        % Matrix (11X4)
 QQ(n,2)=q20(n).*q20(n);
 QQ(n,3)=q30(n).*q30(n);
 QQ(n,4)=q40(n).*q40(n);
 QQ(n,5)=q50(n).*q50(n);
end;
                        % Interpolation points=(parts+1)
parts=500;              % number of points interpolated
  Ma1=pci(nn,PP(:,1)',parts);
  Ma2=pci(nn,PP(:,2)',parts);
  Ma3=pci(nn,PP(:,3)',parts);
  Ma4=pci(nn,PP(:,4)',parts);
  Ma5=pci(nn,PP(:,5)',parts);
  Mb1=pci(nn,QQ(:,1)',parts);
  Mb2=pci(nn,QQ(:,2)',parts);
  Mb3=pci(nn,QQ(:,3)',parts);
  Mb4=pci(nn,QQ(:,4)',parts);
  Mb5=pci(nn,QQ(:,5)',parts);
MA(:,1)=Ma1(:,2);
MA(:,2)=Ma2(:,2);
MA(:,3)=Ma3(:,2);
MA(:,4)=Ma4(:,2);
MA(:,5)=Ma5(:,2);
MB(:,1)=Mb1(:,2);
MB(:,2)=Mb2(:,2);
MB(:,3)=Mb3(:,2);
MB(:,4)=Mb4(:,2);
MB(:,5)=Mb5(:,2);
```

```
AX(:,1)=Mal(:,1);
for n=1:5                          % Integration over mode shape
 IO(n)=trapz(AX,MA(:,n));
 IB(n)=trapz(AX,MB(:,n));
end;
 dd=parts/10;
 for n=1:5                         % Integration over element
  for i=1:10
    for st=1:dd
              ns(st)=AX(dd*(i-1)+st,1);
            ma(st)=MA(dd*(i-1)+st,n);
            mb(st)=MB(dd*(i-1)+st,n);
    end;
    ko(i,n)=trapz(ns,ma);
    kb(i,n)=trapz(ns,mb);
  end;
 end;
%-------------------------------------------------------
                                   % Damage index
for j=1:5
  for i=1:10
   num(i,j)=(kb(i,j)+IB(j))*IO(j);
   den(i,j)=(ko(i,j)+IO(j))*IB(j);
   tot(i,j)=num(i,j)/den(i,j);
  end;
end;

for i=1:10
  B(i)=sum(tot(i,:));
end;

% Normelising
me=MEAN(B);
st=STD(B);
Z=(B-me)/st;

Np(np)=np;
  for n=1:10
    ZZ(n,np)=Z(n);
  end;
end;

rx=1:10;
        figure(1);
waterfall(rx,Np,ZZ);
xlabel('Measurement nodes');
ylabel('Damage scenario');
zlabel('Method related results');
grid;
        figure(2);
waterfall(rx,Np,ZZ);
VIEW(0,0);
xlabel('Measurement nodes');
ylabel('Damage scenario');
zlabel('Method related results');
grid;
```

Combined curvature motion shape method

```
% nubt.M
% A.Engelbrecht
% Damage detection
clear all;
% Length        L [m]
     L=0.8;
     mes=0:0.08:0.8;   % Measurement points
% Width         b [m]
     b=0.0318;
% Thickness     h [m]
     h=0.00952;
        % Consider beam with 50 elements
```

```
d=L/50;
Iz=(1/12)*b*h^3;
Iy=(1/12)*h*b^3;
Jx=(1/12)*b*h*(b^2 + h^2);
A=b*h;

IIw=0:1:500;  % frequency
IIw=IIw';
% ------------------------Undamaged beam---------------
                % Coordinates of nodes
%     node#    unused          x     y     z
node=[ 1     0   0   0         0     0     0
       2     0   0   0         d     0     0
       3     0   0   0       2*d     0     0
       4     0   0   0       3*d     0     0
       5     0   0   0       4*d     0     0
       6     0   0   0       5*d     0     0
       7     0   0   0       6*d     0     0
       8     0   0   0       7*d     0     0
       9     0   0   0       8*d     0     0
      10     0   0   0       9*d     0     0
      11     0   0   0      10*d     0     0
      12     0   0   0      11*d     0     0
      13     0   0   0      12*d     0     0
      14     0   0   0      13*d     0     0
      15     0   0   0      14*d     0     0
      16     0   0   0      15*d     0     0
      17     0   0   0      16*d     0     0
      18     0   0   0      17*d     0     0
      19     0   0   0      18*d     0     0
      20     0   0   0      19*d     0     0
      21     0   0   0      20*d     0     0
      22     0   0   0      21*d     0     0
      23     0   0   0      22*d     0     0
      24     0   0   0      23*d     0     0
      25     0   0   0      24*d     0     0
      26     0   0   0      25*d     0     0
      27     0   0   0      26*d     0     0
      28     0   0   0      27*d     0     0
      29     0   0   0      28*d     0     0
      30     0   0   0      29*d     0     0
      31     0   0   0      30*d     0     0
      32     0   0   0      31*d     0     0
      33     0   0   0      32*d     0     0
      34     0   0   0      33*d     0     0
      35     0   0   0      34*d     0     0
      36     0   0   0      35*d     0     0
      37     0   0   0      36*d     0     0
      38     0   0   0      37*d     0     0
      39     0   0   0      38*d     0     0
      40     0   0   0      39*d     0     0
      41     0   0   0      40*d     0     0
      42     0   0   0      41*d     0     0
      43     0   0   0      42*d     0     0
      44     0   0   0      43*d     0     0
      45     0   0   0      44*d     0     0
      46     0   0   0      45*d     0     0
      47     0   0   0      46*d     0     0
      48     0   0   0      47*d     0     0
      49     0   0   0      48*d     0     0
      50     0   0   0      49*d     0     0
      51     0   0   0      50*d     0     0
      52     0   0   0         0     1     0];
                          % Use beam elements
eltl=[ Inf abs('beam1')
% n#1   n#2 pl# il#   nr   0
   1    2    1    1    52   0
   2    3    1    1    52   0
   3    4    1    1    52   0
   4    5    1    1    52   0
   5    6    1    1    52   0
```

```
   6    7    1    1    52   0
   7    8    1    1    52   0
   8    9    1    1    52   0
   9   10    1    1    52   0
  10   11    1    1    52   0
  11   12    1    1    52   0
  12   13    1    1    52   0
  13   14    1    1    52   0
  14   15    1    1    52   0
  15   16    1    1    52   0
  16   17    1    1    52   0
  17   18    1    1    52   0
  18   19    1    1    52   0
  19   20    1    1    52   0
  20   21    1    1    52   0
  21   22    1    1    52   0
  22   23    1    1    52   0
  23   24    1    1    52   0
  24   25    1    1    52   0
  25   26    1    1    52   0
  26   27    1    1    52   0
  27   28    1    1    52   0
  28   29    1    1    52   0
  29   30    1    1    52   0
  30   31    1    1    52   0
  31   32    1    1    52   0
  32   33    1    1    52   0
  33   34    1    1    52   0
  34   35    1    1    52   0
  35   36    1    1    52   0
  36   37    1    1    52   0
  37   38    1    1    52   0
  38   39    1    1    52   0
  39   40    1    1    52   0
  40   41    1    1    52   0
  41   42    1    1    52   0
  42   43    1    1    52   0
  43   44    1    1    52   0
  44   45    1    1    52   0
  45   46    1    1    52   0
  46   47    1    1    52   0
  47   48    1    1    52   0
  48   49    1    1    52   0
  49   50    1    1    52   0
  50   51    1    1    52   0];  % Ref. node
                      % Material properties for Aluminium
  %     MatId MatType  E [N/m^2]     nu     rho [kg/m^3]
pl=[     1       1      7.1e10      0.35       2762
         2       1      6.39e10      0.35       2762]; %   10 % damage
  % Section properties
  %     SecId SecType  Jx [kgm^2]  Iz [kgm^2]  Iy [kgm^2]    A [m^2]
il=[    1       1      Jx          Iy          Iz           A];
                      % Assemble mass and stiffness matrix
[ml,kl,mdofl]=fe_mk(node,eltl,pl,il);
                      % Active degrees of freedom
                      % Consider 2 degrees of freedom (translation & rotation).03 can be
added
[adofl,indl]=fe_c(mdofl,[.02 ]);  %.06
                      % Node 1 is fixed in translation and rotation
[adofl,indl]=fe_c(adofl,[1],[],2);  %[1,51]
                      % Compute mass normalised normal modes
opt=[0 3 0 0 1e-05];    % opt(2)=no. nodes=7
[model,freql]=fe_eig(ml,kl,opt,mdofl,adofl);
 bl=fe_c(mdofl,[31.02])'; % exiting node 7 direction 02
                      % Responce node 2,3,4 exs. direction 8 construct FRFs
 cdl=fe_c(mdofl,[1.08 6.08 11.08 16.08 21.08 26.08 31.08 36.08 41.08 46.08 51.08]);
 pbl=model'*bl; % model input matrix
 cpl=cdl*model; % mode forms from sensors
 IIxf=nor2xf(freq1,0.01,pbl,cpl,IIw*2*pi); % Undamaged
%-----------------------------------------------------------------------
for kol=1:11       % damage IIxe ; Undamaged IIxf
```

```
                        % Include phase and amplitude
 for n=1:length(IIw)
    if abs(angle(IIxf(n,kol)))>(pi/2)
      teken(n)=-1;
    end;
    if abs(angle(IIxf(n,kol)))<(pi/2)
      teken(n)=1;
    end;
  alfa(n,kol)=teken(n)*abs(IIxf(n,kol));  % undamaged
 end;
end;
   for n=1:length(IIw)  % Difference at measurement points
       delta(n,:)=pcs(mes,abs(IIxf(n,:)));
   end;
%-------------------------------------------------------------------
for np=1:10
np
pln={1 1 1 1 1 1 1 1 1 1};
pln(np)=2;
elt2=[ Inf abs('beam1')
% n#1   n#2 pl# il#  nr  0
    1    2    1    1    52   0
    2    3    1    1    52   0
    3    4    pln(1)    1    52   0
    4    5    1    1    52   0
    5    6    1    1    52   0
    6    7    1    1    52   0
    7    8    pln(2)    1    52   0
    8    9    1    1    52   0
    9   10    1    1    52   0
   10   11    1    1    52   0
   11    12    1    1    52   0
   12    13    pln(3)    1    52   0
   13    14    1    1    52   0
   14    15    1    1    52   0
   15    16    1    1    52   0
   16    17    1    1    52   0
   17    18    pln(4)    1    52   0
   18    19    1    1    52   0
   19    20    1    1    52   0
   20    21    1    1    52   0
   21    22    1    1    52   0
   22    23    pln(5)    1    52   0
   23    24    1    1    52   0
   24    25    1    1    52   0
   25    26    1    1    52   0
   26    27    1    1    52   0
   27    28    1    1    52   0
   28    29    pln(6)    1    52   0
   29    30    1    1    52   0
   30    31    1    1    52   0
   31    32    1    1    52   0
   32    33    1    1    52   0
   33    34    pln(7)    1    52   0
   34    35    1    1    52   0
   35    36    1    1    52   0
   36    37    1    1    52   0
   37    38    1    1    52   0
   38    39    pln(8)    1    52   0
   39    40    1    1    52   0
   40    41    1    1    52   0
   41    42    1    1    52   0
   42    43    1    1    52   0
   43    44    pln(9)    1    52   0
   44    45    1    1    52   0
   45    46    1    1    52   0
   46    47    1    1    52   0
   47    48    1    1    52   0
   48    49    pln(10)    1    52   0
   49    50    1    1    52   0
   50    51    1     1    52   0];
```

```
                                % Use beam elements
                                % Assemble mass and stiffness matrix
[m2,k2,mdof2]=fe_mk(node,elt2,pl,il);
                                % Active degrees of freedom
                                % Consider 2 degrees of freedom .03 can be added
[adof2,ind2]=fe_c(mdof2,[.02]); %.06
                                % Node 1 is fixed in translation and rotation
[adof2,ind2]=fe_c(adof2,[1],[],2); %[1,51]
                                % Compute mass normalised normal modes
[mode2,freq2]=fe_eig(m2,k2,opt,mdof2,adof2);
 b2=fe_c(mdof2,[31.02])'; % exiting node 5 direction 2
                                % response node 2,3,4 exs. direction 8
 cd2=fe_c(mdof2,[1.08 6.08 11.08 16.08 21.08 26.08 31.08 36.08 41.08 46.08 51.08]);
 pb2=mode2'*b2; % model input matrix
 cp2=cd2*mode2; % mode forms from sensors
 IIxe=nor2xf(freq2,0.01,pb2,cp2,IIw*2*pi); % Damaged
%-------------------------------------------------------------------------
for kol=1:11                      % damage IIxe ; Undamaged IIxf
 for n=1:length(IIw)
     if abs(angle(IIxe(n,kol)))>(pi/2)
        teken(n)=-1;
     end;
     if abs(angle(IIxe(n,kol)))<(pi/2)
       teken(n)=1;
     end;
  beta(n,kol)=teken(n)*abs(IIxe(n,kol));  % beta beskadig ;alfa onbeskadig
   end;
end;
   for n=1:length(IIw)
       gama(n,:)=pcs(mes,abs(IIxe(n,:)));
   end;
  for n=1:length(delta)
    for m=1:11
      dcurv(n,m)=abs((gama(n,m))-(delta(n,m)));
    end;
    al(n)=max(dcurv(n,:));
  end;
 for t=1:11
   Op(t)=sum(dcurv(:,t));
   no(t)=t;
 end;
for n=1:10
 Pp(n)=Op(n);
end;
piek(np)=find(Pp==max(Pp))

Np(np)=np;
antw(np,:)=Op;
end;   % end np

               figure(1);
WATERFALL(no,Np,antw);
axis([1 11 1 10 0 5e-5]);
VIEW(0,30);
xlabel('Measurement nodes');
ylabel('Damage scenario');
zlabel('Method related results');
grid;
            figure(2);
waterfall(no,Np,antw);
axis([1 11 1 10 0 5e-5]);
xlabel('Measurement nodes');
ylabel('Damage scenario');
zlabel('Method related results');
grid;
```

Function used with Combined curvature motion shape method

PCI

```
% pci.m (piecewise cubic spline interpolation)
% Burden & Faire pp 130
% Adapted by A.Engelbrecht 2000
% MX(:,1)gives the interpolated x-values
% MX(:,2)gives the interpolated y-values

function MX=pci(x,a,par)
for j=1:length(a)-1
 h(j)=x(j+1)-x(j);
end;
% Introduce matrix Mb
for j=1:length(a)-2
 Mb(j+1,1)=(3/h(j+1)*(a(j+2)-a(j+1)))-(3/h(j)*(a(j+1)-a(j)));
end;
Mb(length(a),1)=0;
Alpha(1,1)=1;                    % Natural boundary
Alpha(length(a),length(a))=1;

for j=1:length(a)-2
 Alpha(j+1,j)=h(j);
 Alpha(j+1,j+1)=2*(h(j)+h(j+1));
 Alpha(j+1,j+2)=h(j+1);
end;
c=inv(Alpha)*Mb;
for j=1:length(c)-1
 b(j)=((a(j+1)-a(j))/h(j))-(h(j)*(c(j+1)+2*c(j))/3);
end;
for j=1:length(c)-1
 d(j)=(c(j+1)-c(j))/(3*h(j));
end;
c=c';                            % graphs = [points - 1]
%-----------------------------------------------------------------------
                % Interpolation for each function
dd=(par/10);
t=1;
for j=1:length(a)-1
  pp=0;
  for n=1:dd
     MX(t,2)=polyval([d(j) c(j) b(j) a(j)],pp);
     MX(t,1)=x(j)+pp;
     t=t+1;
     pp=pp+(h(j)/dd);
  end;
end;    % End point
MX(t,2)=a(length(a));
MX(t,1)=x(length(x));
```

PCS

```
% pcs.m (piecewise cubic spline and second derivative at points)
% Burden & Faire pp 130
% Adapted by A.Engelbrecht 2000
% Delta= second derivatives at given points

function delta=pcs(x,a)
for j=1:length(a)-1
 h(j)=x(j+1)-x(j);
end;
for j=1:length(a)-2
 Mb(j+1,1)=(3/h(j+1)*(a(j+2)-a(j+1)))-(3/h(j)*(a(j+1)-a(j)));
end;
Mb(length(a),1)=0;
Alpha(1,1)=1;
Alpha(length(a),length(a))=1;
for j=1:length(a)-2
 Alpha(j+1,j)=h(j);
```

```
 Alpha(j+1,j+1)=2*(h(j)+h(j+1));
 Alpha(j+1,j+2)=h(j+1);
end;
c=inv(Alpha)*Mb;
for j=1:length(c)-1
 b(j)=((a(j+1)-a(j))/h(j))-(h(j)*(c(j+1)+2*c(j))/3);
end;
for j=1:length(c)-1
 d(j)=(c(j+1)-c(j))/(3*h(j));
end;
c=c';
%-------------------------------------------------------------
% Value at second derivetive function
for j=1:length(h)
   delta(j)=polyval(polyder(polyder([d(j) c(j) b(j) a(j)])),0);
   %delta(j)=polyval(polyder([a(j) b(j) c(j) d(j)]),0);
   %delta(j)=polyval([d(j) c(j) b(j) a(j)],0);
end;
en=length(b);
poe=(x(length(x))-x(length(x)-1));
delta(en+1)=polyval(polyder(polyder([d(en) c(en) b(en) a(en)])),poe);
%delta(en+1)=polyval([d(en) c(en) b(en) a(en)],poe);
```

Modal analysis

```
% DLOADO.M     Load and prepare data
%                              Modal analysis on beams
%            Prepared by Andre Engelbrecht
clear
% Load data
load to01.txt;
load to02.txt;
load to03.txt;
load to04.txt;
load to05.txt;
load to06.txt;
load to07.txt;
load to08.txt;
load to09.txt;
load to10.txt;
load to11.txt;
% Damaged analysis
% Write frequency in IIw format (Hz)
w=to02(:,1);
% Write FRFs in IIxf format
m(:,1)=10.^(to01(:,2)/20);
p(:,1)=(pi/180)*to01(:,3);
xf(:,1)=m(:,1).*exp(i*p(:,1));
m(:,2)=10.^(to02(:,2)/20);
p(:,2)=(pi/180)*to02(:,3);
xf(:,2)=m(:,2).*exp(i*p(:,2));
m(:,3)=10.^(to03(:,2)/20);
p(:,3)=(pi/180)*to03(:,3);
xf(:,3)=m(:,3).*exp(i*p(:,3));
m(:,4)=10.^(to04(:,2)/20);
p(:,4)=(pi/180)*to04(:,3);
xf(:,4)=m(:,4).*exp(i*p(:,4));

m(:,5)=10.^(to05(:,2)/20);
p(:,5)=(pi/180)*to05(:,3);
xf(:,5)=m(:,5).*exp(i*p(:,5));
m(:,6)=10.^(to06(:,2)/20);
p(:,6)=(pi/180)*to06(:,3);
xf(:,6)=m(:,6).*exp(i*p(:,6));
m(:,7)=10.^(to07(:,2)/20);
p(:,7)=(pi/180)*to07(:,3);
xf(:,7)=m(:,7).*exp(i*p(:,7));
m(:,8)=10.^(to08(:,2)/20);
p(:,8)=(pi/180)*to08(:,3);
```

```
xf(:,8)=m(:,8).*exp(i*p(:,8));
m(:,9)=10.^(to09(:,2)/20);
p(:,9)=(pi/180)*to09(:,3);
xf(:,9)=m(:,9).*exp(i*p(:,9));
m(:,10)=10.^(to10(:,2)/20);
p(:,10)=(pi/180)*to10(:,3);
xf(:,10)=m(:,10).*exp(i*p(:,10));
m(:,11)=10.^(to11(:,2)/20);
p(:,11)=(pi/180)*to11(:,3);
xf(:,11)=m(:,11).*exp(i*p(:,11));
save O_frf w xf
```

MA_O

```
% MA_O.M          Modal analysis - Beam
%                          First load and prepare data with DLOAD.M
%                          Structural Dynamics Toolbox Version 3
% Initialisation
format short e
clear;clear global;close all;clc;
%%iicom('clear');
global IDopt IIpo IIpol IIres IIres1 XFopt XFdof IIxf IIxe IIxh IIxi IIw
% Load measured FRFs at specified frequencies
load O_frf
bg=11;
bw=[bg:801];
IIw=w(bw);
f=IIw;
nfrf=[1:11]; IIxf=xf(bw,nfrf);
% IDopt Identification options (p.2-79)
% 11 sensors 1 actuator collocated at 7
IDopt=[3 2 11 1 size(IIxf,1) 1   11 1   0 0 0   1 7];
%%idopt('info');
% XFopt XF options (see page 2-150 and 'help xfopt')
% Set options according to IDopt information
%%xfopt('default'); xfopt('info')
% XFdof XF degrees-of-freedom (see pp.2-150 and 2-151)
for indx=1:11
   XFdof(indx,1)=indx+0.02;    %RespNodeID.RespDOFID
   XFdof(indx,2)=7.02;                 %ExciNodeID.ExciDOFID
   XFdof(indx,3)=indx;                 %Address
   XFdof(indx,4)=0;                            %RespGroup
   XFdof(indx,5)=0;                            %ExciGroup
   XFdof(indx,6)=4;                            %FunType FRF
   XFdof(indx,7)=0;                            %FunID
   XFdof(indx,8)=indx;                 %LoadCase
   XFdof(indx,9)=0;                            %ZaxisValue
end
XFgroup=[]; XFload=[];
% Invoke graphical user interface and interactive curve fitting
iigui; idcom;
% Plot
%%iicom(';ch1;cax1;show abs; cax2; show pha');
% Find approximate normal modes
% cps=output shape matrix (describes sensors)
% pbs=input shape matrix (describes actuators)
%[f2,ga2,pbs2,cps2]=res2nor(IIres,IIpo,IDopt);
[f2,ga2,pbs2,cps2]=id_nor(IIres,IIpo,IDopt);
IIxe=nor2xf(f2,ga2,pbs2,cps2,IIw*2*pi);
iiplot;
IIxh=IIxe + res2xf(IIres,IIpo,IIw*2*pi,IDopt,[5 6]);
iiplot;pause
L=0.8;  % Lengte     (x)    L [m]
                % Beskou balk met 10 elemente
d=L/10;
% Definition of geometry (drawing scales)
% node#      unused      x     y     z
node=[ 1     0  0  0     0     0     0
       2     0  0  0     d     0     0
       3     0  0  0     2*d   0     0
       4     0  0  0     3*d   0     0
       5     0  0  0     4*d   0     0
```

UNIVERSITEIT VAN PRETORIA
UNIVERSITY OF PRETORIA
YUNIBESITHI YA PRETORIA

```
     6     0   0   0     5*d   0     0
     7     0   0   0     6*d   0     0
     8     0   0   0     7*d   0     0
     9     0   0   0     8*d   0     0
    10     0   0   0     9*d   0     0
    11     0   0   0    10*d   0     0];

% Degrees of freedom (Only possible motion Y)
mdof=[1.02 2.02 3.02 4.02 5.02 6.02 7.02 8.02 9.02 10.02 11.02]';
% Plot modes
figure(1)
L=[1 2 3 4 5 6 7 8 9 10 11];
LDraw(1,1)=length(L); LDraw(1,82+[1:length(L)])= L;
% Mode shapes (opt: p2-41)
% See fecom p2-28 for data on manipulation of deformation diagram (gui)
mode =[cps2];
%save mode_o f mode;
opt=[2 2 50 11 0.5];
feplot(node,LDraw,mode,mdof,opt);
```

UNIVERSITEIT VAN PRETORIA
UNIVERSITY OF PRETORIA
YUNIBESITHI YA PRETORIA

APPENDIX B EXPERIMENTAL SETUP

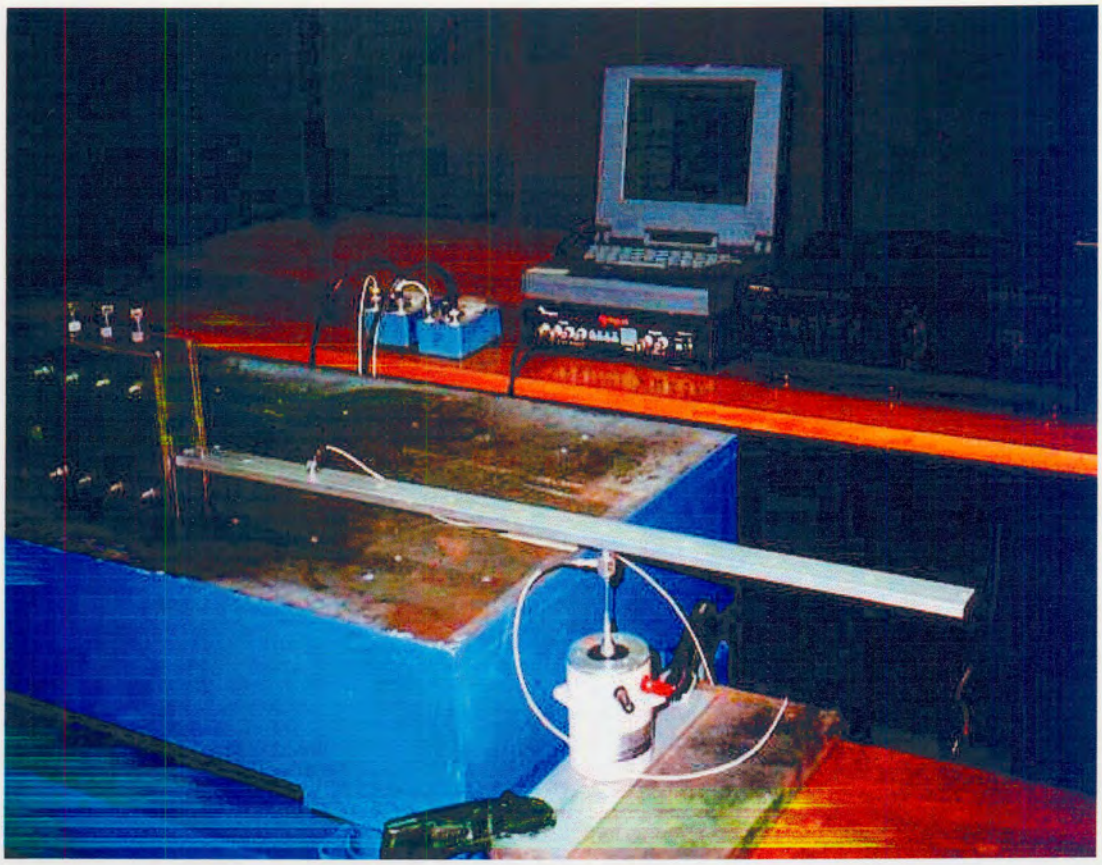

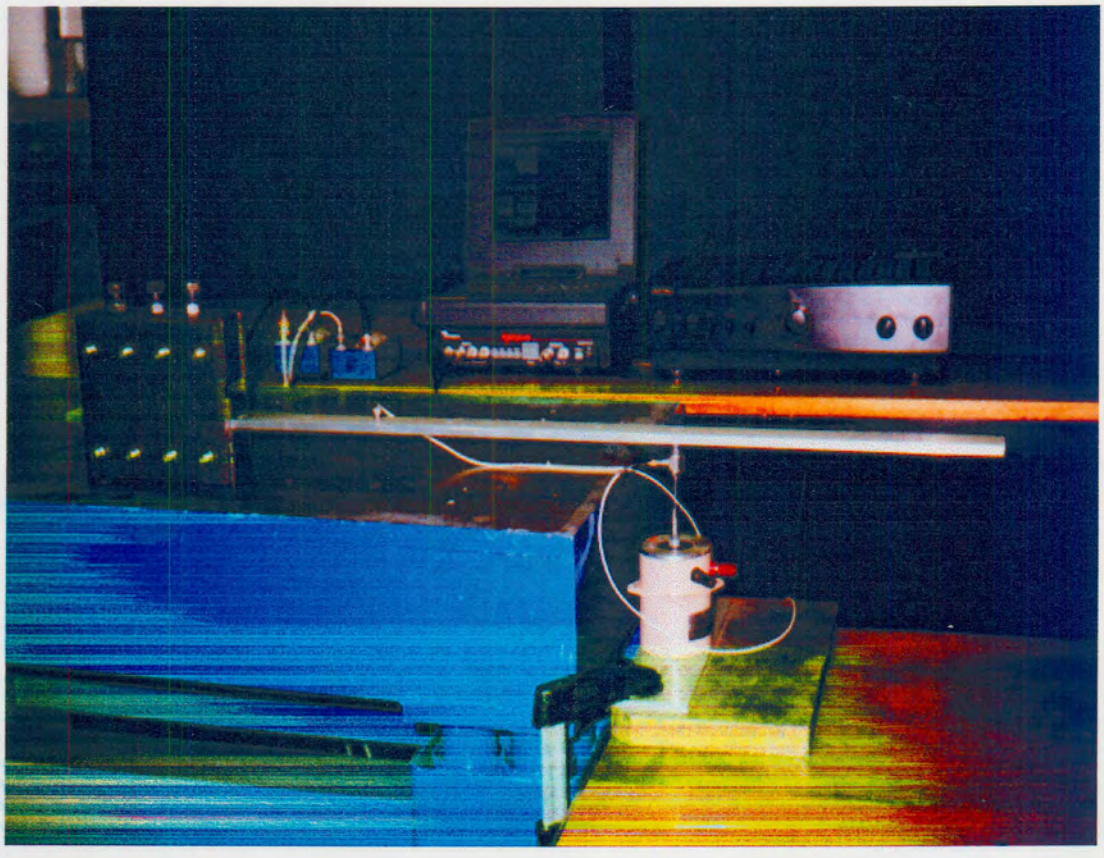

UNIVERSITEIT VAN PRETORIA
UNIVERSITY OF PRETORIA
YUNIBESITHI YA PRETORIA

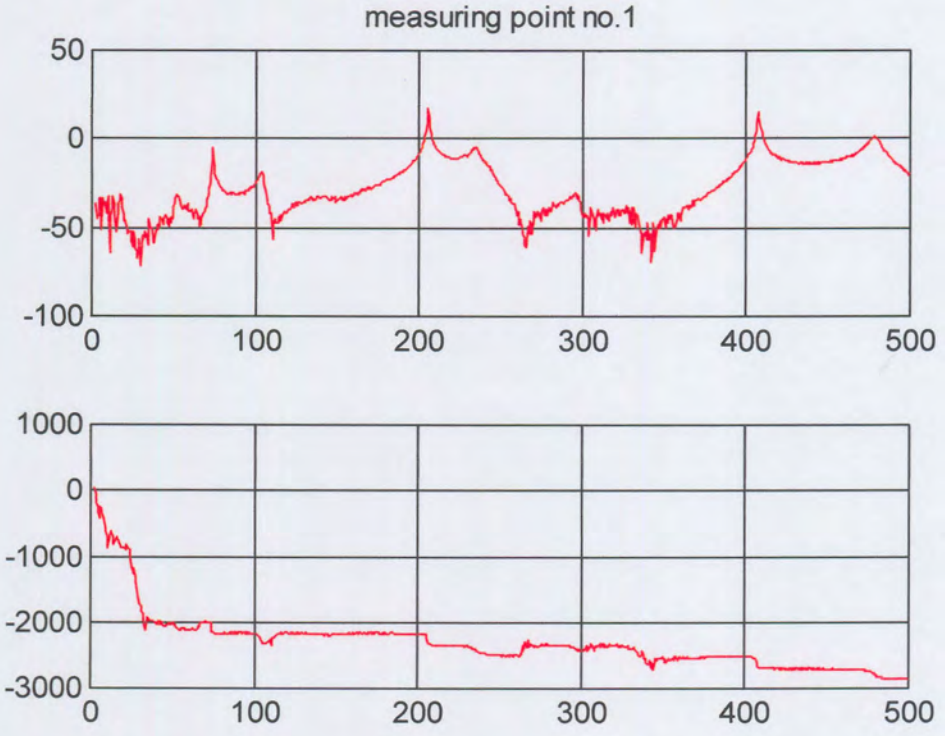

Frequency

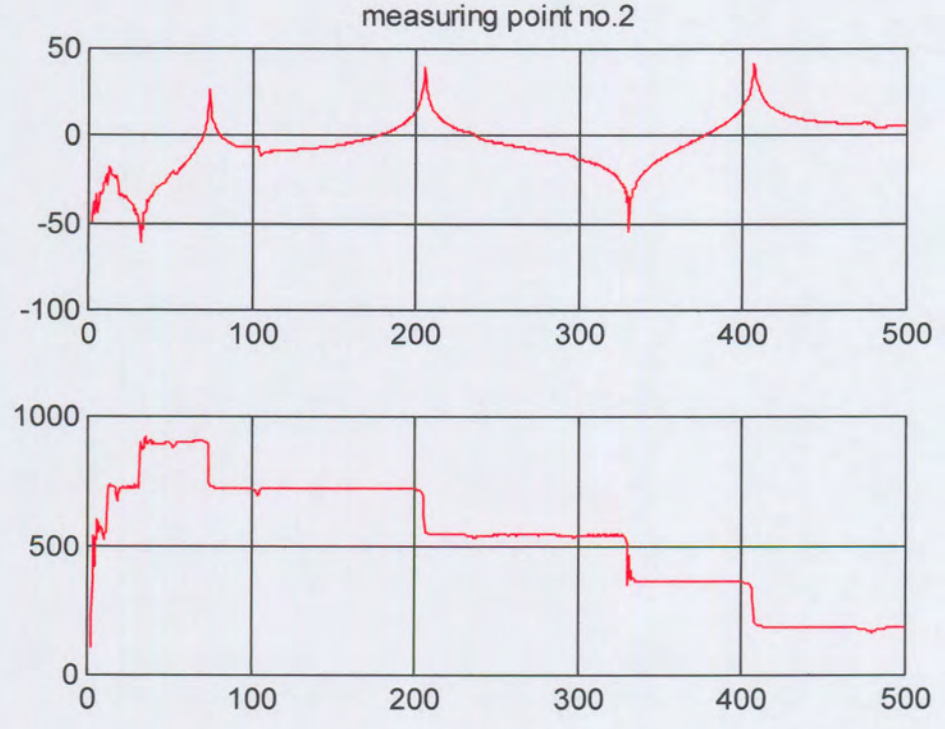

Frequency

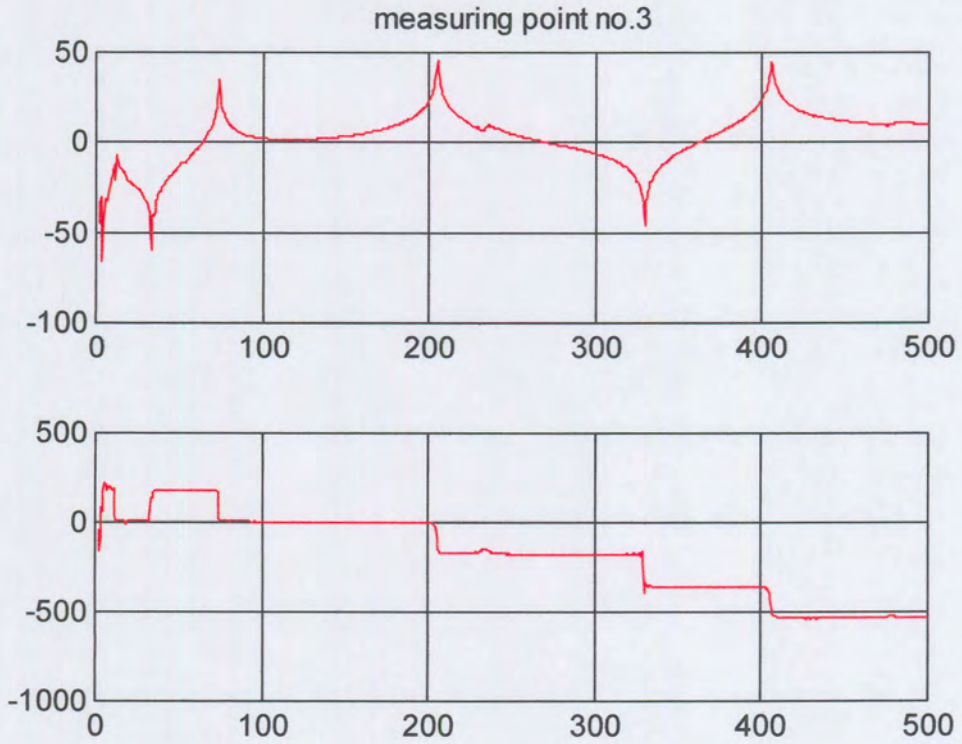

Frequency

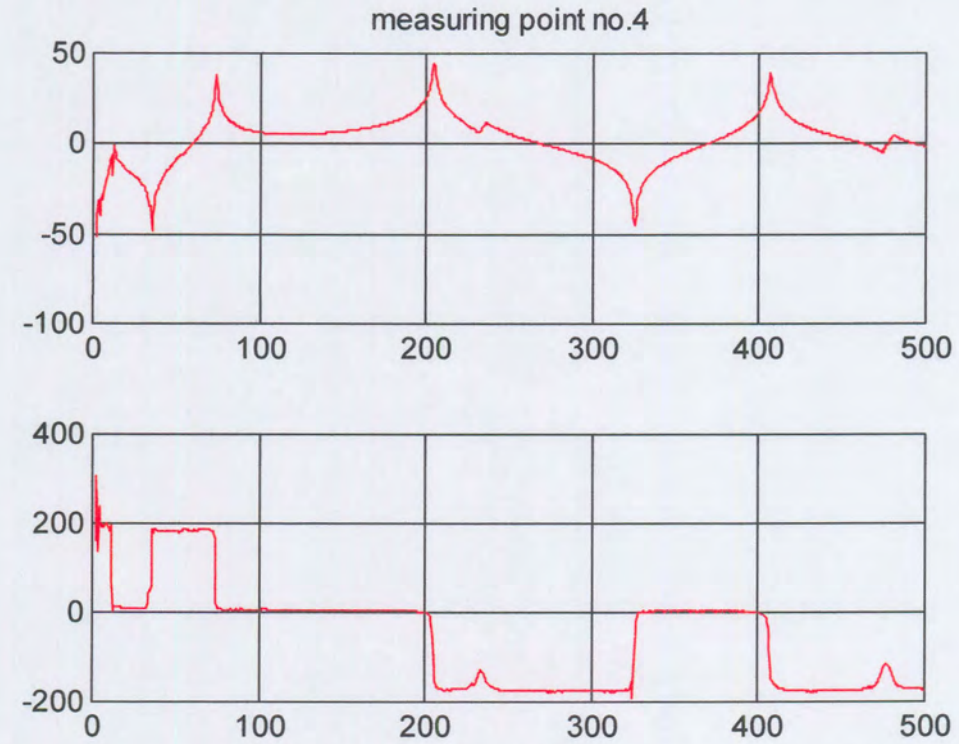

Frequency

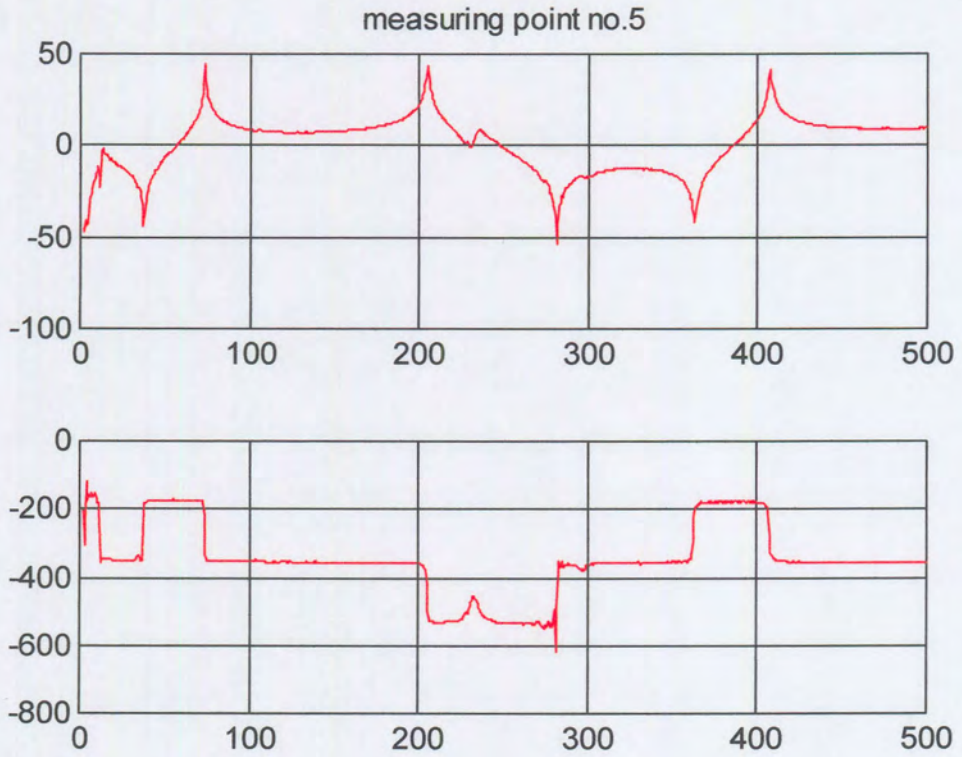

Frequency

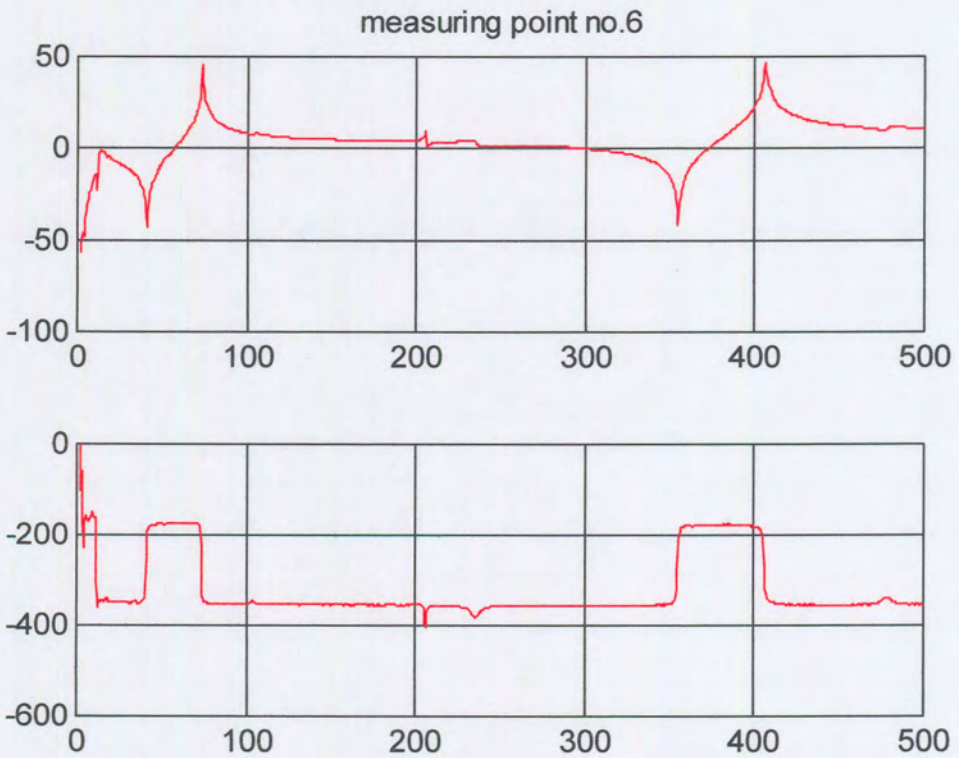

Frequency

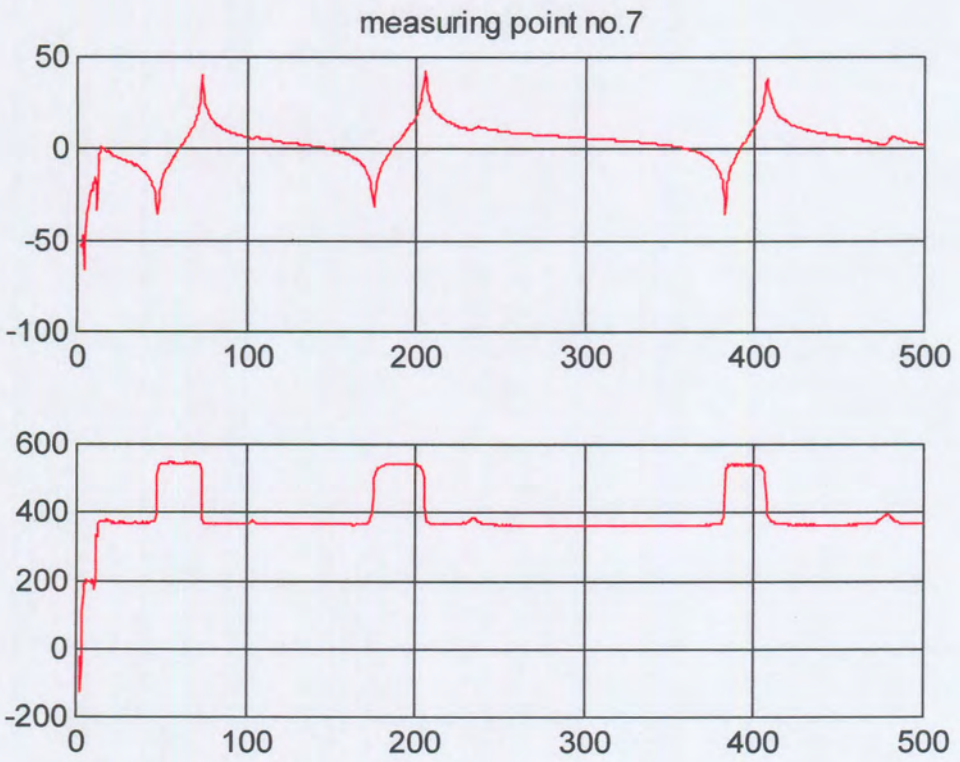

Frequency

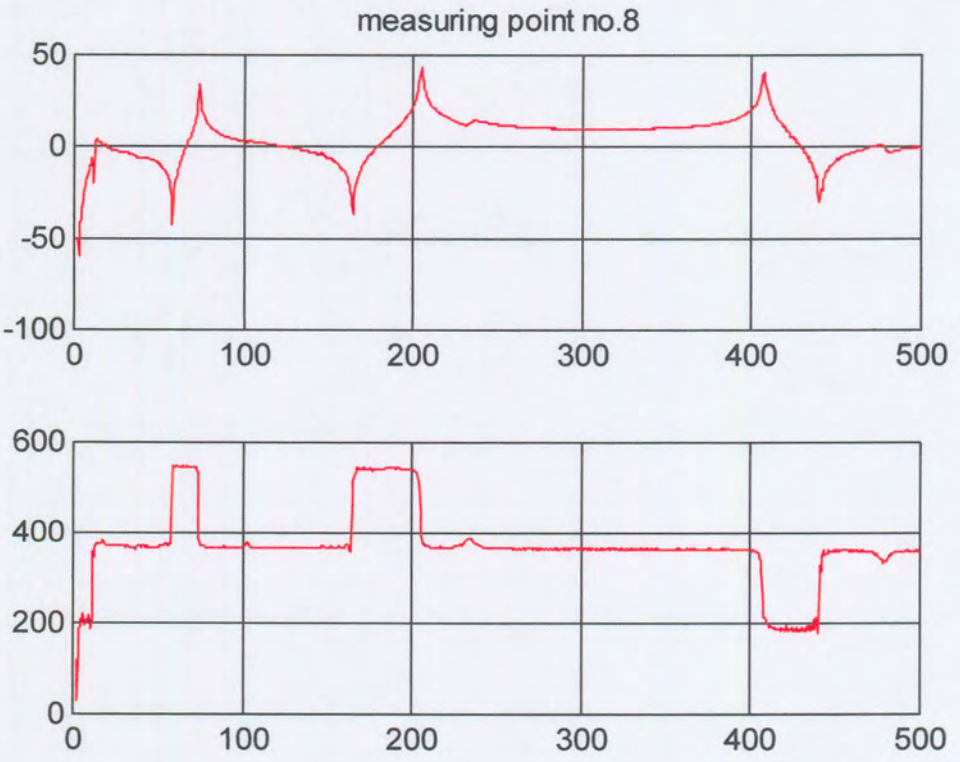

Frequency

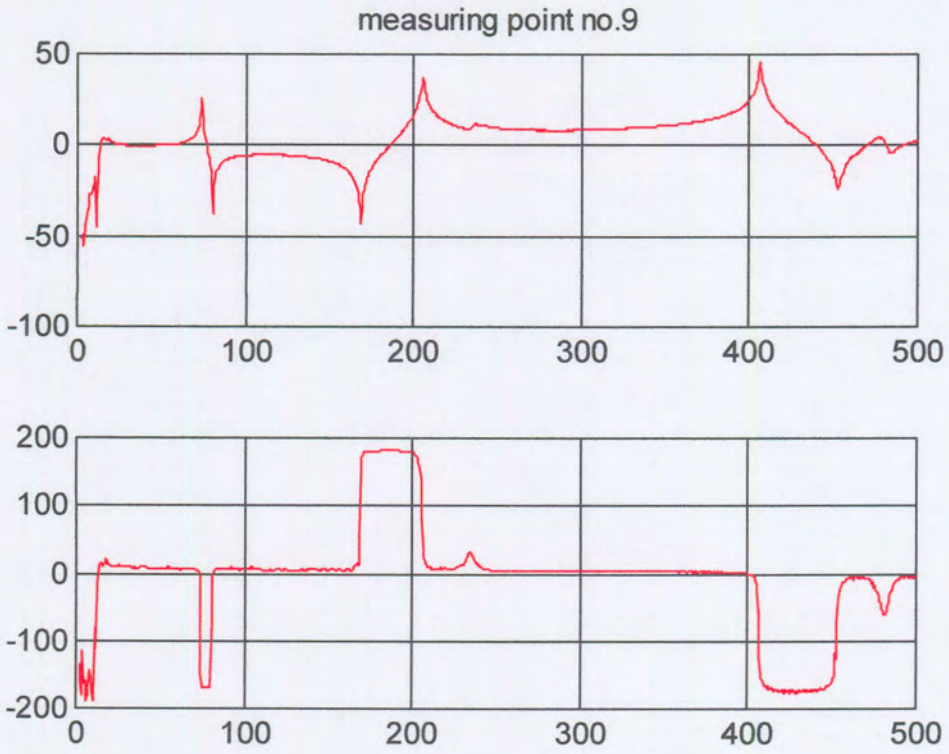

Frequency

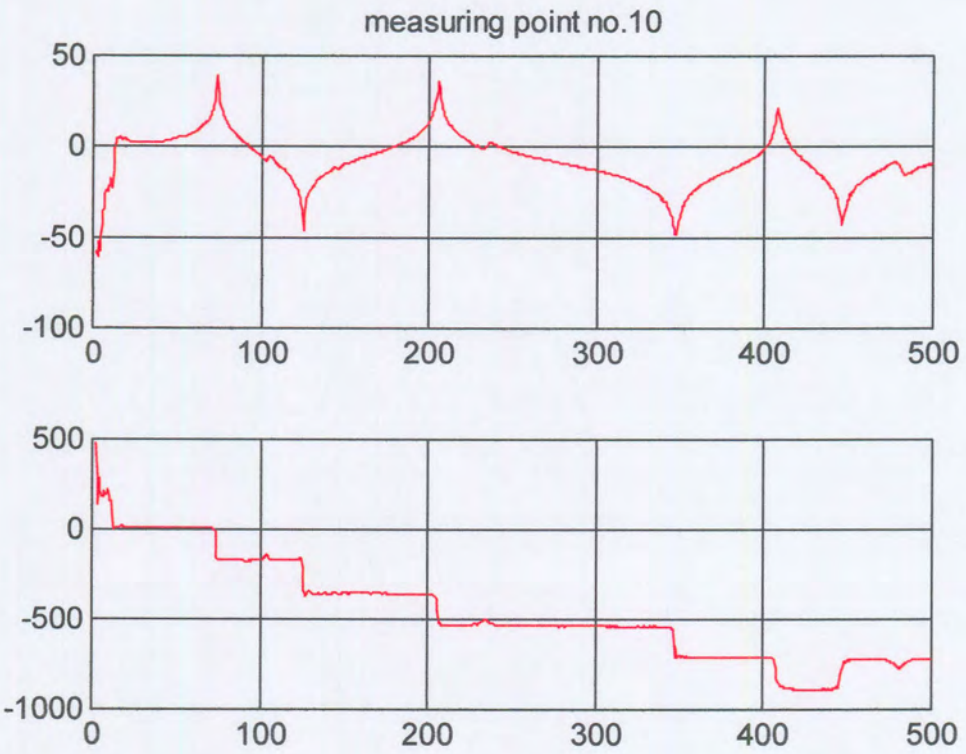

Frequency

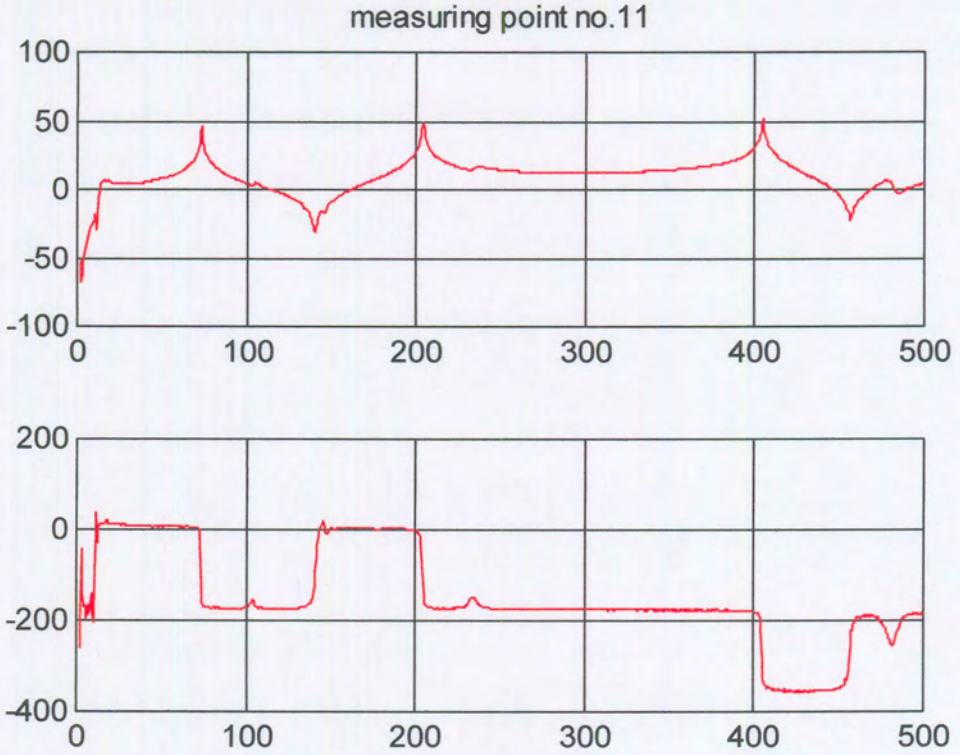
measuring point no.11
100
50
0
-50
-100
0
100
200
300
400
500
200
0
-200
-400
0
100
200
300
400
500
Frequency

Modal analysis measurement point no.2

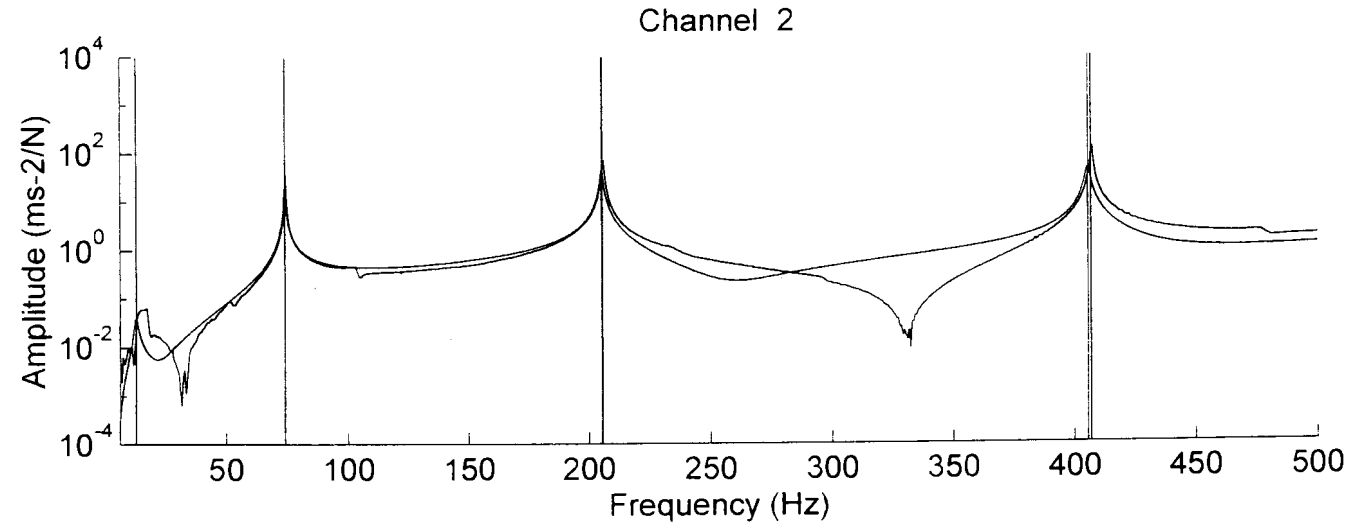

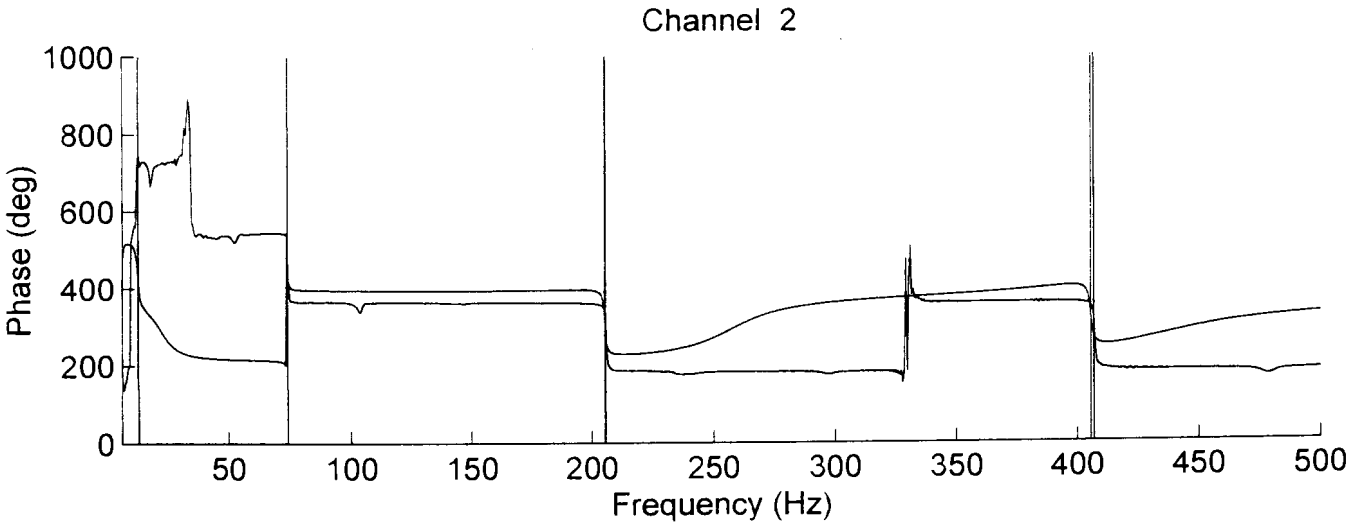

UNIVERSITEIT VAN PRETORIA
UNIVERSITY OF PRETORIA
YUNIBESITHI YA PRETORIA